学 位 論 文

Auxiliary mass method in finite temperature field theory

有限温度場の理論における補助質量の方法

平成11年12月博士（理学）申請

東京大学大学院理学系研究科
物理学専攻

小 幕 英 三

doctor thesis

Auxiliary mass method in finite temperature field theory

Kenzo Ogure

Institute for Cosmic Ray Resarch, University of Tokyo,
Midori-cho, Tanashi-shi, Tokyo 188 JAPAN

Desember 21, 1999

Abstract

We proposed the auxiliary mass method to improve the bad convergence of the perturbation theory at finite temperature. We applied this method to the Z_2-invariant scalar model and the O(N)-invariant scalar model. We found that the phase transition is of second order in these models. We then calculated critical exponents of the second order phase transition and obtained good results. We next applied the method to the Abelian Higgs model and then found that there is an end-point, where the phase transition crosses over from the second order phase transition to the first order phase transition. We further applied the method to the electroweak phase transition. We investigated the phase diagram in Higgs mass-top quark mass plane. We concluded from this phase diagram that we need an extension of the particle physics beyond the standard one in order to explain the baryon number of the present universe by the electroweak baryogenesis. We tried to improve the approximation which we used. We derived the evolution equation of the next to leading approximation, which becomes a simultaneous partial differential equation.

Contents

Chapter 1

Introduction

1.1 Phase transition and field theory

We have many kinds of phase transitions and utilize them in our daily lives often unconsciously. If we look for them with a little attention, we will easily find many examples: water, liquid crystals, superconductors, and so on. Water not only quenches our thirst but also rotates a steam turbine. Liquid crystal makes a monitor compact and superconductors possess various applications in science and engineering.

Of course, phase transitions are important phenomena in theoretical and experimental physics: elementary particle physics, nuclear physics, condensed matter physics, and cosmology. For example, QCD chiral phase transition at high temperature might occur in heavy ion collision experiments [1], which enable us to make progress to understand the QCD vacuum. Besides, QCD may have rich phase structure with respect to the family number [2, 3, 4, 5, 6] and the theta angle [7]. Phase transitions of QCD are, therefore, very interesting and important in elementary particle physics, nuclear physics, and cosmology. The electroweak phase transition is also an important one in cosmology since it may account for the baryon number of the present universe [8]. Since researches on this line indicate need of an extension of the elementary particle physics beyond the standard model, it is also important in elementary particle physics [9, 10]. Needless to say, we have various phase transitions in condensed matter physics: magnetic, liquid-vapor, superfluidity, superconductivity, liquid crystal, and so on. They are very interesting

because both of their academic aspects and applications.

The phase transitions are well described by the quantum field theory since most systems are continuous in space at least approximately. Natural introduction of gauge fields often help the description of the phase transitions: for example, superconductivity [11] and liquid crystal [12]. What is more, the quantum field theory has progressed remarkably in its technical aspects both perturbatively and non-perturbatively: Feynman diagram, path integral, renormalization, renormalization group, instanton, magnetic monopole, Schwinger-Dyson(SD) equation, and so on. We can say that it is now a *phase* for us to investigate a *phase transition* by the quantum field theory based on the technical foundation. Actually, some steps have been already made. For example, renormalization group method is suitable to investigate critical properties of a second order phase transition [13] and SD equation is often used to investigate the QCD phase transition [14, 15].

In the present paper, we focus on the investigations into the phase transitions using the *finite temperature field theory*. This theory is attractive since it is based only on the statistical principle. We, however, often have difficulty in use of the perturbation theory around the critical temperature because of bad infrared behaviour of higher loop Feynman diagram. Overcoming this difficulty is the main purpose of the present paper. Before we enter into details of the problem, we explain intuitively how the difficulty arises in the next section.

1.2 Perturbation theory in the finite temperature field theory

The perturbation theory of the finite temperature field theory often breaks down. This failure can be understood by considering particles in thermal bath [16, 17]. Suppose there is only one scalar field, which interacts each other with a small self-coupling constant, λ and the temperature, T is much larger than the scalar field mass, m_T. The subscript, T reminds us that the mass in the thermal bath is different from that at the zero temperature. In the perturbation theory, we calculate quantities like an effective potential or n-point functions as a series of the coupling constant by the Feynman diagram. At the zero temperature, we can get reliable results by calculating only a few

first terms since the contribution of the remaining terms are expected to be small,

$$\langle 0|\lambda aaa^\dagger a^\dagger \mathcal{O}|0\rangle \sim O(\lambda\langle 0|\mathcal{O}|0\rangle) \ll \langle 0|\mathcal{O}|0\rangle. \tag{1.1}$$

We must, however, take into account the interaction with the thermal bath at the finite temperature. In the thermal bath, we expect that there are large number of thermally excited low energy particles. The number is expected as,

$$n_B = \frac{1}{1-e^{-\frac{E}{T}}} = \frac{1}{1-e^{-\frac{\sqrt{\mathbf{k}^2+m_T^2}}{T}}} \sim \frac{T}{m_T} \qquad (\mathbf{k}^2 \sim m_T^2,\ T \gg m_T). \tag{1.2}$$

We expect that the perturbation terms are enhanced because of these particles,

$$\langle n_B|\lambda aaa^\dagger a^\dagger \mathcal{O}|n_B\rangle = \langle 0|\frac{a^{n_b}}{n_B!}\lambda aaa^\dagger a^\dagger \mathcal{O}|n_B\rangle \sim O((\frac{\lambda T^2}{m_T^2}+\frac{\lambda T}{m_T}+\cdots)\langle n_B|\mathcal{O}|n_B\rangle). \tag{1.3}$$

We observe from this that the perturbation terms are not negligible if the number $\frac{T}{m_T}$ is large enough. We can not, therefore, truncate the series of the Feynman diagram even if the coupling constant is small. We will see this in Sec.2.2.1 quantitatively by calculating the Feynman diagram actually and find that the leading term in Eq.(1.3) can be summed easily using the ring resummation method. The expansion parameter therefore becomes $\frac{\lambda T}{m_T}$ after the resummation. This resummation is, however, not sufficient to investigate properties of this simple model as we will see in Sec.4.1.1.

We notice that this problem is caused by the low energy particles in the thermal bath and then arises only when $T \gg m_T$. We utilize this fact in the auxiliary mass method, which we will explain in Ch.3.

The present paper is organized as follows. In Ch.2, we review the finite temperature theory and breakdown of its perturbation theory. We introduce some known approaches to cope with the breakdown here. In Ch.3, we show the idea of the auxiliary mass method, which is the main subject of the present paper. We derive the evolution equation, which is the most important tool in this method. In Ch.4, we apply the method to scalar field theories concretely. In Ch.5, we apply this method to gauge field theories. In Ch.6, we try to improve the approximation, which is employed in the auxiliary mass method. We write detail calculations in Appendices.

Chapter 2

Finite temperature field theory

2.1 Imaginary time formalism

The finite temperature field theory has various variations [1]: imaginary time formalism [18], real time formalism [19], and thermo dynamics [20]. Of course, we can choose any methods, which are equivalent in equilibrium. We should choose a method by considering what quantities we calculate. We use the imaginary time formalism, which is simple and sufficient to calculate equilibrium thermo dynamical quantities like free energy throughout the present paper since we calculate only the effective potential essentially. In the present section, we review the imaginary time formalism shortly.

The most fundamental quantity in the statistical dynamics is the partition function,

$$\begin{aligned} Z(\beta) &= Tr \exp(-\beta H) \\ &= \int_{all\ \ state} d\phi_a \langle \phi_a | \exp(-\beta H) | \phi_a \rangle. \end{aligned} \tag{2.1}$$

This quantity is quite similar to the partition function of the ordinary quantum field theory. We, therefore, expect that we can utilize the path integral technic, and actually we can. All we have to pay attention to are two differences: the time evolution operator, $exp(-iHt)$, is replaced by the statistical weight, $exp(-\beta H)$, and all states should be summed up. We rewrite the expression in Eq.(2.1) to path integral form as follows,

$$Z(\beta) = \lim_{n\to\infty} \int d\phi_a \, \langle \phi_a | (1 - \triangle\beta H)^n | \phi_a \rangle \qquad (\triangle\beta = \frac{\beta}{n})$$

$$\begin{aligned} &= \lim_{n\to\infty} \int d\phi_a \int \prod_{i=1}^{n-1} d\phi_i \langle \phi_a | (1 - \triangle\beta H) | \phi_{n-1} \rangle \langle \phi_{n-1} | (1 - \triangle\beta H) | \phi_{n-2} \rangle \cdots \\ &\qquad \cdots \times \langle \phi_1 | (1 - \triangle\beta H) | \phi_a \rangle \\ &= \lim_{n\to\infty} \int d\phi_a \int \frac{\prod_{i=1}^{n-1} d\phi_i d\pi_i}{(2\pi)^{n-1}} \int \frac{d\pi_0}{2\pi} \langle \phi_a | \pi_{n-1} \rangle \langle \pi_{n-1} | (1 - \triangle\beta H) | \phi_{n-1} \rangle \times \cdots \\ &\qquad \cdots \times \langle \phi_1 | \pi_0 \rangle \langle \pi_0 | (1 - \triangle\beta H) | \phi_a \rangle. \end{aligned} \tag{2.2}$$

Using a relation,

$$\begin{aligned} &\langle \phi_i | \pi_{i-1} \rangle \langle \pi_{i-1} | (1 - \triangle\beta H) | \phi_{i-1} \rangle \\ &= (1 - \triangle\beta H(\pi_{i-1}, \phi_{i-1})) \ \exp\{ i \int d^3\mathbf{x} \, \pi_{i-1} \, (\phi_i - \phi_{i-1}) \}, \end{aligned} \tag{2.3}$$

we get the path integral form of the partition function,

$$\begin{aligned} &Z(\beta) \\ &= \lim_{n\to\infty} \int d\phi_a \int \frac{\prod_{i=1}^{n-1} d\phi_i d\pi_i}{(2\pi)^{n-1}} \int \frac{d\pi_0}{2\pi} (1 - \triangle\beta H(\pi_{n-1}, \phi_{n-1})) \\ &\qquad \exp\{ i \int d^3\mathbf{x} \, \pi_{n-1} \, (\phi_a - \phi_{n-1}) \} \times \cdots \\ &\qquad \cdots \times (1 - \triangle\beta H(\pi_0, \phi_a)) \exp\{ i \int d^3\mathbf{x} \, \pi_0 \, (\phi_1 - \phi_a) \} \\ &= \lim_{n\to\infty} \int d\phi_a \int \frac{\prod_{i=1}^{n-1} d\phi_i d\pi_i}{(2\pi)^{n-1}} \int \frac{d\pi_0}{2\pi} \exp\{ \triangle\beta \sum_{j=0}^{n-1} \int d^3\mathbf{x} [i\pi_j \, (\frac{\phi_{j+1} - \phi_j}{\triangle\beta}) - H_j | \} \\ &\qquad (\phi_n = \phi_0 \equiv \phi_a) \\ &\equiv \int \mathcal{D}[\pi] \int_p \mathcal{D}[\phi] \ \exp\{ \int_0^\beta d\tau \int d^3\mathbf{x} \, (i \, \pi \, \frac{\partial \phi}{\partial \tau} - H) \}. \end{aligned} \tag{2.4}$$

Here, the subscript "p" under $\mathcal{D}[\phi]$ reminds us the periodicity,

$$\phi(\mathbf{x}, 0) = \phi(\mathbf{x}, \beta). \tag{2.5}$$

We simplify Eq.(2.4) in most cases as in the ordinary quantum field theory. For example, in case

$$\mathcal{H} = \frac{1}{2}\pi^2 + \frac{1}{2}(\nabla\phi)^2 + \frac{1}{2}m^2\phi^2 + U(\phi), \tag{2.6}$$

we can carry out the Gaussian integral with respect to π,

$$\begin{aligned} Z(\beta) &= N\int_p \mathcal{D}[\phi]\exp\int_0^\beta d\tau\int d^3\mathbf{x}\{-\frac{1}{2}(\frac{\partial\phi}{\partial\tau})^2-\frac{1}{2}(\nabla\phi)^2-\frac{1}{2}m^2\phi^2-U(\phi)\} \\ &= N\int_p \mathcal{D}[\phi]\exp\int_0^\beta d\tau\int d^3\mathbf{x}\ \mathcal{L}_E. \end{aligned} \tag{2.7}$$

Here, we defined as,

$$\mathcal{L}_E \equiv -\frac{1}{2}(\frac{\partial\phi}{\partial\tau})^2-\frac{1}{2}(\nabla\phi)^2-\frac{1}{2}m^2\phi^2-U(\phi). \tag{2.8}$$

In order to derive the Feynman rules, we separate a contribution of an external field from the potential,

$$U(\phi)=\tilde{U}(\phi)-J(x)\ \phi(x). \tag{2.9}$$

We then have from Eq.(2.7),

$$\begin{aligned} Z(\beta;J) &= N\int_p \mathcal{D}[\phi]\exp[-\int_0^\beta d\tau\int d^3\mathbf{x}\{\frac{1}{2}\phi(-\frac{\partial^2}{\partial\tau^2}-\nabla^2+m^2)\phi \\ &\qquad +\tilde{U}(\phi)-J(x)\phi(x)\}]. \end{aligned} \tag{2.10}$$

We next introduce a propagator, $\Delta_F(x)$, which is periodic in the interval $0\le\tau\le\beta$ and satisfy the following equation,

$$(-\frac{\partial^2}{\partial\tau^2}-\nabla^2+m^2)\Delta_F(x-y)=\delta(\tau_x-\tau_y)\delta(\mathbf{x}-\mathbf{y}). \tag{2.11}$$

The propagator can be written as follows,

$$\begin{aligned} \Delta_F(\tau_x-\tau_y,\mathbf{x}-\mathbf{y}) &= iT\sum_{n=-\infty}^{n=\infty}\int\frac{d^3\mathbf{k}}{(2\pi)^3}\frac{-i}{\omega_n^2+\mathbf{k}^2+m^2}e^{-i\omega_n(\tau_x-\tau_y)+i\mathbf{k}\cdot(\mathbf{x}-\mathbf{y})} \\ &\qquad (\omega_n\equiv 2\pi nT). \end{aligned} \tag{2.12}$$

Changing the field variable as,

$$\phi'(x)=\phi(x)-\int_0^\beta d\tau_y\int d^3\mathbf{y}\Delta_F(\tau_x-\tau_y,\mathbf{x}-\mathbf{y})J(\tau_y,\mathbf{y}), \tag{2.13}$$

we get a final form from Eq.(2.10),

$$\begin{aligned} Z(\beta;J) &= Z_F(\beta)\exp\{-\int_0^\beta d\tau_x\int d^3\mathbf{x}\ \tilde{U}(\frac{\delta}{\delta J})\} \\ &\quad\times\exp\{\frac{1}{2}\int_0^\beta d\tau_x\int d^3\mathbf{x}\int_0^\beta d\tau_y\int d^3\mathbf{y}\ J(\tau_x,\mathbf{x})\Delta_F(\tau_x-\tau_y,\mathbf{x}-\mathbf{y})J(\tau_y,\mathbf{y})\} \end{aligned} \tag{2.14}$$

$$Z_F(\beta) \equiv \int_p D[\phi']\exp[-\int_0^\beta d\tau\int d^3\mathbf{x}\{\frac{1}{2}\phi'(-\frac{\partial^2}{\partial\tau^2}-\nabla^2+m^2)\phi'\]. \tag{2.15}$$

We derive the Feynman rule from this as the ordinary quantum field theory. In momentum space, the propagator is replaced as,

$$\frac{i}{p_0^2-p_i^2-m^2}\longrightarrow\frac{-i}{(2\pi nT)^2+p_i^2+m^2}\equiv\frac{-i}{\omega_n^2+p_i^2+m^2} \tag{2.16}$$

and the loop integral factor is replaced as,

$$\int\frac{d^4p}{(2\pi)^4}\longrightarrow iT\sum_{n=-\infty}^{\infty}\int\frac{d^3p}{(2\pi)^3}. \tag{2.17}$$

These changes are easily interpreted by considering the differences between the ordinary quantum field theory and the finite temperature field theory. Since the time evolution operator, $exp(-iHt)$, is replaced by the statistical weight, $exp(-\beta H)$, the metric becomes Euclidean. The Fourier transformations replaced by Fourier expansion because of the compactness of the interval of the integral in the imaginary time direction. While we derived the Feynman rule only for the simple model, the rule is the same for other Bose fields.

While we do not derive the rules for Fermi fields, we only write down the result. The propagator in momentum space is replaced as,

$$\frac{i}{p_\mu\gamma^\mu-m}\longrightarrow\frac{-i}{-i\gamma_0(2n+1)\pi T+\gamma_ip^i+m}\equiv\frac{-i}{-ip_0\omega_n+\gamma_ip^i+m} \tag{2.18}$$

and the loop integral is replaced as,

$$\int\frac{d^4p}{(2\pi)^4}\longrightarrow iT\sum_{n=-\infty}^{\infty}\int\frac{d^3\mathbf{p}}{(2\pi)^3}. \tag{2.19}$$

The only difference between Bose field and Fermi field is the imaginary time frequency for Fermi field is not $\omega_n = 2n\pi T$ but $\omega_n = (2n+1)\pi T$. Although this seems to be a slight difference, it is very important in use of the perturbation theory. The propagator of the Bose field does not have the scale T for $n = 0$. On the other hand, the propagator of the Fermi does have the scale T for any n. As we will see in the next section, the perturbation theory often breaks down only for the Bose field because of this difference.

2.2 Breakdown of the perturbation theory and ring resummation

2.2.1 Breakdown of the perturbation theory

In Sec.2.1, we showed that the perturbation theory of the finite temperature field theory can be defined using the finite temperature Feynman diagram. Though we can calculate a few first terms using it, we often can not rely on the results as we mentioned in Sec.1.2. In the present section, we show this fact by actually calculating the Feynman diagram [21].

While we take the scalar field theory as an example here, we can apply the result to other Bose fields. The Lagrangian density is,

$$\mathcal{L} = -\frac{1}{2}(\frac{\partial\phi}{\partial\tau})^2 - \frac{1}{2}(\nabla\phi)^2 + \frac{1}{2}\mu^2\phi^2 - \frac{\lambda\phi^4}{4!} + c.t. \quad . \tag{2.20}$$

This Lagrangian density has Z_2-symmetry at zero temperature, which breaks down spontaneously in case, $\mu^2 > 0$. The mass at the broken vacuum, $\bar{\phi} \neq 0$ is $m^2(\bar{\phi}) = -\mu^2 + \frac{\lambda\bar{\phi}^2}{2}$.

We first consider high temperature behaviour of general one loop graphs with zero external momentum, of which mass dimension is D. From the dimensional analysis, we can write this amplitude, M as follows,

$$M = T^D f(\frac{m}{T}) \tag{2.21}$$

In high temperature limit, $\frac{m}{T} \to 0$, the amplitude behaves as $M \propto T^D$ if $f(0)$ is well-defined.

For example, we consider the one loop graph of the two point function in Fig.2.1. From the above dimensional analysis, we expect that this graph

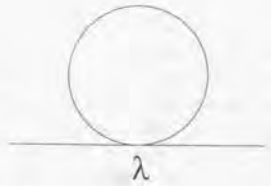

Figure 2.1: A two point function at one loop level. An amplitude of this graph is of order λT^2. This behaviour makes the loop expansion parameter larger at high temperature.

should be of order λT^2 because of the absence of the infrared divergence. We confirm this fact by explicit calculation. The amplitude of this graph is,

$$i\Gamma^{(2)}(m^2(\phi);T) = (-i\lambda)i\frac{T}{2}\sum_{n=-\infty}^{n=\infty}\int\frac{d^3\mathbf{k}}{(2\pi)^3}\frac{-i}{(2\pi nT)^2 + \mathbf{k}^2 + m^2(\phi)}. \tag{2.22}$$

Though we can not express this amplitude by elementary functions, we can expand this with respect to m/T, *high temperature expansion*. We left the derivation to the Appendix.A and only show the result,

$$\begin{aligned} i\Gamma^{(2)}(m^2(\phi);T) &= -\frac{i\lambda T^2}{24} + \frac{i\lambda mT}{8\pi} + \frac{i\lambda m^2}{32\pi^2}\left\{\frac{1}{\epsilon} + \log(\frac{M_R^2}{T^2}) - \log(4\pi) + \gamma_E\right\} \\ &\quad + \mathcal{O}(\frac{m^6}{T^2}). \end{aligned} \tag{2.23}$$

As we expected, we have the leading contribution of order λT^2. Since this amplitude has ultraviolet divergence, we regularised it using the dimensional regularisation with renormalization scale M_R. We notice that the divergent term is identical to that at zero temperature. Therefore, once we renormalize it at zero temperature using any method like MS or $\overline{MS}$ scheme, we do not have any divergence at finite temperature. Although we showed this fact only for the simple model at one-loop level, we can generalize it for any renormalizable models at arbitrary level [1, 22]. The physical interpretation of this fact is that the temperature influence only long range physics and does not change the ultraviolet behaviour. We think that the divergence in Eq.(2.23) is renormalized by appropriate method below.

On the other hand, how can we know high temperature behaviour of a graph, of which $f(0)$ is ill-defined? In this case, we notice the fact that the infrared divergence arises only for the zero mode of the finite temperature Bose field propagator(see Eq.(2.16)) since the scale T prevents them from the infrared divergence for the other modes. According to this observation, we deal with only the zero mode as an exception. Since the propagator does not depend on T for the zero mode, the three dimensional integrals does not depend on T. The only dependence on T comes from the loop factor (see Eq.(2.17)). As a consequence, the contribution from the zero mode is always proportional to T. For example, an amplitude of the 4-point function in Fig.2.2(a) with zero external momentum behaves as,

$$\begin{aligned}\Gamma^{(4)} &\propto T\sum_{n=-\infty}^{n=\infty}\int\frac{d^3\mathbf{k}}{(2\pi)^3}\frac{1}{\{(2\pi nT)^2+\mathbf{k}^2+m^2(\phi)\}^2}\\ &= T\int\frac{d^3\mathbf{k}}{(2\pi)^3}\frac{1}{\{\mathbf{k}^2+m^2(\phi)\}^2}\\ &\qquad +2T\sum_{n=1}^{\infty}\int\frac{d^3\mathbf{k}}{(2\pi)^3}\frac{1}{\{(2\pi nT)^2+\mathbf{k}^2+m^2(\bar{\phi})\}^2}\\ &= \mathcal{O}(T)+\mathcal{O}(T^0).\end{aligned}\tag{2.24}$$

From the above example, one can observe that an ultraviolet quadratic divergent graph behaves as $\propto T^2$ and the other graphs behave as $\propto T$ in case the space dimension is three. Although we only investigated the behaviour of one loop graphs, we can generalize these idea to more complicated graphs. In many cases, we can know the high temperature behaviour without explicit calculations.

Using the above general properties, we next see the breakdown of the perturbation theory at high temperature. We take a loop expansion of the 4-point function with zero external momentum as an example of the breakdown. While the leading graph in the loop expansion is Fig.2.3, this does not depend on the temperature. Temperature-dependent contribution arises from one-loop graphs, Fig.2.2(a),(b), and (c). According to the above paragraph, we expect that these graphs have amplitudes of order, $\lambda(\frac{\lambda T}{m})$, $\lambda(\frac{\lambda T}{m})(\frac{\lambda\bar{\phi}^2}{m^2})$, and $\lambda(\frac{\lambda T}{m})(\frac{\lambda\bar{\phi}^2}{m^2})^2$ respectively without explicit calculations. We can actually confirm these by explicit calculations using the results

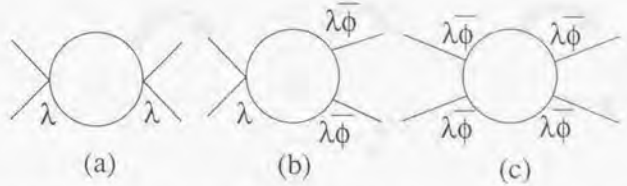

Figure 2.2: Feynman graphs of four point function at two loop level. The amplitude of these graphs are $\lambda(\frac{\lambda T}{m})$, $\lambda(\frac{\lambda T}{m})(\frac{\lambda\bar{\phi}^2}{m^2})$, and $\lambda(\frac{\lambda T}{m})(\frac{\lambda\bar{\phi}^2}{m^2})^2$ respectively.

Figure 2.3: The leading graph of 4-point functions in the loop expansion. The amplitude of this graph is independent of the temperature.

in Appendix.A,

$$\begin{aligned}\Gamma^{(4)}_{(a)} &\sim \lambda^2 T\sum_{n=-\infty}^{n=\infty}\int\frac{d^3k}{(2\pi)^3}\frac{1}{\{(2\pi nT)^2+\mathbf{k}^2+m^2(\phi)\}^2}\sim\lambda(\frac{\lambda T}{m})\qquad(2.25)\\ \Gamma^{(4)}_{(b)} &\sim \lambda^3\bar{\phi}^2 T\sum_{n=-\infty}^{n=\infty}\int\frac{d^3k}{(2\pi)^3}\frac{1}{\{(2\pi nT)^2+\mathbf{k}^2+m^2(\phi)\}^3}\sim\lambda(\frac{\lambda T}{m})(\frac{\lambda\bar{\phi}^2}{m^2})\\ \Gamma^{(4)}_{(c)} &\sim \lambda^4\bar{\phi}^4 T\sum_{n=-\infty}^{n=\infty}\int\frac{d^3k}{(2\pi)^3}\frac{1}{\{(2\pi nT)^2+\mathbf{k}^2+m^2(\phi)\}^4}\sim\lambda(\frac{\lambda T}{m})(\frac{\lambda\bar{\phi}^2}{m^2})^2.\end{aligned}$$

We observe that the loop expansion parameter is $(\frac{\lambda T}{m})$ if we assume that the mass squared is of order $m^2\sim\lambda\bar{\phi}^2$ even at finite temperature. The new expansion parameter, $(\frac{\lambda T}{m})$ can be larger than $\mathcal{O}(1)$ in a second order phase transition even for small λ since the mass vanish at the critical temperature. This situation is similar for weakly first order phase transition of which correlation length is long around the critical temperature.

What is worse, the loop expansion parameter can be much larger for some

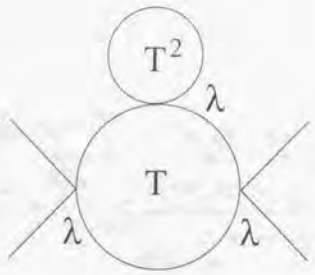

Figure 2.4: A two loop graph of 4-point function. This has amplitude of order $\lambda(\frac{\lambda T}{m})(\frac{\lambda T^2}{m^2})$.

type of graphs. We consider a two loop graph Fig.2.4, which can be seen as the graph Fig.2.2(a) with the graph Fig.2.1. At the zero temperature, we expect that the amplitude of the graph Fig.2.4 is smaller than that of the graph Fig.2.2(a) by λ. The amplitude of the graph in Fig.2.4, however, changes by $(\frac{\lambda T^2}{m^2})$ from that of the graph Fig.2.2(a) at high temperature. We observe this without explicit calculation as follows. When we add the graph Fig.2.1 to graph Fig.2.2(a), we multiply the factor λT^2 to the amplitude of Fig.2.2(a) and increase a propagator in loop integral. Since this propagator has zero mode, which has unique mass scale m, the amplitude changes by $(\frac{\lambda T^2}{m^2})$. Of course, we can confirm this by explicit calculation using the results in AppendixA. Similarly, we observe that all graphs in Fig.2.5 have the loop expansion parameter, $(\frac{\lambda T^2}{m^2})$.

In the present section, we showed that the perturbation theory is often not reliable at high temperature. The loop expansion parameter is $(\frac{\lambda T}{m})$ for most graphs and $(\frac{\lambda T^2}{m^2})$ for some type of graphs. In the next section, we review the ring resummation method [21, 23], which improves convergence of the graphs. Using this method, loop expansion parameter becomes only $(\frac{\lambda T}{m})$.

2.2.2 Ring diagram

The graphs, which have the worst loop expansion parameter $(\frac{\lambda T^2}{m^2})$, arise systematically (see Fig.2.5). We can sum up the dominant part of these graphs beforehand and make the loop expansion parameter $(\frac{\lambda T}{m})$ by utilizing this rule. We first make $\mathcal{O}(\lambda T^2)$ part of Fig.2.1, $-\frac{i\lambda T^2}{24}$, be represented by the mark in Fig.2.6. We then sum up the graphs in Fig.2.7 by sifting the

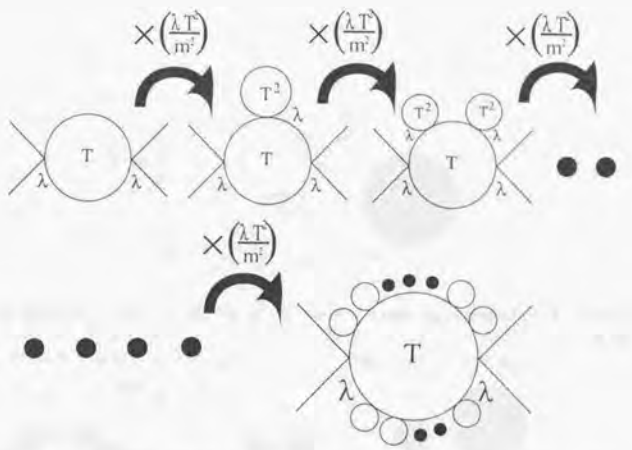

Figure 2.5: Graphs, which have worse loop expansion parameter, $\frac{\lambda T^2}{m^2}$.

mass as follows,

$$m^2(\phi) \longrightarrow m^2(\phi) + \frac{\lambda T^2}{24}, \tag{2.26}$$

because of the identity,

$$\frac{-i}{\omega_n^2 + q^2 + m^2(\phi)} + \frac{-i}{\omega_n^2 + q^2 + m^2(\phi)}\left(\frac{-i\lambda T^2}{24}\right)\frac{-i}{\omega_n^2 + q^2 + m^2(\phi)} + \cdots\cdots$$

$$= \frac{-i}{\omega_n^2 + q^2 + m^2(\phi) + \frac{\lambda T^2}{24}}. \tag{2.27}$$

Defining ring resummed propagator as Fig.2.8, we can represent the summation of the graphs in Fig.2.7 as Fig.2.9.

We, however, must perform the loop expansion carefully from two loop level in order to avoid double counting. For example, a part of two loop graph in Fig.2.10 has already been contained in one loop resummed graph in Fig.2.9. We therefore should subtract the part as Fig.2.11. The amplitude of the sum of these graphs change from one loop graph Fig.2.9 by $\mathcal{O}(\frac{\lambda T}{m})$,

Figure 2.6: The leading contribution of the graph in Fig.2.1 at high temperature.

Figure 2.7: Graphs, which are summed at one loop ring resummation.

Figure 2.8: Ring propagator.

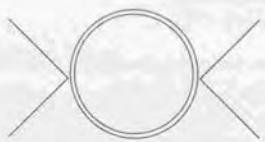

Figure 2.9: One loop diagram in ring resummed perturbation theory.

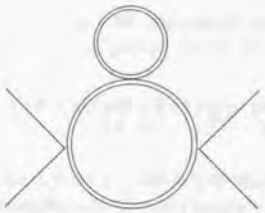

Figure 2.10: A two loop diagram in ring resummed perturbation theory. A part of this diagram has already been counted in one loop level(Fig.2.9).

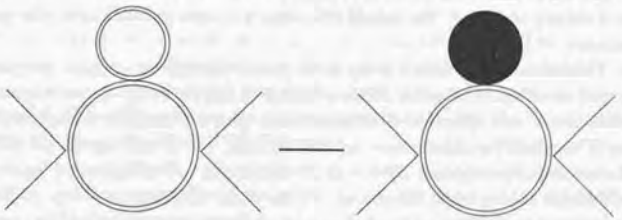

Figure 2.11: Double counted part is subtracted as the counter term method

The loop expansion parameter is improved to $(\frac{\lambda T}{m})$. As we mentioned in Sec.1.2, we can sum up the leading contribution in Eq.(1.3) and make the loop expansion parameter $(\frac{\lambda T}{m})$.

We notice that this procedure is the same as the counter term method. We actually perform the ring resummation by rewriting the Lagrangian density as,

$$\mathcal{L} = \frac{1}{2}(\partial_\mu\phi)^2 + \frac{1}{2}(\mu^2 - \frac{\lambda T^2}{24})\phi^2 - \frac{\lambda\phi^4}{4!} + \frac{\lambda T^2}{48}\phi^2 + c.t. \qquad (2.28)$$

and deal the term $\frac{\lambda T^2}{48}\phi^2$ as a counter term. We call the temperature dependent mass term as thermal mass below.

As a summary, we note three important points again: (1) We need shift the mass squared by $\mathcal{O}(\lambda T^2)$. (2) We should subtract double counted part as the counter term method. (3) The loop expansion parameter is $\frac{\lambda T}{m}$ even after

the ring resummation. Following the ordinary convention, we call the ring resummed perturbation theory as simply "the perturbation theory" below.

2.2.3 The other methods in the finite temperature field theory

In Sec.2.2.1, we explained the breakdown of the perturbation theory. In Sec.2.2.2, we then introduced the ring resummation method, which improves the bad convergence of the perturbation theory to some extent. This method is, however, not sufficient to investigate all phase transitions as we will see in Sec.4.1.1. Many efforts are, therefore, made to use the finite temperature field theory reliably. We introduce some known approaches in the present section.

The lattice field theory is the most powerful method at finite temperature as well as the perturbation theory. Since we discretise the finite temperature field theory and simulate behaviours of a phase transition using the Monte Carlo method on computers in this method, we do not have the difficulty of the bad convergence of the loop expansion. We, however, have other difficulties in this case. Of course, we have the doubling problem of Fermion at finite temperature as in the case of zero temperature. Besides, we have another problem at high temperature. Since the interval of the imaginary time direction is $\frac{1}{T}$, it is short at high temperature. We can not have many sites in this short distance. For example, in most simulations of the SU(2) gauge+Higgs theory, we have only two sites in the direction, $N_\tau = 2$. It is doubtful if we reach the continuum limit in such few sites. There are two ideas to overcome the problem. We introduce these two approaches shortly.

We first introduce the *dimensional reduction approach* [24, 25, 26, 27, 28]. The aim of this approach is to make an effective three dimensional theory, which does not have the imaginary time direction and does have remarkably good properties in the Monte Carlo simulation. To make it, we utilize a fact that the propagator in Eq.(2.16) can be seen to have a light mass mode(zero-mode) and infinite number of heavy modes(non-zero mode) at high temperature. Similar to the decoupling theorem [29, 30], we can integrate out the heavy modes and have the effective three dimensional theory only of the light field. While we do not derive the explicit form of this effective theory, we notice some properties of this theory here: (1)

Although we can use the perturbation theory in the effective theory, the loop expansion parameter is, of course, not improved. (2) In the lattice Monte Carlo simulation, we do not have the problem of the imaginary time direction because of its absence. (3) Since Fermions do not have the light mode(zero-mode), we can integrate out them completely. This fact allows us to use the lattice simulation easily.

We next introduce the *anisotropic lattice approach* [31, 32, 33]. This is a rather simple idea. We take the lattice spacing of the imaginary time direction smaller than that of the other directions. Though this makes a lattice action complicated, we can have sufficient sites in the imaginary direction.

We next introduce approaches different from the lattice theory. Roughly speaking, most of them are based on the idea to improve the perturbation theory by taking into account some non-perturbative effects. The subject of the present paper, *auxiliary mass method*, also belongs to this kind. There are many other methods belonging to this kind: the optimized perturbation theory [34], the self-consistent Hartree approximation [35], the C.J.T.method [36, 37, 38], the ϵ-expansion [39], the gap equation method [40, 41]. We have not yet gotten a method, with which we can investigate any phase transition reliably, in spite of these efforts. It is therefore meaningful to develop the new method, auxiliary mass method, to reveal properties of phase transitions.

Chapter 3

Auxiliary mass method

3.1 Idea of the auxiliary mass method

In the present section, we introduce the basic idea of the auxiliary mass method [42, 43, 44, 45, 46, 47, 48, 49]. As we showed in Sec.2.2.1, the loop expansion parameter was $\frac{\lambda T^2}{m^2}$ at high temperature. This enhancement of the loop expansion parameter is caused by the interaction with the thermal bath, where thermally excited particles with energy $E \sim m$ filled the space. In this case, the perturbation theory does not give us reliable informations for $T \gtrsim \frac{m}{\sqrt{\lambda}}$. As we showed in Sec.2.2.2, the loop expansion parameter was able to be improved to $\frac{\lambda T}{m}$ by the ring resummation method. In this case, the perturbation theory will not give reliable answer for $T \gtrsim \frac{m}{\lambda}$.

We utilize the fact that that the loop expansion parameter is $\mathcal{O}(\lambda)$ in case $m \sim T$. We can, therefore, use the perturbation theory reliably at the temperature if we can do it at zero temperature. Throughout the present paper, we only deal with such theories; the auxiliary mass method can not deal with theory of which perturbation theory is unreliable even at the zero temperature. The first procedure of the auxiliary mass method is adding the large auxiliary mass $M \sim T$ to the true mass. We then calculate the effective potential/action using the perturbation theory. This effective potential/action is reliable thanks to the auxiliary mass.

This is, however, not the effective potential/action at the true mass, which we need. The second procedure is then extrapolating the effective potential/action at the large mass to the effective potential/action at the

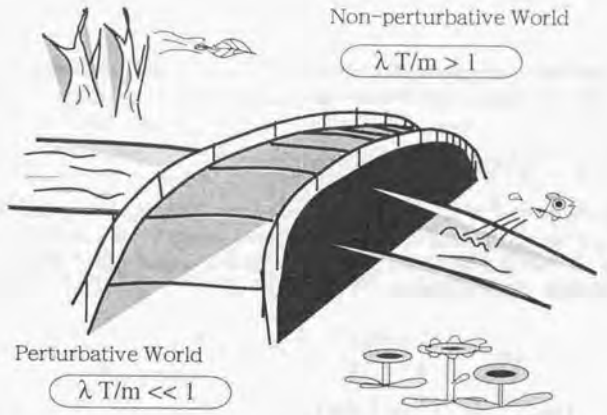

Figure 3.1: Image of the auxiliary mass method is shown. *Perturbative World* means the large mass region, where the loop expansion parameter is $O(\lambda)$. We first calculate the effective potential/action here by the perturbation theory. The bridge means the evolution equation, which relates the effective potential/action at different mass. We get the effective potential/action at the Non-perturbative World by solving this equation from the Perturbative World.

true mass. In order to carry this out, we construct an evolution equation of the effective potential/action as the mass varies. We calculate the effective potential/action at the true mass by solving the evolution equation from the large mass to the true mass with the initial condition, which is calculated in the first procedure. The whole process for calculating the effective potential/action by the auxiliary mass method is shown in Fig.3.1.

In the final stage, we read physical quantities from the effective potential/action example, we can observe the order of the phase transition. If the phase transition is of first order, we observe the phase transition temperature and the strength of it. If the phase transition is of second order, we observe the critical temperature and the critical exponents.

The most important procedure in this method is constructing the evolution equation. Of course, we can not get a solvable evolution equation unless we approximate somehow. In the next section, we get the exact evolution

equation. Though we can not solve it by itself, we get solvable evolution equations from it under some approximations.

3.2 Evolution equation

In the present section, we derive the evolution equation of the effective action with respect to mass squared. We consider the O(N)-invariant scalar model as an example. We define Lagrangian density, action, partition function, and effective action as follows,

$$\begin{aligned}
\mathcal{L}_E &= -\frac{1}{2}\left(\frac{\partial\phi_a}{\partial\tau}\right)^2 - \frac{1}{2}(\nabla\phi_a)^2 + \frac{1}{2}\mu^2\phi^2 - \frac{\lambda\phi^4}{4!} + \phi_a J^a + c.t. \\
S[\phi_a; J_a] &= \int_0^{\frac{1}{T}} d\tau \int d^3\mathbf{x}\ \mathcal{L}_E \\
Z[J_a] &= e^{W[J_a]} = \int \mathcal{D}[\phi_a]\ e^{S[\phi_a; J_a]} \\
\Gamma[\bar{\phi}^2] &= W[J_a] - \int_0^{\frac{1}{T}} d\tau \int d^3\mathbf{x}\ \bar{\phi}_a J_a. \\
&\quad (\bar{\phi}_a = \frac{\delta W[J_a]}{\delta J_a},\ \bar{\phi}^2 = \bar{\phi}_a\bar{\phi}_a,\ a = 1, 2, \cdots, N)
\end{aligned} \tag{3.1}$$

We take a derivative of the effective potential,

$$\begin{aligned}
\frac{\partial\Gamma[\bar{\phi}^2]}{\partial m^2} &= \frac{\partial W[J_a]}{\partial m^2} - \int_0^{\frac{1}{T}} d\tau \int d^3\mathbf{x}\ \bar{\phi}_a \frac{\partial J_a}{\partial m^2} + c.t. \\
&= \frac{1}{Z}\int \mathcal{D}[\phi_a] \int_0^{\frac{1}{T}} d\tau \int d^3\mathbf{x} \left(-\frac{1}{2}\phi^2 + \phi_a \frac{\partial J_a}{\partial m^2}\right) e^{S[\phi_a; J_a]} \\
&\quad - \int_0^{\frac{1}{T}} d\tau \int d^3\mathbf{x}\ \bar{\phi}_a \frac{\partial J_a}{\partial m^2} + c.t. \\
&= -\frac{1}{2}\int_0^{\frac{1}{T}} d\tau \int d^3\mathbf{x} \langle\phi_a(\tau, \mathbf{x})\phi_a(\tau, \mathbf{x})\rangle + c.t.\ .
\end{aligned} \tag{3.2}$$

Since the full two point function in the last line can be represented by the effective action itself, we have,

$$\frac{\partial\Gamma[\bar{\phi}^2]}{\partial m^2} = -\frac{1}{2}\int_0^{\frac{1}{T}} d\tau \int d^3\mathbf{x} \left\{\bar{\phi}_a^2 + \left(-\frac{\delta^2\Gamma}{\delta\bar{\phi}_a^2}\right)\right\} + c.t.\ . \tag{3.3}$$

Here, the functional second derivative of the effective action with respect to the field expectation values, $\frac{\delta^2\Gamma}{\delta\bar{\phi}_a^2}$, is the full 1PI connected 2-point function at same point since the effective action is the generating functional of 1PI connected n-point functions. We represent this quantity explicitly in Appendix.D using the derivative expansion of the effective action. This is the evolution equation, which extrapolates the information at $\frac{\lambda T}{m} \ll 1$ to $\frac{\lambda T}{m} \gtrsim 1$(the bridge in Fig.3.1). Though this self-consistent equation is exact, it can not be solved exactly. We must approximate the equation somehow. We propose two approximations below and find that one of them works successfully.

Chapter 4

Phase transitions of scalar field theories

4.1 The Z_2-invariant scalar field theory

4.1.1 Investigation by the perturbation theory

In the present section, we investigate the phase transition of the Z_2-invariant scalar field theory by the perturbation theory. From the investigation, we see that the ring resummation is not sufficient to improve the perturbation theory [50, 51].

The Lagrangian density is,

$$\mathcal{L}_E = -\frac{1}{2}(\frac{\partial\phi}{\partial\tau})^2 - \frac{1}{2}(\nabla\phi)^2 + \frac{1}{2}\mu^2\phi^2 - \frac{\lambda\phi^4}{4!} + c.t. . \tag{4.1}$$

We have the effective potential at the tree level,

$$V^{(0)}(\bar{\phi}) = -\frac{1}{2}\mu^2\bar{\phi} + \frac{1}{4!}\lambda\bar{\phi}^4. \tag{4.2}$$

This does not depend on the temperature since temperature dependence arise from one loop level. The Z_2-symmetry is spontaneously broken in case $\mu^2 > 0$ at zero temperature.

We next calculate the one loop contribution at finite temperature,

$$V^{(1)} = \frac{T}{2}\sum_{n=-\infty}^{\infty}\int\frac{d^3k}{(2\pi)^3}\log\{(2\pi nT)^2 + \mathbf{k}^2 + m_T^2(\bar{\phi})\} + c.t. .$$

$$\left(m_T^2(\bar{\phi}) = -\mu^2 + \frac{\lambda}{2}\bar{\phi}^2 + \frac{\lambda T^2}{24}.\right) \tag{4.3}$$

We performed the ring resummation by shifting the mass here. This contribution can be expressed in Fig.4.1. According to Appendix.B, the equation(4.3) can be converted to the following form,

$$\begin{aligned} V^{(1)} &= V_0^{(1)} + V_T^{(1)} \\ V_0^{(1)} &= -\frac{i}{2}\int_{-i\infty}^{i\infty}\frac{dp_0}{2\pi}\int\frac{d^3\mathbf{p}}{(2\pi)^3}\log(-p^2 + m_T^2(\bar{\phi})) + c.t. \qquad (4.4) \\ V_T^{(1)} &= \frac{T}{2\pi^2}\int_0^\infty dr\ r^2\ \log\{1 - \exp(-\frac{1}{T}\sqrt{r^2 + m_T^2(\bar{\phi})})\}. \qquad (4.5) \end{aligned}$$

The contribution from $V_0^{(1)}$ is the same as the one loop contribution at zero temperature except the mass squared is shifted by the ring resummation. The ultraviolet divergence of this does depend on the temperature due to the mass shift. This temperature dependence seems to be incompatible with the statement in Sec.2.2.1 that the temperature does not cause new divergence. This is, however, artificial problem. The temperature dependent divergence is cased by the ring resummation, which sums up infinite diagrams. We summed higher loop divergences of the ordinary perturbation theory at the one loop diagram of the ring resummed perturbation theory. In this case, we summed two divergent diagrams in Fig.4.2 since they are contained in Fig.4.1. We can, therefore, subtract the divergences using the counter terms for the diagram for Fig.4.2. We use $\overline{MS}$ renormalization scheme with renormalization scale M_R and have,

$$V_0^{(1)} = \frac{m_T^4(\bar{\phi})}{4(4\pi)^2}\left\{\log\frac{m_T^2(\bar{\phi})}{M_R^2} - \frac{3}{2}\right\}. \tag{4.6}$$

On the other hand, the contribution from $V_T^{(1)}$ is convergent. Though this integral can not be expressed by elemental functions, it can be evaluated by numerical calculation. We plot the effective potential within one loop level $V_1 \equiv V^{(0)} + V^{(1)}$ qualitatively in Fig.4.3 around the critical temperature. This graph indicates that the phase transition is of first order. We know, however, that the phase transition is of second order from the other investigations: lattice simulations and renormalization group [13][52][53][54][55].

Figure 4.1: Graphical representation of the one loop contribution to the effective potential in the perturbation theory. Double line is the ring propagator defined in Fig.2.8

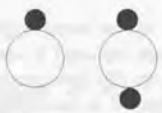

Figure 4.2: Two divergent diagrams, which are contained in the one loop graph in Fig.4.1.

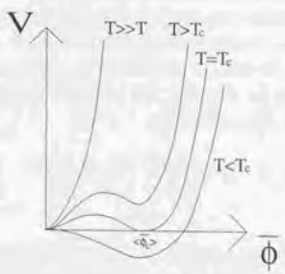

Figure 4.3: Schematic graph of the one loop effective potential around the critical temperature. This figure indicates that the phase transition is of first order.

Why did we fail in the investigation into such a simple model by the perturbation theory? The loop expansion parameter around the critical temperature answers this question. In order to look for the parameter, we expand V_1 by the high temperature expansion(see Appendix A),

$$\begin{aligned} V_1(\bar{\phi};T) &= \frac{1}{2}(-\mu^2+\frac{\lambda T^2}{24})\bar{\phi}^2-\frac{T}{12\pi}(-\mu^2+\frac{\lambda T^2}{24}+\frac{\lambda}{2}\bar{\phi}^2)^{\frac{3}{2}}+\frac{\lambda}{4!}\bar{\phi}^4 \\ &\quad +\frac{\{m_T^2(\bar{\phi})\}^2}{4(4\pi)^2}\left\{\log\frac{(4\pi T)^2}{M_R^2}-\frac{3}{2}\right\}+\mathcal{O}(\frac{m_T^6}{T^2}). \end{aligned} \tag{4.7}$$

We omit $\bar{\phi}$ independent terms, which have nothing to do with properties of the phase transition here[1]. To understand the behaviour of the effective potential, we neglect the last term in Eq.(4.7), which is small,

$$V_1(\bar{\phi};T) = \frac{1}{2}(-\mu^2+\frac{\lambda T^2}{24})\bar{\phi}^2-\frac{T}{12\pi}(-\mu^2+\frac{\lambda T^2}{24}+\frac{\lambda}{2}\bar{\phi}^2)^{\frac{3}{2}}+\frac{\lambda}{4!}\bar{\phi}^4. \tag{4.8}$$

We can understand the behaviour of the effective potential in Fig.4.3 from this. The effective potential increases near the origin because of the first term ($\propto \bar{\phi}^2$). Apart from the region, it decreases because of the second term ($\sim -\bar{\phi}^3$). For large $\bar{\phi}$, it is increasing function because of the last term. According to this discussion, we expect that all the three terms in Eq.(4.8) is comparable around $\bar{\phi}_c$,

$$(-\mu^2+\frac{\lambda T^2}{24})\bar{\phi}_c^2 \sim \frac{T}{12\pi}(-\mu^2+\frac{\lambda T^2}{24}+\frac{\lambda}{2}\bar{\phi}_c^2)^{\frac{3}{2}} \sim \frac{\lambda}{4!}\bar{\phi}_c^4. \tag{4.9}$$

From these relations, we conclude that the mass around $\bar{\phi}_c$ is of order,

$$m_T^2(\bar{\phi}) = -\mu^2+\frac{\lambda T^2}{24}+\frac{\lambda}{2}\bar{\phi}^2 \sim \lambda^2 T^2. \tag{4.10}$$

The loop expansion parameter, $\frac{\lambda T}{m_T}$ is, therefore, $O(1)$ at the vicinity of $\bar{\phi}_c$ around the critical temperature. This is why we could not obtain the correct properties by the perturbation theory.

[1] Strictly speaking, it has relation with the specific heat. We are, however, interested in the order of the phase transition and neglect the $\bar{\phi}$ independent terms

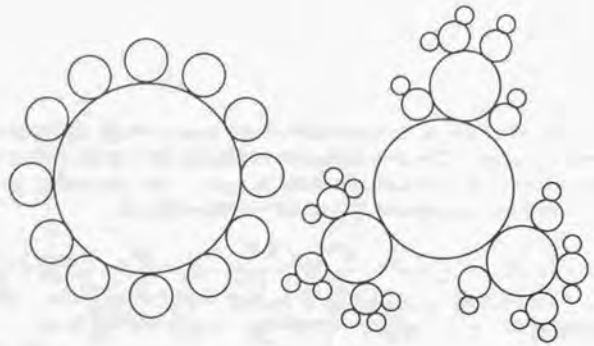

Figure 4.4: Examples of super-daisy diagrams. The graph (a) is often simply referred to as a 'daisy diagram'.

4.1.2 Investigation by the auxiliary mass method

Super daisy approximation

In Sec.3, we have explained the idea of the auxiliary mass method and have derived the evolution equation, which is the most important tool in the method. The equation, however, can not be solved exactly. We must, then, approximate somehow. In the present section, we introduce one of the approximations, *super daisy approximation* [44]. In this approximation, we sum up, so called, super daisy diagrams in Fig.4.4.

We first derive the evolution equation, which can sum up all the super daisy diagrams. We define the effective potential $V(\bar{\phi})$ as usual,

$$-\frac{\Omega}{T}V(\bar{\phi}) = \Gamma_T(\bar{\phi}(x))\Big|_{\phi(x)=\bar{\phi}=const}, \tag{4.11}$$

where $\Omega = \int d^3\boldsymbol{x}$. Substituting this definition to Eq.(3.3) for $N = 1$ and using a technic in appendix B, we get,

$$\frac{\partial V}{\partial m^2} = \frac{1}{2}\bar{\phi}^2 + \frac{1}{4\pi i}\int_{-i\infty+\epsilon}^{+i\infty+\epsilon} dp_0 \int \frac{d^3\boldsymbol{p}}{(2\pi)^3}\frac{1}{-p_0^2+\boldsymbol{p}^2+m^2+\frac{\lambda}{2}\bar{\phi}^2+\Pi}\frac{1}{e^{\beta p_0}-1}$$

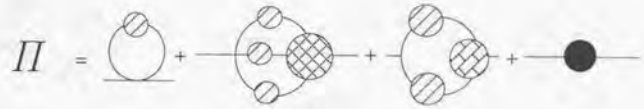

Figure 4.5: 1 PI self-energy graphs of Π. The line with the *striped blob* represents the full propagator. The *circle with a net* expresses the full 4-point vertex (the second term on the RHS). The *circle with bricks* represents the full 3-point vertex (the third term on the RHS). The *black blob* represents the counter term (the fourth term on the RHS).

$$\begin{aligned}
&+\frac{1}{4\pi i}\int_{-i\infty}^{+i\infty} dp_0 \int \frac{d^3\boldsymbol{p}}{(2\pi)^3}\frac{1}{-p_0^2+\boldsymbol{p}^2+m^2+\frac{\lambda}{2}\bar{\phi}^2+\Pi} \\
&+(Z_m Z_\phi - 1)\Big[\frac{1}{2}\bar{\phi}^2 \\
&+\frac{1}{4\pi i}\int_{-i\infty+\epsilon}^{+i\infty+\epsilon} dp_0 \int \frac{d^3\boldsymbol{p}}{(2\pi)^3}\frac{1}{-p_0^2+\boldsymbol{p}^2+m^2+\frac{\lambda}{2}\bar{\phi}^2+\Pi}\frac{1}{e^{\beta p_0}-1} \\
&+\frac{1}{4\pi i}\int_{-i\infty}^{+i\infty} dp_0 \int \frac{d^3\boldsymbol{p}}{(2\pi)^3}\frac{1}{-p_0^2+\boldsymbol{p}^2+m^2+\frac{\lambda}{2}\bar{\phi}^2+\Pi}\Big],
\end{aligned} \tag{4.12}$$

where $\Pi = \Pi(\boldsymbol{p}^2, -p_0^2, \bar{\phi}, m^2, \tau)$ is the sum of all the one particle irreducible (1PI) self-energy graphs. The first term of Eq. (4.12) is the simple background field contribution. The second term gives the finite temperature contribution. The third term expresses the effect which remains finite at zero temperature. The last term is the counter term contribution. The factors, Z_m and Z_ϕ, represent renormalization constants for the mass and the field respectively. In the following we ignore the third and fourth terms in Eq.(4.12), assuming that only the first two terms are important in regard to the phase transition [43]. Due to this approximation, we neglect the loop contribution remaining finite at $T = 0$. These contributions are usually small around the critical temperature since their contribution to the effective potential is $\sim \frac{m_T^4}{64\pi^2}\log\frac{m_T^2}{M_R^2}$ and $\frac{m_T}{T}$ is small around the critical temperature [43].

The function Π is expressed by the full propagator, the full three and the

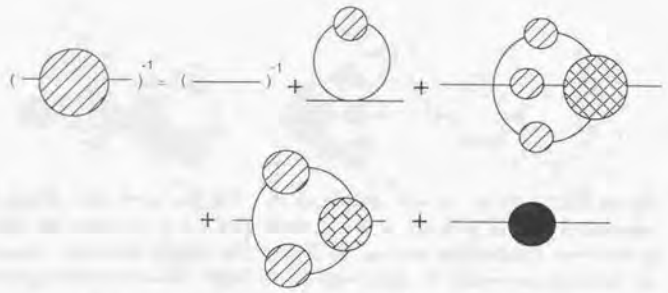

Figure 4.6: Schwinger-Dyson equation for the full propagator in $\lambda\phi^4$ theory. The symbols are the same as in Fig.4.5.

full four point functions (Fig.4.5) according to the Schwinger-Dyson equation. The Schwinger-Dyson equation expresses the inverse of the full propagator by the relation expressed by Fig.4.6. On the right-hand side of Fig.4.5, the first and the fourth terms are independent of the external momentum, and the second and the third terms depend on them. Since we only sum up all the super daisy diagrams in the present section, we retain only the momentum independent term (the first and fourth term in Fig.4.5). We stress that the effective potential consists of all the super-daisy diagrams without over-counting by this approximation. In this approximation, we have relation (see Fig.4.7),

$$\Pi = \lambda(\frac{\partial V}{\partial m^2} - \frac{1}{2}\bar{\phi}^2). \tag{4.13}$$

Using relation (4.13) and integrating Eq.(4.12) over p_0 [1, 22, 56][2], we obtain the evolution equation, which sums up all the super daisy diagrams,

$$\frac{\partial V}{\partial m^2} = \frac{1}{2}\bar{\phi}^2 + \frac{1}{2\pi^2}\int_0^\infty dp \frac{p^2}{2\sqrt{p^2 + m^2 + \lambda\frac{\partial V}{\partial m^2}}}$$

[2]Similar technic is used in Appendix B. In this case, the singularity is not a cut but a pole.

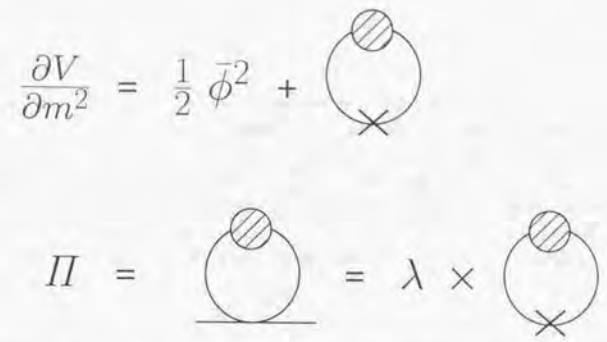

Figure 4.7: The relation between the self-energy Π and the derivative of the effective potential V with respect to the mass squared in the super daisy approximation. (See the first two terms of Eq.(4.12).)

$$\times \frac{1}{\exp\left(\frac{1}{T}\sqrt{p^2 + m^2 + \lambda\frac{\partial V}{\partial m^2}}\right) - 1}. \tag{4.14}$$

We next calculate the effective potential at the true mass using an identity,

$$V(m^2 = -\mu^2) = V(m^2 = M^2) + \int_{M^2}^{-\mu^2} \frac{\partial V}{\partial m^2} dm^2. \tag{4.15}$$

We set the initial mass M as large as T so that we can evaluate the effective potential, $V(m^2 = M^2)$, reliably by the perturbation theory. We use the one loop effective potential[3] as the initial condition and omit the zero temperature contribution as we did in the evolution equation,

$$V(m^2 = M^2) = \frac{1}{2}M^2\bar{\phi}^2 + \frac{\lambda}{4!}\bar{\phi}^4$$

[3]Strictly speaking, we should sum up the all the super daisy graphs in calculating the initial effective potential. The difference between one loop effective potential and the super daisy effective potential is, however, numerically small thanks to the auxiliary mass. We, therefore, use the one loop effective potential as the initial condition.

$$+\frac{T^2}{2\pi^2}\int_0^\infty dp/p^2 \log\left[1-\exp\left(-\frac{1}{T}\sqrt{p^2+M^2+\frac{\lambda}{2}\bar{\phi}^2}\right)\right]. \tag{4.16}$$

We do not perform the ring resummation method in calculating this since we need not to do it thanks to the large auxiliary mass.

The integral in the evolution equation (4.14) is well-defined when the effective mass squared, $m^2+\lambda\frac{\partial V}{\partial m^2}$, is real and positive. Below the critical temperature, however, the effective mass squared can be negative or complex. We need an analytic continuation of the integral in Eq.(4.14). To make the analytic continuation, we change the variable of integration p to z as,

$$z=\sqrt{\frac{p^2}{T^2}+Z^2}-Z. \tag{4.17}$$

This change of variable allows us rewrite Eq.(4.14) as,

$$\frac{\partial V}{\partial m^2}=\frac{1}{2}\bar{\phi}^2+\frac{T^2}{4\pi^2}\int_0^\infty dz\frac{\sqrt{z(z+2Z)}}{e^{z+Z}-1}, \tag{4.18}$$

where $Z=\frac{1}{T}\sqrt{m^2+\lambda\frac{\partial V}{\partial m^2}}$. This equation is equivalent to Eq.(4.14) for $Z>0$ and calculable for $Z<0$. It is ,therefore, the analytic continuation of Eq.(4.14) for $Z<0$. To find $\partial V/\partial m^2$ we solve Eq.(4.18). This equation is double valued. We choose the branch as the following criterion.

As is well-known, the effective potential becomes complex at small $\bar{\phi}$ below the critical temperature. This indicates the instability of the state, and the imaginary part of the effective potential is interpreted as being related to the decay rate of the state [57]. The imaginary part arises from the integral of the evolution equation in our method (see Eq.(4.18)). It is natural to suppose that the imaginary part of the effective potential is negative in order to interpret it as representing the decay rate. We therefore choose the branch of Eq.4.18 so that the imaginary part be negative.

We solved the Eq.(4.16) numerically. Let us show the numerical results. For the graphs in Fig.(4.8) $\sim$ (4.10) we set[4] the four-point coupling as $\lambda=1$. We show the real part of the effective potential around the critical temperature in Fig.4.8. We observe a small barrier between the symmetric vacuum

[4]We varied the value of λ and found no qualitative change.

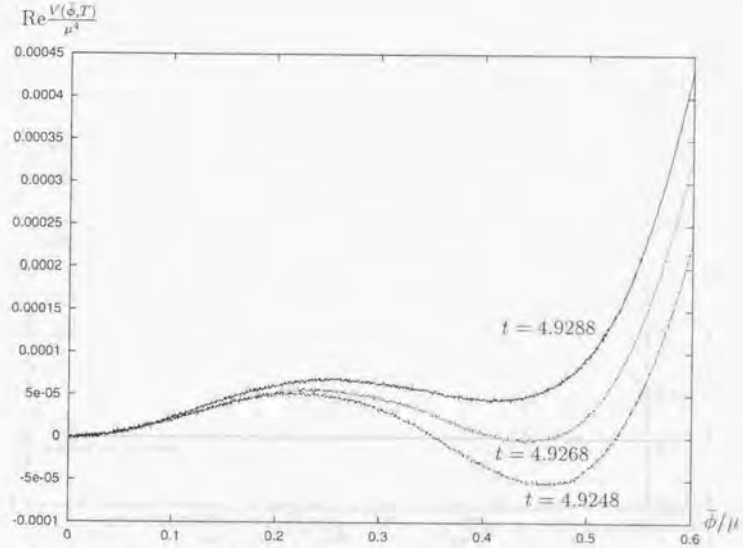

Figure 4.8: Real part of the effective potential at $T=\mu t$. We see a small barrier to indicate a first order phase transition.

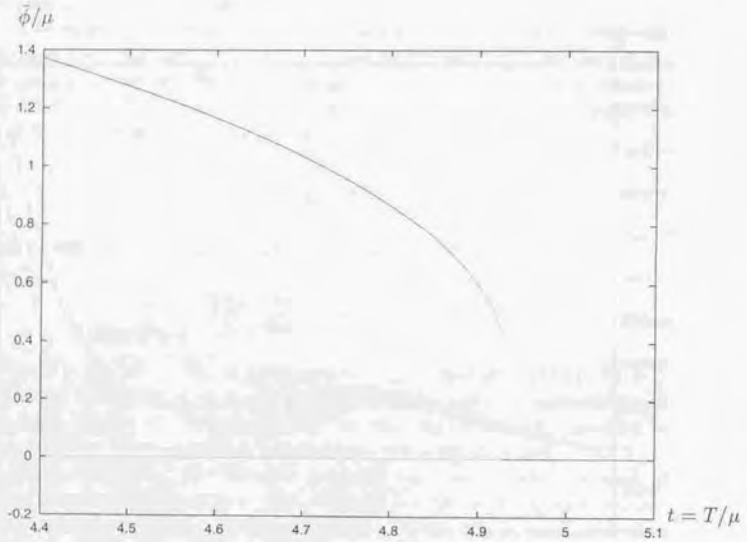

Figure 4.9: The field expectation value near the critical temperature at the stable point. We see a finite jump of $\bar{\phi}/\mu$ at $t = 4.93\mu$ to indicate a first order phase transition.

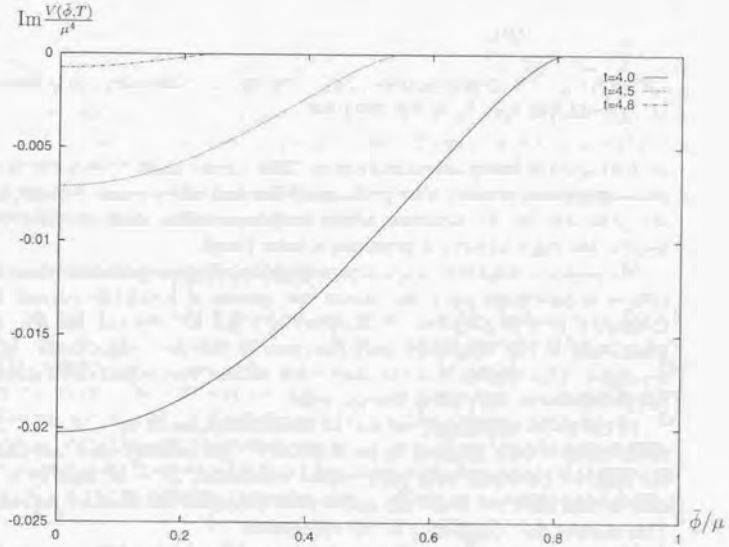

Figure 4.10: Imaginary part of the effective potential at $T = \mu t$. We see that as $\bar{\phi}/\mu$ becomes smaller, the larger the imaginary part becomes larger.

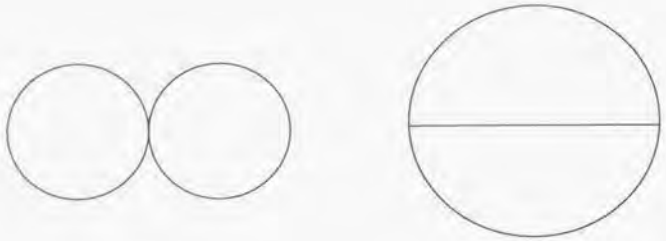

(a) (b)

Figure 4.11: Two loop diagrams which contribute to the effective potential. (a) is daisy-like and (b) is not daisy-like.

($\bar{\phi} = 0$) and the broken vacuum ($\bar{\phi} \neq 0$). This clearly shows that a first order phase transition occurs. The presence of the first order phase transition is also indicated by the behavior of the field expectation value at the stable point since Fig.4.9 shows it possesses a finite jump.

We obtain a negative imaginary part of the effective potential below the critical temperature since we choose the branch of Eq.(4.18) so that the imaginary part be negative. It is shown in Fig.4.10. We can see that the magnitude of the imaginary part increases as the field expectation value decreases. This implies that the state with smaller field expectation value is less stable below the critical temperature.

In the above discussion, we set the initial condition at $m = M = T$. The initial mass is only required to be of order T. We actually have calculated the effective potential with other initial conditions, $M = 2T$ and $M = \frac{T}{2}$, and we then have not found any appreciable change of the effective potential. This ensures the consistency of our calculation.

Now we compare our method with other approach, the CJT method [36]. One can also gather up the super-daisy graphs without over-counting by this method. It is carried out by truncating the CJT expansion at $O(\lambda)$, that is, taking into account only Fig.4.11 (a). A first order phase transition is also indicated in this model with the CJT method [37]. This is consistent with our result. Though both methods can sum up super daisy diagrams without over-counting, there are several different points. First, we do not use a high-temperature approximation. Second, we calculate both the imaginary and real parts of the effective potential below the critical temperature. Third, we

can make another approximation which cannot be made by the CJT method as we will see in the next section.

Though the phase transition of the Z_2-invariant scalar mode is of second order [13], the super daisy approximation indicates the first order phase transition. The result obtained by the super daisy approximation is not good even qualitatively. We think the reason by comparing with the case of the perturbation theory. In the perturbation theory, the effective potential indicates a first order phase transition at the one loop level [50]. There are two graphs at two loop level (see Fig.4.11). If one includes the contribution of Fig.4.11(a) alone [50], the phase transition is still indicated to be of first order [5]. A second order phase transition is indicated when the contributions both of Fig.4.11(a) and Fig.4.11(b) are included [6]. From this, we expect that the contribution of Fig.4.11(b), which is not daisy-like, plays an important role in determining the effective potential. We next try the other approximation to take into these non-daisy type contributions.

Local potential approximation

In the super daisy approximation, we retain only the first term in Fig.4.5. We use the other approximation, "*local potential approximation*"[7] , here. This approximation can take into account all the graphs in Fig.4.5. The graphs except the first one are, however, taken into account approximately. The second and third diagrams depend on the external momentum. We approximate the external momentum to be zero. Since the effective potential is a generating function of n-point functions with zero external momentum, neglect of the momentum dependence in Π allows us to replace as follows in Eq.(4.12),

$$m^2 + \frac{\lambda}{2}\bar{\phi}^2 + \Pi(0, 0, \bar{\phi}, m^2, T) \to \frac{\partial^2 V}{\partial \bar{\phi}^2}. \tag{4.19}$$

We can take into account the super daisy diagrams correctly in this approximation since they are produced by momentum-independent parts of Π.

[5] In Ref.[50] only Fig.4.11(a) was included.

[6] The author of Ref.[51] calculated the effective potential including both Fig.4.11(a) and Fig.4.11(b). They did not, however, investigate the 2-loop result in detail since their purpose is not to do it. We calculated the expectation value of the field using their effective potential and found the phase transition to be of second order.

[7] This terminology is used in Wilsonian renormalization group. [58, 59]

Besides, we can take into account contributions of other graphs approximately. We obtain a partial differential equation for the effective potential by integrating over p_0 and the angle variables in Eq.(4.12),

$$\frac{\partial V}{\partial m^2} = \frac{1}{2}\bar{\phi}^2 + \frac{1}{4\pi^2}\int_0^\infty dp p^2 \frac{1}{\sqrt{p^2 + \frac{\partial^2 V}{\partial \bar{\phi}^2}}\exp\left(\frac{1}{T}\sqrt{p^2 + \frac{\partial^2 V}{\partial \bar{\phi}^2}}\right) - 1}. \quad (4.20)$$

All what we should do to obtain the effective potential at the true mass is to solve this equation from the initial condition Eq.(4.16) to the true mass. We note that this equation is corresponding to the leading approximation of the derivative expansion of the effective action as we will see in Ch.6.

Since Eq.(4.20) is complicated non-linear partial differential equation, we solve it numerically. The numerical method is shown in the Appendix.C. The real parts of the effective potentials for various temperatures are shown in Fig.4.12. A stable field expectation value $\bar{\phi}_c$, where the effective potential has its minimum, comes to be zero smoothly as the temperature increases. This indicates that second order phase transition takes place in this model. The imaginary part of the effective potential below the critical temperature is shown in Fig.4.13. One can observe that it increases as a field expectation value decreases; this illustrates that the state with smaller field expectation value is less stable below the critical temperature. The critical temperature as a function of the coupling constant λ is shown in Fig.4.14. This shows a similar behavior to the leading result obtained in Ref.[23], but has a slight difference ($\sim 2\%$)[8]. We next determine some critical exponents, β, δ, γ , and α, since we observe a second order phase transition. The amplitude ratio $\frac{\chi_+}{\chi_-}$ is also determined. The results are summarized in table.4.1.

First, we pay attention to the location of the stable point $\bar{\phi}_c$. We show $\bar{\phi}_c$ as a function of the reduced temperature, $\tau \equiv \frac{T-T_c}{T_c}$, in Fig.4.15. It decreases monotonically and vanishes smoothly as temperature increases. We then focus on its behaviour near the critical temperature T_c to determine one of the critical exponents β, which relates the order parameter to the reduced temperature near T,

$$\phi_c \propto \tau^\beta \quad (\tau \sim 0,\ T < T_c). \quad (4.21)$$

[8]This critical temperature is determined by the condition that the mass at the finite temperature vanishes.

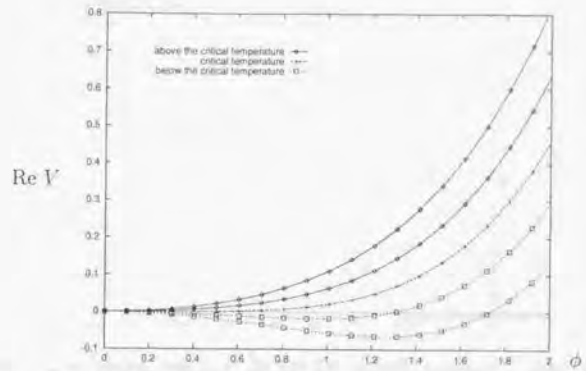

Figure 4.12: The real part of the effective potential ($\lambda = 1$). The values of the origin are set to zero. A stable point come to be zero smoothly as temperature increases. This indicates the phase transition is of second order.

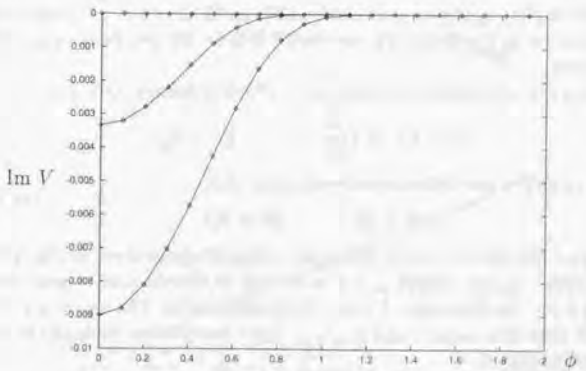

Figure 4.13: The imaginary part of the effective potential ($\lambda = 1$). The magnitude, which shows the instability of the state, increases as a field expectation value decreases.

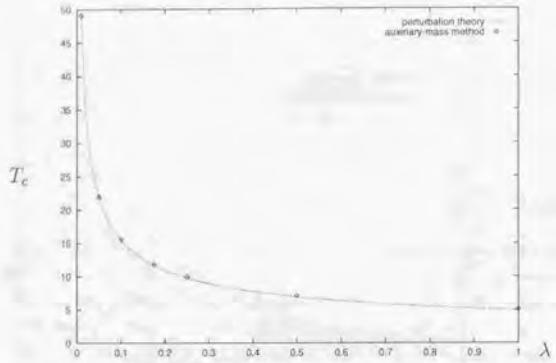

Figure 4.14: The phase diagram of the Z_2 invariant scalar theory. Second-order phase transition is observed on the boundary. The dots represent values calculated using auxiliary-mass method. The dotted line represents the result of the perturbation theory at the leading approximation.

We plot $\log(\bar{\phi}_c)$ against $\log(\tau)$ in Fig.4.16; we fit the data to a linear function and draw it in Fig.4.16. We determine β from the gradient of it. We find $\beta = 0.385$.

We next determine the exponent δ, which is defined as follows,

$$\bar{\phi} \propto J^{1/\delta} = (\frac{\partial V}{\partial \bar{\phi}})^{1/\delta} \qquad (T = T_c). \tag{4.22}$$

One can derive the following relation from this,

$$V \propto \bar{\phi}^{\delta+1} \qquad (T = T_c). \tag{4.23}$$

We show the effective potential at the critical temperature in Fig.4.17. We plot $\log(V)$ against $\log(\bar{\phi})$ in Fig.4.18. We fit the data to a linear function in Fig.4.18. We determine δ from the gradient of it. The result is $\delta = 4.0$

We then determine γ and χ_-/χ_+. They are defined through the susceptibility as follows,

$$\chi \equiv \left.\frac{\partial \bar{\phi}}{\partial J}\right|_{J=0} \sim \chi_+ \tau^{-\gamma^+} \qquad (\tau \sim 0, T > T_c), \tag{4.24}$$

$$\chi \equiv \left.\frac{\partial \bar{\phi}}{\partial J}\right|_{J=0} \sim \chi_- \tau^{-\gamma^-} \qquad (\tau \sim 0, T < T_c). \tag{4.25}$$

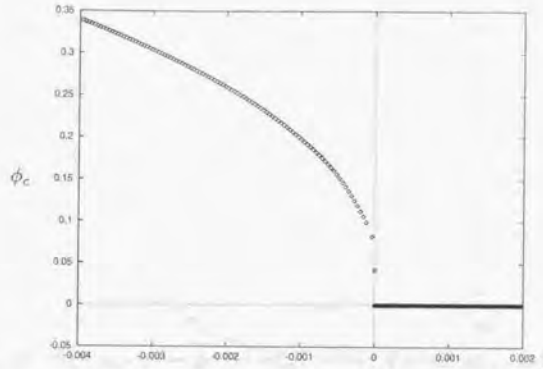

Figure 4.15: Stable field expectation value as a function of the reduced temperature ($\lambda = 1$). It decreases monotonically and vanishes smoothly as temperature increases.

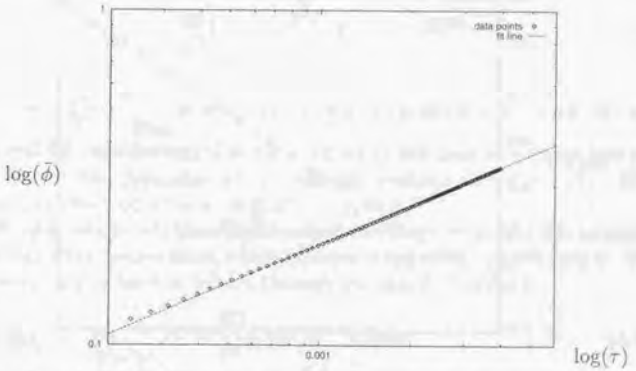

Figure 4.16: Plots of $\log(\bar{\phi}) - \log(\tau)$ ($\lambda = 1$). The data are fit by linear function. Using its gradient, β is determined.

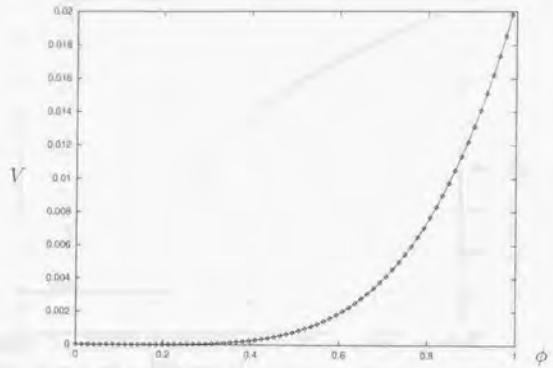

Figure 4.17: The effective potential at the critical temperature ($\lambda = 1$).

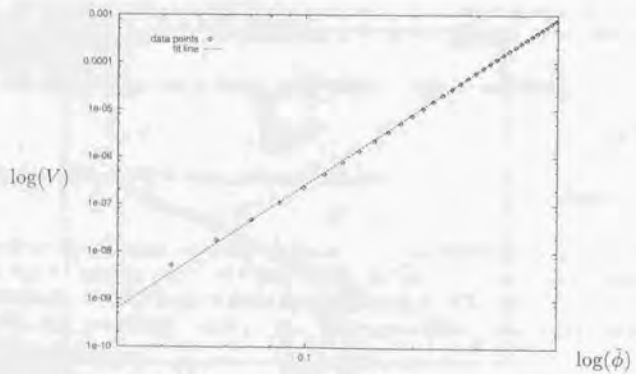

Figure 4.18: Plots of $\log(V) - \log(\tilde{\phi})$ ($\lambda = 1$). The data are fit by linear function. Using its gradient, δ is determined.

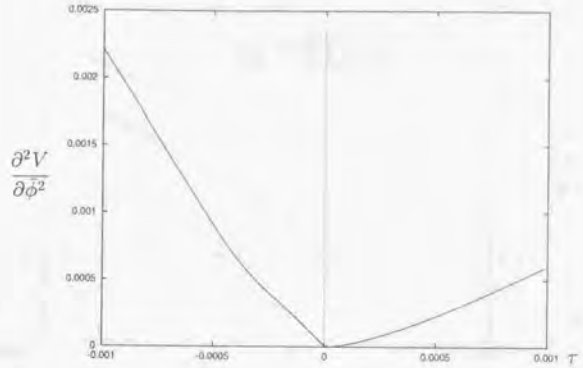

Figure 4.19: The curvature at the stable point, $\frac{\partial^2 V}{\partial \tilde{\phi}^2}$, as temperature varies ($\lambda = 1$).

To calculate χ, we relate χ to the curvature using the following identity derived from the definition of the effective potential,

$$\left.\frac{\partial \tilde{\phi}}{\partial J}\right|_{J=0} = \left(\frac{\partial^2 V}{\partial \tilde{\phi}^2}\right)^{-1}\Bigg|_{\tilde{\phi}=\tilde{\phi}_c}. \tag{4.26}$$

We show $\left(\frac{\partial^2 V}{\partial \tilde{\phi}^2}\right)^{-1}\Big|_{\tilde{\phi}=\tilde{\phi}_c}$ as a function of the temperature in Fig.4.19. We also plot $\log(\frac{\partial^2 V}{\partial \tilde{\phi}^2})$ against $\log(\tau)$ in Fig.4.20; we fit the data to a linear function in Fig.4.20. We determine γ^+, γ^- from the gradient of it and χ_-/χ_+ from intercepts. We find $\gamma^+ = \gamma^- = 1.37, \chi_-/\chi_+ = 3.4$

Finally, we pay attention to the second derivative of the effective potential with respect to temperature, which is proportional to the specific heat C. The exponent α is defined as follows through the specific heat[9],

$$C \propto \frac{\partial^2 V}{\partial \tau^2} \propto \tau^{-\alpha} \quad (\tau \sim 0). \tag{4.27}$$

This derivative is shown in Fig.4.21 as a function of the temperature. We determine α using this. The result is $\alpha = 0.12$.

[9]Though the amplitude ratio of the specific heat can also be defined, it is not determined because of the numerical reason.

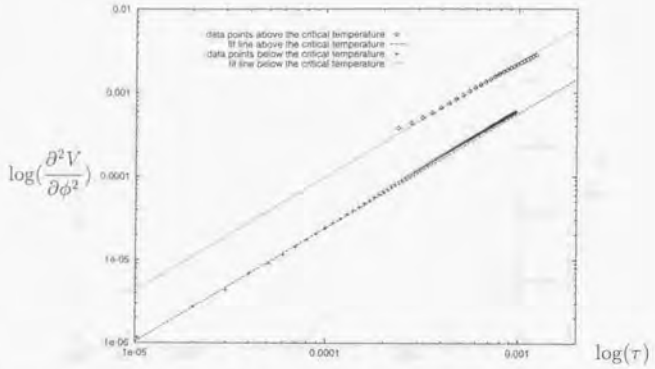

Figure 4.20: Plots of $\log(\frac{\partial^2 V}{\partial \phi^2}) - \log(\tau)$ ($\lambda = 1$). The data are fit by linear function. We determine γ from their gradients and χ_-/χ_+ from their intercepts.

The results are summarized in table.4.1 and compared with results obtained by various methods. In the present section, the critical exponents and the amplitude ratio were determined using the auxiliary-mass method by the numerical method in the appendix.C. The results are summarized in table.4.1. We found that the phase transition of the Z_2-invariant scalar theory is indicated to be of second order as it should be. Though the critical exponents calculated here do not satisfy the scaling rules, they satisfy the inequalities of critical exponents. For example, inequalities given by Griffiths [62],

$$\gamma^- \geq \beta(\delta - 1), \tag{4.28}$$

$$\gamma^+(\delta + 1) \geq (2 - \alpha)(\delta - 1) \tag{4.29}$$

are satisfied. In the following, we compare our result with other methods.

First, the results are compared with the values obtained by the perturbative finite-temperature field theory with daisy resummation. Since first order phase transition is indicated at one loop level [51, 50], the critical exponents can not be determined by the perturbation theory. At two loop level, second order phase transition is observed and the critical exponents are de-

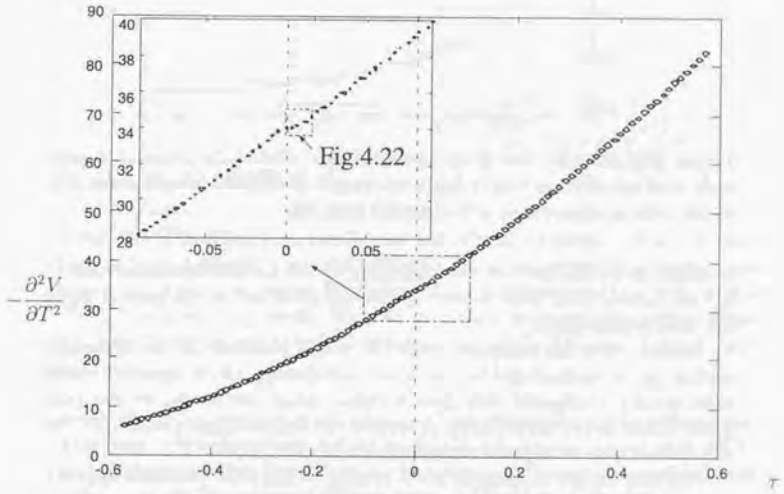

Figure 4.21: The second derivative of the effective potential with respect to temperature. ($\lambda = 1$).

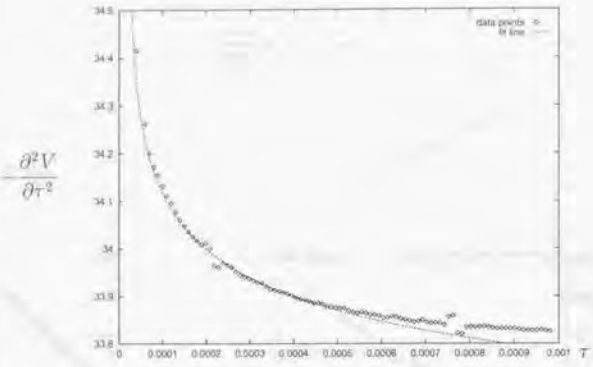

Figure 4.22: Specific heat C as a function of τ around the critical temperature. One can observe that it blows up around the critical temperature. One of the critical exponent α is determined from this.

termined to be the same as those obtained by the Landau approximation [10]. In comparison with these values, the results obtained in the present paper are considerably good.

Second, they are compared with the values obtained by the renormalization group method and by the lattice simulation, which agree with each other greatly. Compared with these accurate values, our results are not quite good. These errors are probably caused by the replacement in Eq.(4.19). We will discuss how to improve the approximation in Ch.6.

Anyway, we get reasonably good results by the local potential approximation using the finite temperature field theory both qualitatively and quantitatively. We, therefore, investigate the other models by the approximation in the remaining of the present paper.

4.2 The O(N)-invariant scalar model

In the present section, we investigate the O(N)-invariant scalar model by the auxiliary mass method with the local potential approximation. Phase transition of the O(N)-invariant scalar model at high temperature is very important since many physical systems belong to the same universality class as it: critical liquid-vapor phase transition (N=1), alloy (e.g. β-brass) phase transition (N=1), uniaxial ferromagnet phase transition (N=1), superfluid phase transition (N=2), ferromagnet phase transition (N=3), and chiral phase transition with two flavor massless quarks (N=4) [13, 63].

Applying this method to the O(N)-invariant scalar model, the Euclidean Lagrangian density is given by the following,

$$\mathcal{L}_E = -\frac{1}{2}\left(\frac{\partial\phi_a}{\partial\tau}\right)^2 - \frac{1}{2}(\boldsymbol{\nabla}\phi_a)^2 - \frac{1}{2}m^2\phi_a^2 - \frac{\lambda}{4!}(\phi_a^2)^2 + J_a\phi_a + c.t. \ , \quad (a = 1, 2, \cdots N) \quad (4.30)$$

Here, J_a are external source functions and the index. We assume that the coupling constant, λ is small and therefore the perturbation theory at zero

[10] We used the two-loop order effective potential calculated in [51]. We determined the critical exponents from this both numerically and analytically.

				γ	ν	β	α	δ	η	χ_+/χ_-
F-T	auxiliary-mass method			1.37		0.385	0.12	4.0		3.4
	perturbation theory	1-loop		*	*	*	*	*	*	*
		2-loop		1.0	0.5	0.5	0.0	3.0	0.0	2.0
R-G	perturbation theory[61]	fixed dim.		1.24	0.630	0.325	0.11	4.82	0.317	4.82
		ϵ-exp.		1.24	0.631	0.327	0.11	4.79	0.349	4.70
	non -perturbative	sharp cut off [58]		1.38	0.69	0.345		5.0	0.0	
		smooth cut off [59]	∂^0	1.32	0.66	0.33		5.0	0.0	
			∂^2	1.20	0.628	0.32		4.69	0.054	
lattice Monte Carlo [60]					0.629				0.027	
experiment [61]		binary fluids		1.236	0.625	0.325	0.112			4.3
		liquid-vapor		1.24	0.625	0.316	0.107			5.0
		antiferromagnets		1.25	0.64	0.328	0.112			4.9
Landau approximation				1.0	0.5	0.5	0.0	3.0	0.0	2.0

Table 4.1: The critical exponents and the critical amplitude ratio obtained from various methods. Since the first order phase transition is indicated, the critical exponents can not be determined using finite-temperature field theory (F-T) within one-loop order. We note that there are many non-perturbative methods based on the renormalization group (R-G) idea which we do not refer here.

temperature is reliable. We first calculate the effective potential with auxiliary large mass $m = M(\sim T)$ at the one-loop level as,

$$V = \frac{1}{2}M^2\bar{\phi}^2 + \frac{\lambda}{4!}\bar{\phi}^4 + \frac{T}{2\pi^2}\int_0^\infty dr\ r^2 \log\left[1 - \exp\left(-\frac{1}{T}\sqrt{r^2 + M^2 + \frac{\lambda}{2}\bar{\phi}^2}\right)\right] + (N-1)\ \frac{T}{2\pi^2}\int_0^\infty dr\ r^2 \log\left[1 - \exp\left(-\frac{1}{T}\sqrt{r^2 + M^2 + \frac{\lambda}{6}\bar{\phi}^2}\right)\right]. \quad (4.31)$$

Here $\bar{\phi}$ is a field expectation value. The last term in this equation is a contribution from the NG-modes. We keep only the finite-temperature part of the effective potential here, too. We note that the daisy-resummation is not necessary because of the large mass. We then construct a non-perturbative evolution equation which connects the effective potential at an auxiliary large mass squared, $m^2 \sim T^2$, and that of the true mass squared, $m^2 = -\mu^2$.

We then derive the evolution equation for the O(N)-invariant scalar model. From Eq.(3.3) and the definition of the effective potential,

$$-\frac{\Omega}{T}V(\bar{\phi}) = \Gamma_T(\bar{\phi}^2(x))\Big|_{\phi_a(x)=\bar{\phi}_a=const}, \quad (4.32)$$

we obtain the evolution equation,

$$\frac{\partial V}{\partial m^2} = \frac{1}{2}\bar{\phi}^2 + \frac{1}{4\pi i}\int_{-i\infty+\epsilon}^{+i\infty+\epsilon} dp_0 \int \frac{d^3\boldsymbol{p}}{(2\pi)^3} \frac{1}{-p_0^2 + \boldsymbol{p}^2 + m^2 + \frac{\lambda}{2}\bar{\phi}^2 + \Pi_{Sig}} \frac{1}{e^{\frac{p_0}{T}} - 1} + \frac{N-1}{4\pi i}\int_{-i\infty+\epsilon}^{+i\infty+\epsilon} dp_0 \int \frac{d^3\boldsymbol{p}}{(2\pi)^3} \frac{1}{-p_0^2 + \boldsymbol{p}^2 + m^2 + \frac{\lambda}{6}\bar{\phi}^2 + \Pi_{NG}} \frac{1}{e^{\frac{p_0}{T}} - 1}. \quad (4.33)$$

Here $\Pi_{Sig} = \Pi_{Sig}(m^2, \bar{\phi}^2, p_0^2, \mathbf{p}^2, T)$ and $\Pi_{NG} = \Pi_{NG}(m^2, \bar{\phi}^2, p_0^2, \mathbf{p}^2, T)$ are the full self-energy for massive and massless mode in the broken phase respectively. We also use the local potential approximation here, too. we generalize Eq.(4.19) as follows,

$$m^2 + \frac{\lambda}{2}\bar{\phi}^2 + \Pi_{Sig}(0, 0, \bar{\phi}, m^2, \tau) \to \frac{\partial^2 V}{\partial \bar{\phi}^2}$$
$$m^2 + \frac{\lambda}{6}\bar{\phi}^2 + \Pi_{NG}(0, 0, \bar{\phi}, m^2, \tau) \to \frac{1}{\bar{\phi}}\frac{\partial V}{\partial \bar{\phi}}. \quad (4.34)$$

This replacement corresponds to fixing an external momentum of the full self-energy to zero. It allows us to convert Eq.(4.33) to the following partial differential equation,

$$\frac{\partial V}{\partial m^2} = \frac{1}{2}\bar{\phi}^2 + \frac{1}{4\pi^2}\int_0^\infty dp\ p^2 \frac{1}{\sqrt{p^2 + \frac{\partial^2 V}{\partial \bar{\phi}^2}}} \frac{1}{\exp\left(\frac{1}{T}\sqrt{p^2 + \frac{\partial^2 V}{\partial \bar{\phi}^2}}\right) - 1} + \frac{N-1}{4\pi^2}\int_0^\infty dp\ p^2 \frac{1}{\sqrt{p^2 + \frac{1}{\bar{\phi}}\frac{\partial V}{\partial \bar{\phi}}}} \frac{1}{\exp\left(\frac{1}{T}\sqrt{p^2 + \frac{1}{\bar{\phi}}\frac{\partial V}{\partial \bar{\phi}}}\right) - 1}. \quad (4.35)$$

The last term of this evolution equation is a contribution from the NG-mode. All we must do to calculate the effective potential is solving the evolution equation Eq.(4.35) from the initial condition, Eq.(4.31), to the true mass squared, $m^2 = -\mu^2$. This partial differential equation is solved numerically.

We show the effective potential for N=4 around T_c in Fig.4.17. We show the stable point of this effective potential, $\bar{\phi}_c$, in Fig.4.24. We find that the phase transition is of second order from these figures. The same behaviour is found for the other values of N. This is consistent with the other analyses using the lattice field theory and the renormalization group method [13]. We find that the auxiliary-mass method deals with the problem of the infrared divergence well in this model, too.

The critical temperature is shown as a function of N in Fig.4.25. Though they resemble to the results of the perturbation theory at leading order [23], $T_c = 6\sqrt{\frac{2}{\lambda(N+2)}}$, which is determined from the condition that mass with the thermal one vanishes, they have slight differences quantitatively.

We next determine the critical exponents and study how well the auxiliary-mass method works. We first calculate one of the effective potential β. The critical exponent, β relates an order parameter, ϕ_c to a reduced temperature, $\tau \equiv \frac{T_c - T}{T_c}$ as follows,

$$\phi_c \propto \tau^\beta. \quad (4.36)$$

The order parameter ϕ_c as a function of the temperature τ is presented in Fig.4.24 for N=4. We plot ϕ_c as a function of τ in Fig.4.26 for various N in log-scale. These data appear to be well fit by a linear function with different

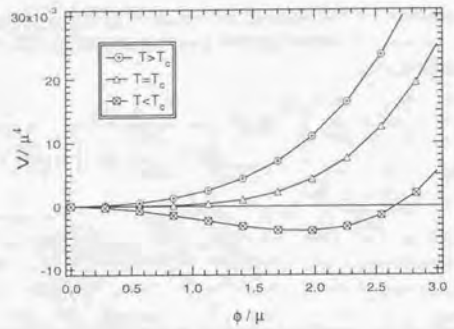

Figure 4.23: The effective potential obtained by the auxiliary-mass method ($N = 4, \lambda = 0.01$). Second-order phase transition occurs at the critical temperature. Similar behaviour is observed for other values of N and λ.

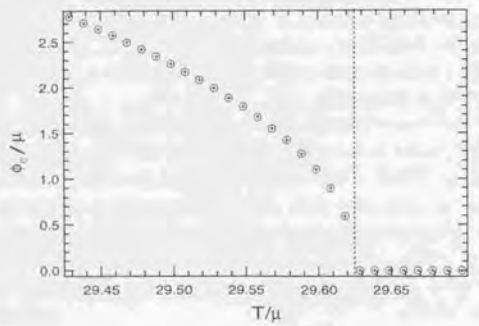

Figure 4.24: The stable field expectation value ϕ_c as a function of the temperature T ($\lambda = 0.01$). It decreases monotonically and vanishes smoothly near the critical temperature.

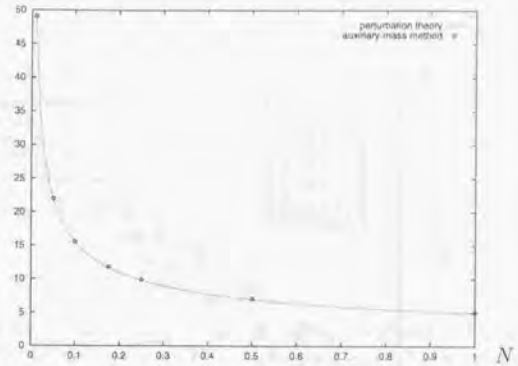

T_c/μ

Figure 4.25: The critical temperature as a function of N at $\lambda = 1$ ($\diamond$). This resembles to a result of the perturbation theory at leading order (—) but has a slight difference quantitatively.

gradients, which correspond to β for each N. The exponent, β is larger for larger values of N. We summarize the results in table 4.2.

We determine γ from a second derivative of the effective potential with respect to $\bar{\phi}$ at the origin. The critical exponent γ is defined as follows,

$$\chi \equiv \left.\frac{\partial\bar{\phi}}{\partial J_1}\right|_{J_a=0} \sim \chi\tau^{-\gamma} \quad (\tau = (T - T_c)/T_c) \tag{4.37}$$

the following identity then relates the second derivative to the susceptibility,

$$\left.\frac{\partial\bar{\phi}}{\partial J_1}\right|_{J_a=0} = \left.\left(\frac{\partial^2 V}{\partial\bar{\phi}^2}\right)^{-1}\right|_{\bar{\phi}=\phi_c}. \tag{4.38}$$

Here ϕ_c is determined from the condition, $\left.\frac{\partial V}{\partial\bar{\phi}}\right|_{\bar{\phi}=\phi_c} = 0$. The second derivative are shown in log-scale in Fig.4.27. We then determine the gradients, which correspond to γ. One can observe that they become steeper as N increases and therefore γ becomes larger for lager N. The results are $\gamma = 1.37$ ($N = 1$), 1.47 ($N = 2$), 1.60 ($N = 3$), 1.66 ($N = 4$). These results are summarized in table 4.2, compared with those obtained by the Landau approximation and most reliable values.

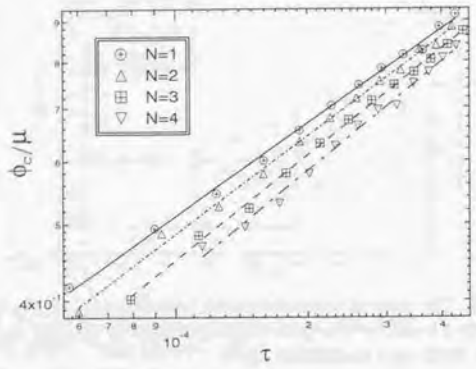

Figure 4.26: Log-scale plots of $\phi_c - \tau$ ($\lambda = 0.01$). The data are fit by linear functions with gradients corresponding to β for each N. We find that the exponent, β is larger for larger N.

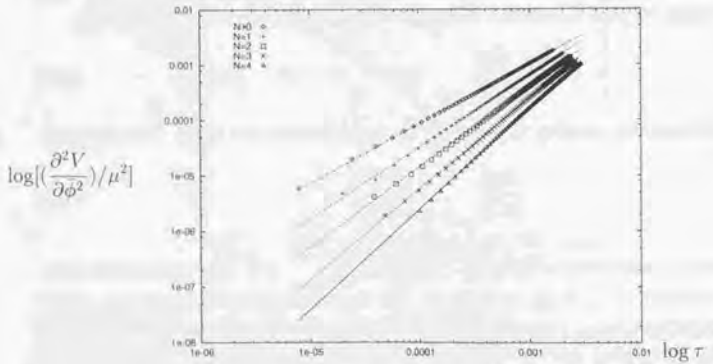

Figure 4.27: Second derivative of the effective potential with respect to ϕ. The gradients are steeper for larger N.

We determine δ using the effective potential at the critical temperature. The critical exponent δ is defined as follows.

$$\bar{\phi} \propto J_1^{1/\delta} = (\frac{\partial V}{\partial \bar{\phi}})^{1/\delta} \qquad (T = T_c). \tag{4.39}$$

The following relation, which derived from Eq.(4.39), enables us to determine δ from the effective potential at the critical temperature,

$$V \propto \bar{\phi}^{\delta+1} \qquad (T = T_c). \tag{4.40}$$

The effective potential at the critical temperature is shown in Fig.4.23. As we obtained γ, we determine δ. The results are $\delta = 4.0$ ($N = 1$), 4.2 ($N = 2$), 4.4 ($N = 3$), 4.4 ($N = 4$).

We summarize the results of the present section in table.4.2. The values of β, γ, δ are much better than the Landau approximation and the dependence on N is close to the most reliable value(MRV). There are, however, slight differences between our results and MRV which will be caused by an approximation in deriving Eq.(4.35).

In conclusion, we have investigated the O(N)-invariant scalar model using the auxiliary-mass method and have obtained good results both qualitatively and quantitatively. These results suggest that the auxiliary-mass method is an effective tool at finite temperature. Besides, we are able to investigate not only the second order phase transitions but also the first order phase transitions since the finite-temperature field theory is based only on the statistical principle. We, therefore, investigate gauge theories, which may have complicated phase structure, by the method in the next chapter.

Table 4.2: The critical exponents β, γ and δ obtained in a present paper and the previous paper. Those of Landau approximation (LA) and the most reliable values (MRV) are also summarized. We used the results of the six-loop approximation using the Padé-Borel resummation for the MRV here.

	β (LA,MRV)	γ (LA,MRV)	δ (LA,MRV)
N=1 [64]	0.39 (0.5, 0.327)	1.37 (1, 1.239)	4.0 (3, 4.8)
N=2 [64]	0.41 (0.5, 0.348)	1.47 (1, 1.315)	4.2 (3, 4.8)
N=3 [64]	0.44 (0.5, 0.366)	1.60 (1, 1.386)	4.4 (3, 4.8)
N=4 [64]	0.45 (0.5, 0.382)	1.66 (1, 1.449)	4.4 (3, 4.8)

Chapter 5

Auxiliary mass method in gauge theories

5.1 The abelian Higgs model

The phase transition of the Abelian Higgs Model is important since this model describes not only the Higgs mechanism in particle physics but also properties of superconductors and liquid crystals in condensed matter physics. In particle physics, a phase transition of an analogous theory, the electroweak phase transition, is investigated by many researchers [28, 40, 48, 65, 51, 66, 67, 68, 69, 70, 71] since it may account for the baryon number of the present universe [8]. We deal with this model in Sec.5.2. In condensed matter physics, B.I.Halperin, T.C.Lubensky and S.K.Ma investigated the phase transition in their pioneering work [72] as a model of *super-normal transition* of superconductors and *nematic—smectic-A transition* of liquid crystals. They used different methods to investigate the phase transition for the type-I superconductor ($\kappa \ll 1$) and the type-II superconductor ($\kappa \gg 1$). The Ginzburg-Landau parameter, κ is defined as a ratio of the London penetration depth λ_L to the coherent length, ξ of a scalar field, $\kappa \equiv \lambda_L/\xi$, which corresponds to a ratio of the scalar particle mass to gauge boson mass in the Abelian Higgs model. They showed that an effective potential around the critical temperature indicates a first order phase transition due to fluctuation of the gauge boson for $\kappa \ll 1$. They then showed that the phase transition is also of first order since the renormalization group flow of the model has no infrared

stable fixed points in 4-ϵ dimension. Lattice simulations, however, indicate that the phase transition is of first order for $\kappa \ll 1$ and of second order for $\kappa \gg 1$ [73, 74, 75, 76, 77, 78].[1] According to this result, the first order phase transition disappears at an end-point. Though many theoretical efforts based on the renormalization group were made to reveal the properties of the phase transition [79, 80, 81, 82, 83, 84, 85, 86, 87, 88, 89], we have not gotten conclusive answer to it yet. In experiments, a superconductor is a suitable material to investigate the phase transition though it is almost impossible to reach the narrow critical region of an ordinary superconductor. Fortunately, the critical region of a high-temperature superconductor is much broader than that of the ordinary one due to its small coherent length and high critical temperature [90]. Though some experiments are started using it [91, 92], they are still insufficient to determine an existence and a location of the end-point. On the other hand, many experiments were done using liquid crystals [93, 94, 95, 96, 97, 98, 99, 100, 101, 102, 103, 104, 105, 106, 107, 108, 109]. Most of them indicate that the end-point exists while a result of Ref.[105] indicates that there is no end-point; the phase transition is always of first order.

It is suitable to investigate the phase transition using the finite temperature field theory [18], which is based only on the statistical mechanics. However, its perturbation theory is often unreliable due to an infrared divergence in case a phase transition is of second order or of weakly first order as we showed in Ch.1 and Ch.2. According to the perturbation theory, the phase transition is of first order for any parameter region[110, 111, 112] though the result is unreliable for $\kappa \gg 1$. We do not have conclusive results to the properties of the phase transition in spite of other efforts: CJT method [38] and gap-equation method [41].

In the present section, we investigate the properties of the phase transition of the abelian Higgs model. The Lagrangian density of this model is the following,

$$\mathcal{L} = -\frac{1}{4}F^{\mu\nu}F_{\mu\nu} + |(\partial_\mu - iqA_\mu)\Phi|^2 - m^2|\Phi|^2 - \frac{\lambda}{3!}|\Phi|^4. \tag{5.1}$$

We take the true mass squared to be negative, $m^2 = -\mu^2$, in order to make a

[1] In a recent work Ref.[78], the authors pointed out that their simulation needs more data to distinguish between a second order phase transition and a more exotic one for cases $\kappa \gg 1$.

theory with spontaneous symmetry breaking(SSB) at zero-temperature. In this notation, G-L parameter is $\kappa = \sqrt{\frac{\lambda}{6q^2}}$. We first take the mass squared of the Higgs boson to be large positive, $m^2 = M^2(\sim T^2)$. We need not introduce the auxiliary mass to the gauge field since we have no 3- or 4-point self-interactions of the gauge field in the Abelian Higgs Model. We shall express the effective potential calculated using the Landau gauge in terms of $\phi = \sqrt{2}|\Phi|$,

$$\begin{aligned}
V(m^2 = M^2) &= \frac{M^2\phi^2}{2} + \frac{\lambda\phi^4}{24} \\
&\quad + J(m_1^2) + J(m_2^2) + 2J(m_A^2) + J(m_{AL}^2) \\
J(m^2) &\equiv \frac{T}{2\pi^2}\int_0^\infty dk\; k^2 \log\{1 - \exp(-\frac{\sqrt{k^2+m^2}}{T})\} \\
m_1^2 &= M^2 + \frac{\lambda}{2}\phi^2, m_2^2 = M^2 + \frac{\lambda}{6}\phi^2, \\
m_A^2 &= q^2\phi^2, m_{AL}^2 = q^2\phi^2 + \frac{q^2T^2}{3}.
\end{aligned} \tag{5.2}$$

This effective potential is reliable due to the auxiliary mass. The ring resummation is needed only for the gauge field.

We next construct an evolution equation which describes the change of an effective potential as the mass varies. Since we give the auxiliary mass only to the Higgs field, we have the same evolution equation as the O(2)-invariant scalar model,

$$\begin{aligned}
\frac{\partial V}{\partial m^2} &= \frac{1}{2}\bar{\phi}^2 + \frac{1}{4\pi^2}\int_0^\infty dp \frac{p^2}{\sqrt{p^2 + \frac{\partial^2 V}{\partial\phi^2}}} \frac{1}{e^{\frac{1}{T}\sqrt{p^2+\frac{\partial^2 V}{\partial\phi^2}}} - 1} \\
&\quad + \frac{1}{4\pi^2}\int_0^\infty dp \frac{p^2}{\sqrt{p^2 + \frac{1}{\phi}\frac{\partial V}{\partial\phi}}} \frac{1}{e^{\frac{1}{T}\sqrt{p^2+\frac{1}{\phi}\frac{\partial V}{\partial\phi}}} - 1}.
\end{aligned} \tag{5.3}$$

We numerically solve this equation to the true mass $m^2 = -\mu^2$ from the initial condition Eq.(5.2) in order to get the effective potential at the true mass. We show the results with initial mass, $M^2 = T^2$, since we need the auxiliary mass, which has the same or larger order of the temperature. We got the same results for $M^2 = 4T^2$ and $M^2 = T^2/4$. We use a mass unit, $\mu = 1$, below.

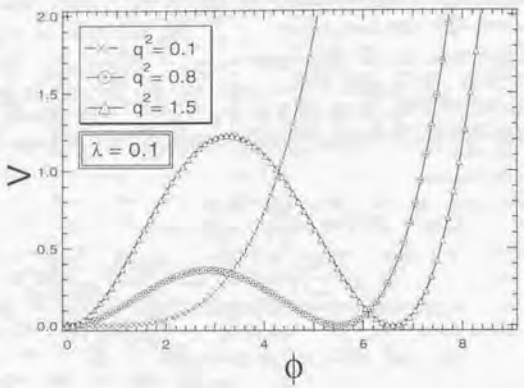

Figure 5.1: The effective potentials at the critical temperature for $\lambda = 0.1, q^2 = 0.1, 0.8, 1.5$. The first order phase transition becomes weaker for smaller values of the gauge coupling constant and disappears finally.

We show the effective potential at the critical temperature for various gauge coupling constants in Fig.5.1. The first order phase transition becomes weaker for smaller values of the gauge coupling constant and disappears finally. This indicates the existence of the end-point. The location of the end-point is clear in Fig.5.2, which shows a ratio of the critical field expectation value to the critical temperature as a function of gauge coupling constant. We observe that the results obtained by the auxiliary mass method and by the one-loop ring resummed perturbation theory are similar for larger values of the gauge coupling constant. This indicates that the perturbation theory is reliable only for strongly first order phase transition as we mentioned above. On the other hand, we show the ratio of the critical field expectation value to the critical temperature as a function of the scalar self-coupling constant for the fixed coupling constant $q^2 = 0.1$ in Fig.5.3. This figure also shows the existence of the end-point and the reliability of the perturbation theory for the strongly first order phase transition.

In order to get the phase diagram, we plot the ratio of the critical field

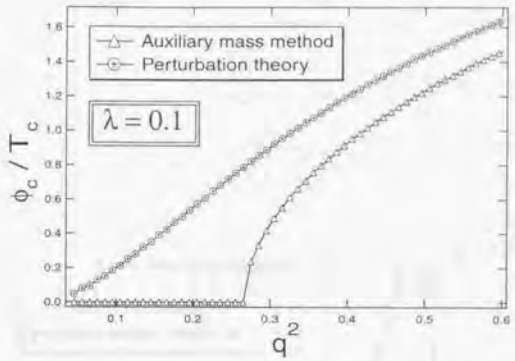

Figure 5.2: The ratio of the critical field expectation values to the critical temperature, ϕ_c/T_c, as a function of the gauge coupling constant q^2. The first order phase transition appears at $q^2 \sim 0.25$. The results obtained by the auxiliary mass method and the perturbation theory are similar for larger values of the gauge coupling constant.

expectation values to the critical temperature as a function of the scalar self-coupling constant and the gauge coupling constant in Fig.5.4. We observe that the phase transition is stronger for larger gauge coupling constant and for smaller scalar self-coupling constant. One can see that there is the boundary between the first order phase transition and the second order phase transition.

We show the phase diagram in Fig.5.5. The boundary between the first order phase transition and the second order phase transition is fit by $q^2 \propto \lambda^\zeta$ approximately. The value of ζ depends on the range of the scalar coupling constant λ. One can observe how well the boundary is fit by the function for various orders of the scalar coupling constant from Fig.5.6. We summarize the values of ζ in table.5.1. They are smaller for smaller scalar coupling constant.

In the present section, we investigated the phase transition of the Abelian Higgs Model using the auxiliary mass method at finite temperature. We found that there exists the end-point where the first order phase transition disappears. We fit the boundary of the first and the second order phase

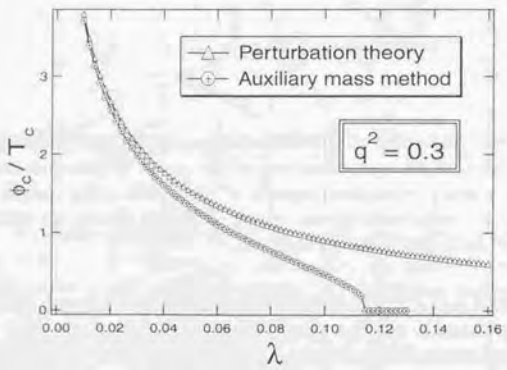

Figure 5.3: The ratio of the critical field expectation value to the critical temperature, ϕ_c/T_c as a function of the scalar coupling constant λ. The first order phase transition disappears at, $\lambda \sim 0.11$. The results obtained by the auxiliary mass method and the perturbation theory are similar for smaller value of scalar self-coupling constant.

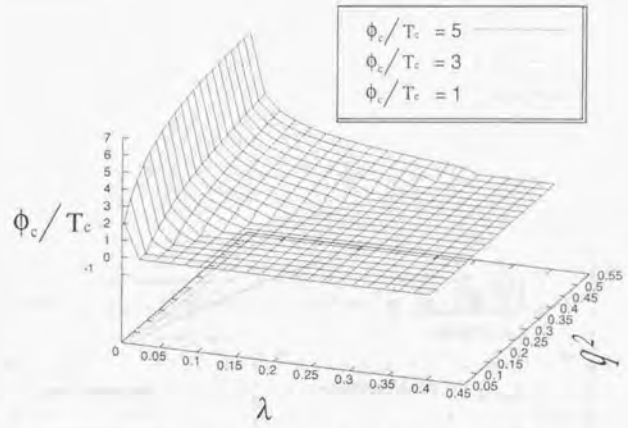

Figure 5.4: The ratio of the critical field expectation value to the critical temperature, ϕ_c/T_c as a function of the gauge coupling constant q^2 and the scalar self-coupling constant, λ. The phase transition is stronger for larger gauge coupling constant and for smaller scalar self-coupling constant.

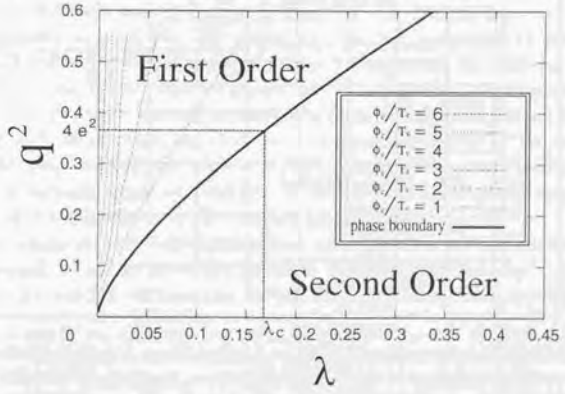

Figure 5.5: The phase diagram of the Abelian Higgs Model. Contours for various values of ϕ_c/T_c are shown. The end-point is $\lambda_c = 0.17$ for the case of superconductor, $q = 2e$.

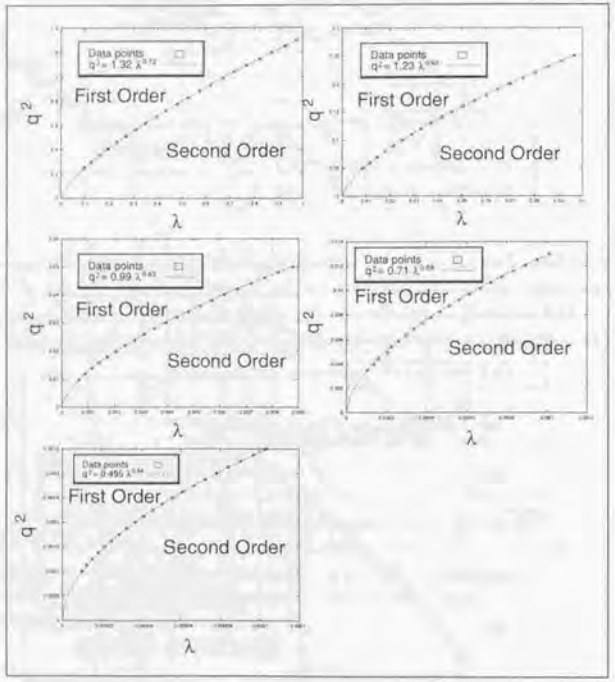

Figure 5.6: The phase diagram of the Abelian Higgs Model for various orders of the scalar coupling λ. The data are fit by a function, $q^2 \propto \lambda$.

λ	$0.1\sim 1$	$10^{-2} \sim 0.1$	$10^{-3} \sim 10^{-2}$	$10^{-4} \sim 10^{-3}$	$10^{-5} \sim 10^{-4}$
ζ	0.72	0.68	0.63	0.58	0.54

Table 5.1: Fit parameter ζ for various orders of scalar coupling constant λ. They are smaller for smaller order of the scalar coupling constant λ.

transition to a function, $q^2 \propto \lambda^\zeta$. The values of the parameter ζ are smaller for smaller scalar coupling constant. Our results would be confirmed by experiments of high-temperature superconductors and liquid crystals or by lattice simulations. In particular, the end-point is $\kappa_c = 0.28$ for the case of superconductor, $q = 2e$.

5.2 Electroweak phase transition

The Electroweak phase transition is one of the most important phase transitions at the early universe since it may account for the baryon number of the present universe [8]. We introduce how the properties of the phase transition are important in the production of the baryon number during the phase transition, *Electroweak baryogenesis*. The phase transition should be of strongly first order for the electroweak baryogenesis since there must be non-equilibrium[2]. In practice, we need two non-equilibrium due to the strongly first order phase transition: *sufficient suppression of the sphaleron rate after the phase transition* and *an existence of a clear wall between the symmetric vacuum and the broken one*. We explain these below in turn.

The sphaleron is a non-perturbative configuration of the SU(2) gauge field through which we have the violation of the baryon number[3]. Though we need the process to have the baryon number production, we must not

[2]This is one of the necessary conditions for the baryogenesis, *the Sakharov's three conditions*. The others are *an existence of the baryon number violation process* and *C and CP violation*. The former is satisfied by the existence of the sphaleron process in the electroweak baryogenesis. Though the latter is also satisfied in the standard model because of the complex phase of the KM matrix, it would need other source of CP violation for the sufficient baryon production.

[3]Though the process violates the baryon number, it conserve difference between a baryon number and a lepton number

have the process after the phase transition frequently. If there are too much sphaleron process after the phase transition, it washes out the produced baryon number[4]. The sphaleron rate, therefore, should be suppressed enough after the phase transition. Comparing the sphaleron rate and the expansion rate of the universe at the time, we have the constraint for the field expectation value of the Higgs field, $\frac{\phi_c}{T_c} \gtrsim 1$, since the sphaleron rate has a dependence, $\Gamma_{sphaleron} \propto e^{-const \times \frac{\phi_c}{T_c}}$ [9, 10].

In almost every scenarios of the electroweak baryogenesis, the wall between the symmetric vacuum and the broken one plays an important role to produce the baryon number. If the phase transition is of second order or of weakly first order, there is no clear wall. We, therefore, can not produce any baryon number in this case. The analysis of the wall is, however, difficult since it is needed to investigate the dynamics of the phase transition. The calculation of the effective potential is not sufficient for this investigation. We then use a sufficient sphaleron rate suppression condition, $\frac{\phi_c}{T_c} \gtrsim 1$, as a criterion of the strongly first order phase transition in the present paper.

This phase transition was first investigated using the perturbation theory of the finite temperature field theory and predicts the first order phase transition from an effective potential [65, 51]. The perturbation theory, however, has difficulty due to an infrared divergence caused by light Bosons and cannot give reliable results in the case where the Higgs Boson mass m_H, is comparable to or greater than the Weak Boson mass since the phase transition gets weaker in this region. This is the problem, which we showed in Sec.1.2 and Sec.2.2.Lattice Monte Carlo simulations, therefore, become the most powerful method and are still used to investigate details of the phase transition [28, 66, 67, 68, 69]. According to these results, the Electroweak phase transition is of first order if m_H is less than an end-point $m_{H,e} \sim 70$ (GeV). It turns to be of second order just on the end-point. Beyond the end-point, we have no phase transition, which means any observable quantities do not have discontinuities. As far as we know, three other non-perturbative methods predict the existence of the end-point [40, 70, 71]. The end-point is determined below 100 GeV by these three methods.

We apply the auxiliary mass method to the Standard Model and investigate the Electroweak phase transition in the present section. We add an auxiliary mass $M \gtrsim T$ only to the Higgs Boson, which becomes very light owing to a cancellation between its negative tree mass and positive thermal mass for small field expectation values around the critical temperature. We notice that the infrared divergence from the Higgs Boson is always serious if the phase transition is of second order or of the weakly first order [51]. In the standard model, transverse modes of the gauge fields also have small masses at small field expectation values since they do not have the thermal mass at one loop order. We discuss the influence of this modes in summary.

An effective potential is then calculated as follows in the Landau gauge [65, 51],

$$\begin{aligned} V(M^2) &= \frac{M^2}{2}\phi^2 + \frac{\lambda}{4!}\phi^4 + f_{BT}(m_H^2(\phi)) + 3f_{BT}(m_{NG}^2(\phi)) \\ &\quad +4f_{BT}(M_W^2(\phi)) + 4f_{G0}(M_W^2(\phi)) \\ &\quad +2f_{BT}(M_{WL}^2(\phi)) + 2f_{G0}(M_{WL}^2(\phi)) \\ &\quad +2f_{BT}(M_Z^2(\phi)) + 2f_{G0}(M_Z^2(\phi)) \\ &\quad +f_{BT}(M_{ZL}^2(\phi)) + f_{G0}(M_{ZL}^2(\phi)) \\ &\quad +f_{BT}(M_{\gamma L}^2(\phi)) + f_{G0}(M_{\gamma L}^2(\phi)) \\ &\quad +12f_{FT}(m_t^2(\phi)) + 12f_{F0}(m_t^2(\phi)) \end{aligned} \tag{5.4}$$

here,

$$\begin{aligned} m_H^2(\phi) &= M^2 + \frac{\lambda}{2}\phi^2,\ m_{NG}^2(\phi) = M^2 + \frac{\lambda}{6}\phi^2, \\ M_W^2(\phi) &= \frac{g_2^2\phi^2}{4},\ M_{WL}^2(\phi) = \frac{g_2^2\phi^2}{4} + \frac{11g_2^2T^2}{6}, \\ M_Z^2(\phi) &= \frac{(g_2^2+g_1^2)\phi^2}{4},\ m_t(\phi) = \frac{g_Y^2\phi^2}{2} \end{aligned}$$

$$\begin{pmatrix} M_{ZL}^2 & 0 \\ 0 & M_{\gamma L}^2 \end{pmatrix} = \mathbf{T}^\dagger \begin{pmatrix} \frac{g_2^2\phi^2}{4} + \frac{11g_2^2T^2}{6} & -\frac{g_1g_2\phi^2}{4} \\ -\frac{g_1g_2\phi^2}{4} & \frac{g_1^2\phi^2}{4} + \frac{11g_1^2T^2}{6} \end{pmatrix} \mathbf{T}$$

$$f_{BT}(m^2) = \frac{T}{2\pi^2}\int_0^\infty dk\ k^2 \log\{1 - \exp(-\frac{\sqrt{k^2+m^2}}{T})\}$$

[4]We assume the baryon number and the lepton number are zero before the phase transition. The entropy has, therefore, maximum at the state where baryon number and the lepton number are zero.

$$
\begin{aligned}
f_{FT}(m^2) &= \frac{T}{2\pi^2}\int_0^\infty dk\; k^2 \log\{1+\exp(-\frac{\sqrt{k^2+m^2}}{T})\} \\
f_{G0}(m^2) &= \frac{m^4}{64\pi^2}\{\log(\frac{m^2}{\bar{\mu}^2})-\frac{5}{6}\} \\
f_{F0}(m^2) &= -\frac{m^4}{64\pi^2}\{\log(\frac{m^2}{\bar{\mu}^2})-\frac{3}{2}\}.
\end{aligned}
$$

In the above equations, λ, g_2, g_1 and g_Y are coupling constants for the Higgs Boson, SU(2) gauge field, U(1) gauge field and top Yukawa respectively. The matrix $\mathbf{T}$ is orthogonal and diagonalizes the mass matrix for the Z Boson and photon at finite temperature. We renormalized the effective potential using the $\overline{MS}$ scheme with a renormalization scale $\bar{\mu}$. A zero-temperature contribution from the Higgs Boson is neglected since it is small in the mass region we consider. The ring diagrams are added only to the Weak Bosons and the Z-Boson since the Higgs Bosons have auxiliary large mass and do not need the resummation. We then extrapolate this effective potential at the auxiliary mass squared M^2 to that of the true mass squared $-\nu^2$ using an evolution equation. Since we add the auxiliary mass only to the Higgs Boson, the evolution equation is same as that for the O(4)-invariant scalar model. We then have the evolution equation from Eq.(4.35)

$$
\begin{aligned}
\frac{\partial V}{\partial m^2} &= \frac{1}{2}\bar{\phi}^2 + \frac{1}{4\pi^2}\int_0^\infty dk \frac{k^2}{\sqrt{k^2+\frac{\partial^2 V}{\partial\bar{\phi}^2}}}\frac{1}{e^{\frac{1}{T}\sqrt{k^2+\frac{\partial^2 V}{\partial\bar{\phi}^2}}}-1} \\
&\quad + \frac{3}{4\pi^2}\int_0^\infty dk \frac{k^2}{\sqrt{k^2+\frac{1}{\bar{\phi}}\frac{\partial V}{\partial\bar{\phi}}}}\frac{1}{e^{\frac{1}{T}\sqrt{k^2+\frac{1}{\bar{\phi}}\frac{\partial V}{\partial\bar{\phi}}}}-1}. \qquad (5.5)
\end{aligned}
$$

A non-perturbative effective potential free from the infrared divergence can be obtained by solving the evolution equation (5.5) with an initial condition Eq.(5.4). We carry out this by numerical calculation.

Before showing our numerical results, we relate the parameters ν^2, λ, g_2, g_1 and g_Y to physical quantities at the zero-temperature [51],

$$
\begin{aligned}
\lambda &= \frac{3m_{H0}^2}{\phi_0^2} - \frac{3}{32\pi^2}\left[\frac{3}{2}g_2^4\left\{\log\left(\frac{M_{W0}^2}{\bar{\mu}^2}\right)+\frac{2}{3}\right\}\right. \\
&\quad \left. + \frac{3}{4}\left(g_1^2+g_2^2\right)^2\left\{\log\left(\frac{M_{Z0}^2}{\bar{\mu}^2}\right)+\frac{2}{3}\right\}\right.
\end{aligned}
$$

$$
\left. - 12 g_Y^4 \log\left(\frac{m_{t0}^2}{\bar{\mu}^2}\right)\right]
$$

$$
\begin{aligned}
\nu^2 &= \frac{m_{H0}^2}{2} - \frac{\phi_0^2}{64\pi^2}\left\{\frac{3}{2}g_2^4 + \frac{3}{4}(g_1^2+g_2^2)^2 - 12 g_Y^4\right\} \qquad (5.6) \\
M_{W0}^2 &= \frac{g_2^2\phi_0^2}{4}, M_{Z0}^2 = \frac{(g_2^2+g_1^2)\phi_0^2}{4}, \\
m_{t0}^2 &= \frac{g_Y^2\phi_0^2}{2}, \phi_0 = 246\ (\mathrm{GeV})
\end{aligned}
$$

Radiative corrections at the one-loop order are included in the equations for ν^2 and λ since they are large, especially in the case where the Higgs Boson mass is small. The effective potential Eq.(5.4) does not depend on $\bar{\mu}$ using λ in Eq.(5.6) in this order. We fix the masses of the Weak Bosons and the Z-Boson as $M_{W0} = 80$ (GeV) and $M_{Z0} = 92$ (GeV) below.

We first investigate the $SU(2) \times U(1)$ gauge plus Higgs theory, corresponding to the case, $m_t = 0$. We show results obtained by setting $M = T$ since similar results were obtained by setting $M = \frac{T}{2}$ and $M = 2T$. This is quite natural since the restriction on M is only $M \gtrsim T$. The effective potentials at the critical temperature are shown in Fig.5.7 for m_H =15, 30, 45 (GeV), respectively. The first order phase transition becomes weaker each other for smaller values of the Higgs mass and disappears finally. They are compared to effective potentials obtained by the ring resumed perturbation theory at the one-loop order without the high temperature expansion in Fig.5.8. We find clearly that they are similar for smaller values of m_H and different for larger values of m_H. This is consistent with the fact that the ring resumed perturbation theory is reliable only for smaller values of the Higgs mass $m_H \ll M_W$ [51]. We plot the ratio of the critical field expectation values to the critical temperature, ϕ_c/T_c as a function of m_H in Fig.5.9. This quantity indicates the strength of the first order phase transition and important in estimating the sphaleron rate, which plays a very important role in the Electroweak Baryogenesis [113, 114]. The end-point is determined as $m_{H,c} = 38$ (GeV) from Fig.5.9. This figure also shows that the results obtained by the auxiliary mass method and the perturbation theory is similar for smaller values of m_H and different for larger values, $m_H \gtrsim 30$ (GeV).

We next investigate more realistic cases in which the top quark mass is finite. The same ratio is shown in Fig.5.10 for various values of m_t. This figure shows that the strength of the first order phase transition is almost

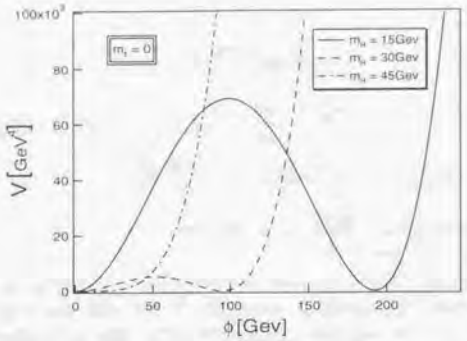

Figure 5.7: The effective potentials at the critical temperature for m_H =15, 30, 45 (GeV). The first order phase transition becomes weaker for smaller values of the Higgs mass and disappears finally.

same for $m_t \lesssim 100$ (GeV) and become weaker for $m_t \gtrsim 100$ (GeV) rapidly. The end-points are then shown in Fig.5.11 as a function of m_t. The graph labeled "1-loop" is obtained using Eq.(5.4) and Eq.(5.6), which take into account the zero-temperature radiative corrections from the top quark and gauge fields. The contribution from the top quark is much larger than that of the gauge fields. On the other hand, the graph labeled as "tree" is obtained without the zero-temperature radiative correction, omitting the contributions from f_{G0} and f_{F0} from Eq.(5.4) and leaving only the first terms of Eq.(5.6) for λ and v^2. They are not much different for smaller values of the top quark mass, $m_t \lesssim 100$ (GeV). Their behavior, however, differs drastically for larger values of the top quark mass, $m_t \gtrsim 100$ (GeV). Surprisingly, the end-point vanishes for $m_t \gtrsim 160$ (GeV) in the "1-loop" results though it increases in the "tree" results. These results tell us that Fermionic degrees of freedom play significant roles in the phase transition through the renormalization effects at the zero-temperature. We also conclude that there are no first order phase transitions for $m_t = 175$ (GeV), no matter how small the Higgs Boson mass.

In the present section, we have calculated the effective potentials of the standard model using the auxiliary mass method at a finite temperature. We first investigated the $SU(2) \times U(1)$ gauge plus Higgs theory, corresponding

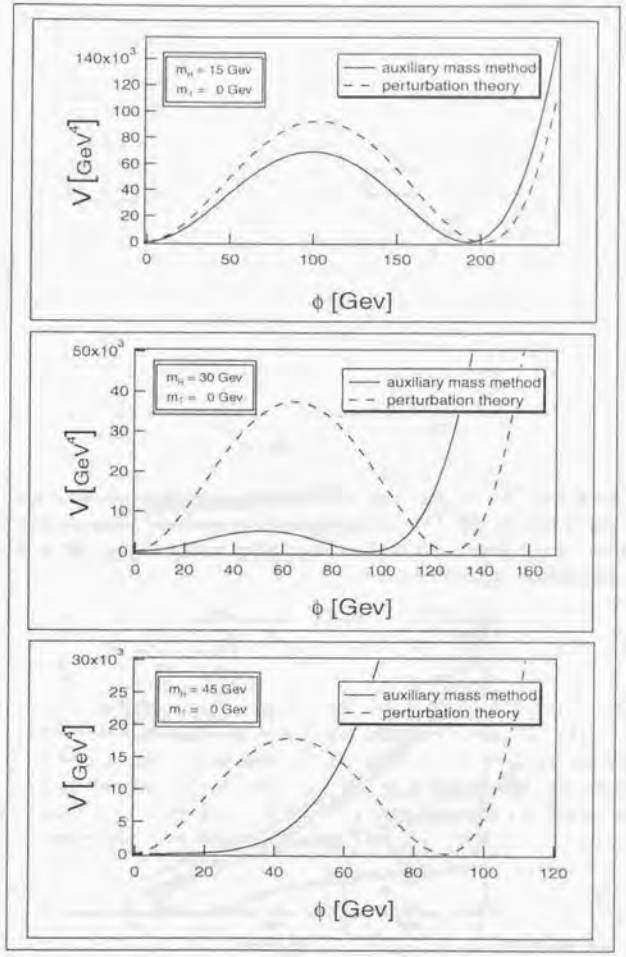

Figure 5.8: The effective potentials at the critical temperature obtained by the auxiliary mass method and the perturbation theory for m_H =15, 30, 45 (GeV). They are similar for smaller values of m_H and different for larger values of m_H.

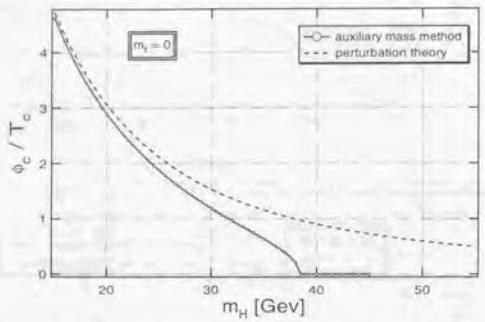

Figure 5.9: The ratio of the critical field expectation values to the critical temperature, ϕ_c/T_c. The results obtained by auxiliary mass method and the perturbation theory are similar for smaller values of m_H and different for larger values, $m_H \gtrsim 30$ (GeV).

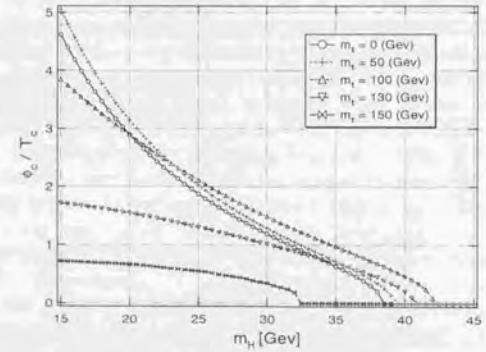

Figure 5.10: The ratio of the critical field expectation values to the critical temperature, ϕ_c/T_c. The phase transition is weaker for larger top quark mass.

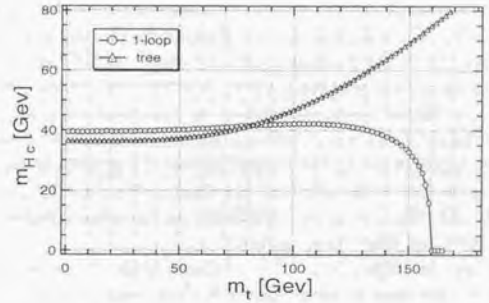

Figure 5.11: The end point of Higgs boson as a function of top quark mass. The graph "tree" is obtained using only the first terms in Eq.(5.6) for ν^2 and λ, which corresponds to matching the parameters with physical observable quantities at tree level. The graph "1-loop" is obtained using all terms in Eq.(5.6) for ν^2 and λ, which corresponds to matching the parameters with physical observable quantities at one-loop level.

to the case $m_t = 0$. The phase transition was of first order and similar to the results obtained by the perturbation theory for smaller $m_H \sim 15$ (GeV). The phase transition became weaker for larger $M_H \sim 30$ (GeV) and finally disappeared in contrast to the results from perturbation theory. We found that the end-point is at $m_{H,c} = 38$ (GeV) in this case. This is consistent with the results of the Lattice Monte Carlo simulation [66, 67, 68, 69] and the other non-perturbative methods [40, 70, 71] qualitatively. The value of the end-point, however, was smaller than those by these methods. We next investigated the more realistic case in which the top quark mass is finite. We found that the end-point was strongly dependent on m_t and disappeared for $m_t \gtrsim 160$ (GeV). The renormalization effects from the top quark were significant. Lattice Monte Carlo simulations, however, do not follow this behavior [28]. We think of two possible reasons:(1)Since our results differ from that of the Lattice Monte Carlo simulation by factors of 2 in a $SU(2) \times U(1)$ gauge plus Higgs theory quantitatively, the similar behavior may be found at a larger top quark mass in the Lattice Monte Carlo simulation.(2)Since the one-loop correction to the *effective potential* at the zero-temperature is significant, the 3D effective theory, which has no Fermionic degrees of freedom, may not reflect the effect appropriately.

We discuss the higher loop effect of gauge fields. Since we did not introduce the auxiliary mass to gauge fields, the loop expansion parameter for the gauge fields was not improved. We, therefore, controlled only the infrared divergence of graphs involving the Higgs Boson field. In this sense, our method improves the infrared divergence partially. We then take "hybrid method" to improve the approximation; auxiliary mass for Higgs boson and perturbative expansion for gauge boson[5]. For example, we explain how to evaluate two loop effect. Using auxiliary mass method, we need not take into account Fig.(5.12) (a1),(a2) and (a3) thanks to the auxiliary mass. Besides, we need not take into account Fig.(5.12) (b1) and (b2), which have large infrared effect ($\propto \phi^2 T^2 log(\phi)$) at ordinary perturbation theory, since the auxiliary mass controls the infrared effect ($\propto \phi^2 T^2 log(M)$). Only graphs we have to take into account are Fig.(5.12) (c1),(c2) and (c3). We must take into account fewer graphs than that of the ordinary perturbation theory since most graphs have good infrared behavior thanks to the auxiliary mass. We expect that

[5]Perturbative expansion for non-Abelian gauge fields can not be calculated at arbitrary order due to the infrared divergence. Our method can not solve this problem.

this two loop effect reduces the qualitative gap between our results and that of Lattice simulations[6].

Finally, the first order phase transition, which is necessary for the Electroweak Baryogenesis, was not found in the Standard Model. We will apply this method to extensions of the Standard Model.

[6]The investigation of the two loop effect is underway

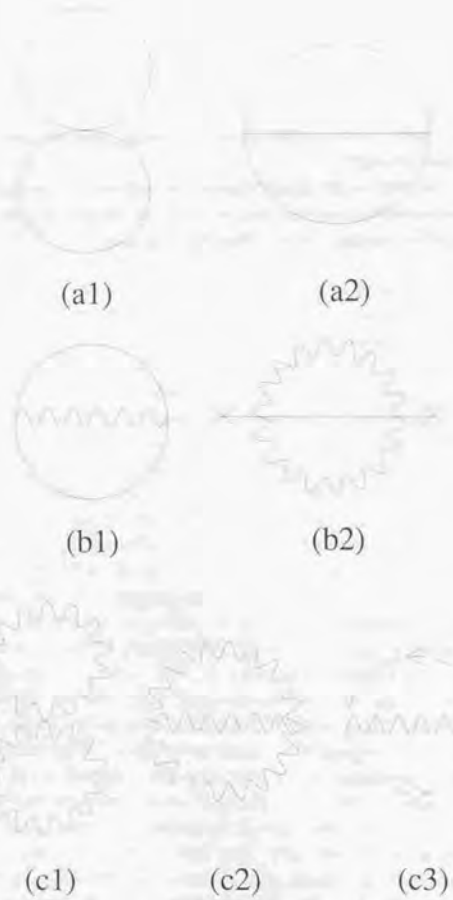

Figure 5.12: Two loop graphs with Higgs boson and gauge boson. (a) graphs with only Higgs boson, which have no infrared divergence thanks to the auxiliary mass. (b) graphs with Higgs boson and gauge field, of which infrared behavior is controlled by the auxiliary mass. (c) graphs with only gauge boson, which have bad infrared behaviour.

Chapter 6

Beyond the local potential approximation

6.1 Evolution equation beyond the local potential approximation

As we have seen in Ch.4 and Ch.5, the local potential approximation works well both qualitatively and quantitatively. We need method to improve the approximation. In the present section, we try to improve the approximation. We show that the local potential approximation corresponds to a leading approximation of the derivative expansion of the effective action. We also derive an evolution equations of the next to leading approximation. We deal only the Z_2-invariant scalar model here.

We calculate the derivative $\frac{\partial\Gamma[\phi_c]}{\partial m^2}$[1]. From Eq.(3.3), we have,

$$\begin{aligned}\frac{\partial\Gamma[\phi_c]}{\partial m^2} &= -\frac{1}{2}\int d^4x < \phi(x)^2 > \\ &= -\frac{1}{2}\int d^4x d^4y < \phi(x)\phi(y) > \delta(y-x) \\ &= -\frac{1}{2}\int d^4x\phi_c(x)^2 - \frac{1}{2}\int d^4x d^4y \left(\frac{\delta^2(-\Gamma[\phi_c])}{\delta\phi_c(x)\delta\phi_c(y)}\right)^{-1}\delta(y-x),\end{aligned} \tag{6.1}$$

here "$\int d^4x$" is an abbreviation of "$\int_0^\beta d\tau \int_{-\infty}^{\infty} d^3x$". We use this notation

[1]See the appendix D in detail.

from now on.

Equation (6.1), however, can not be solved exactly. In order to solve this equation approximately, we limit the functional space and expand $\Gamma[\phi_c]$ in powers of derivatives[115, 59],[2]

$$\Gamma[\phi_c] = \int d^4x \left[-V(\phi_c^2) - \frac{1}{2}K_0(\phi_c^2)(\partial_0\phi_c)^2 - \frac{1}{2}K_s(\phi_c^2)(\nabla\phi_c)^2 + \cdots \right], \quad (6.2)$$

where $\cdots$ denotes terms with higher derivative. Note that the coefficient functional of $(\partial_0\phi_c)^2$ differs from that of $(\nabla\phi_c)^2$ due to the absence of the 4-dimensional Euclidean symmetry. We then expand the both side of Eq.(6.1) with respect to derivative as Eq.(6.2) and match the coefficient function of each terms. In practice, we have to truncate the series in Eq.(6.2) at finite terms. In the present paper, we keep the three terms in Eq.(6.2). This is the next-to-leading approximation of the derivative expansion. We obtain the local potential approximation by taking $K_0 = 1$ and $K_s = 1$ as we will see later.

From Eq.(6.2), l.h.s of Eq.(6.1) becomes,

$$-\frac{\partial\Gamma}{\partial m^2} = \int d^4x \left[\frac{\partial V}{\partial m^2} + \frac{1}{2}\frac{\partial K_0}{\partial m^2}(\partial_0\phi_c)^2 + \frac{1}{2}\frac{\partial K_s}{\partial m^2}(\nabla\phi_c)^2 \right]. \quad (6.3)$$

From Eq.(6.2), up to the second derivative terms,[3]

$$\begin{aligned}
M_{yx} &\equiv -\frac{\delta^2\Gamma[\phi_c]}{\delta\phi_c(x)\delta\phi_c(y)} \\
&= \delta(y-x)\Big[V''(\phi_c(y)) \\
&\quad - \Big\{\frac{1}{2}K_0''(\phi_c(y))(\partial_0\phi_c(y))^2 + K_0'(\phi_c(y))\partial_0\phi_c(y)\partial_{y_0} \\
&\quad + K_0'(\phi_c(y))\partial_0^2\phi_c(y) + K_0(\phi_c(y))\partial_{y_0}^2\Big\} \quad (6.4) \\
&\quad - \{K_0 \leftrightarrow K_s, \partial_{y_0} \leftrightarrow \nabla_y\}\Big] \\
&= \delta(y-x)(-\overline{K}_0\partial_{y_0}^2 - \overline{K}_s\nabla_y^2 + \overline{V}'') \\
&\quad + \delta(y-x)\Big[\widetilde{V}''(\phi_c(y)) \\
&\quad - \Big\{\frac{1}{2}K_0''(\phi_c(y))(\partial_0\phi_c(y))^2 + K_0'(\phi_c(y))\partial_0\phi_c(y)\partial_{y_0} \\
&\quad + K_0'(\phi_c(y))\partial_0^2\phi_c(y) + \widetilde{K}_0(\phi_c(y))\partial_{y_0}^2\Big\} \quad (6.5) \\
&\quad - \{K_0 \leftrightarrow K_s, \partial_{y_0} \leftrightarrow \nabla_y\}\Big] \\
&= A_{yx} - B_{yx}, \quad (6.6) \\
A_{yx} &\equiv \delta(y-x)(-\overline{K}_0\partial_{y_0}^2 - \overline{K}_s\nabla_y^2 + \overline{V}'') \\
B_{yx} &\equiv A_{yx} - M_{yx} \\
\widetilde{V}''(\phi_c(y)) &\equiv V''(\phi_c(y)) - \overline{V}'' \\
\widetilde{K}_0(\phi_c(y)) &\equiv K_0(\phi_c(y)) - \overline{K}_0
\end{aligned}$$

Here, we divide M_{yx} into two parts, A_{yx} and B_{yx}, which remains finite and vanishes at $\phi_c(x) = \bar{\phi}$ respectively. Details of the following calculation are explained in the appendix. The right hand side of Eq.(6.1) can now be expanded around $\phi_c(x) = \bar{\phi}$ up to the second derivative as follows,

$$\begin{aligned}
&\int d^4x d^4y \Big(\frac{\delta^2(-\Gamma[\phi_c])}{\delta\phi_c(x)\delta\phi_c(y)}\Big)^{-1}\delta(y-x) \\
&= \int d^4x (A^{-1})_{xx} \\
&\quad + \int d^4x d^4y d^4z (A^{-1})_{xy} B_{yz} (A^{-1})_{zx} \\
&\quad + \int d^4x d^4y d^4z d^4u d^4v (A^{-1})_{xy} B_{yz} (A^{-1})_{zu} B_{uv} (A^{-1})_{vx} \\
&\quad + \cdots \\
&= \int_{px} \frac{1}{\nu} \\
&\quad + \int_{px} \frac{1}{\nu^2}\Big[-\frac{1}{2}\Big\{\overline{K}_0''(\partial_0\phi_c)^2 + \overline{K}_s''(\nabla\phi_c)^2\Big\}\Big] \\
&\quad + \int_{px} \frac{1}{\nu^3}\Big[\Big\{\overline{K}_0' p_0(\partial_0\phi_c) + \overline{K}_s' p_i(\partial_i\phi_c)\Big\}^2 \\
&\qquad + 2\Big\{\overline{K}_0'(\partial_0\phi_c)^2 + \overline{K}_s'(\nabla\phi_c)^2\Big\}\nu'\Big] \quad (6.7) \\
&\quad \int_{px} \frac{1}{\nu^4}\Big[-2\Big\{\overline{K}_0' p_0\partial_0\phi_c + \overline{K}_s' p_i\partial_i\phi_c\Big\}\Big\{\overline{K}_0 p_0\partial_0\phi_c + \overline{K}_s p_i\partial_i\phi_c\Big\}\nu' \\
&\qquad - \frac{1}{2}\{\nu'\}^2\Big\{\overline{K}_0(\partial_0\phi_c)^2 + \overline{K}_s(\nabla\phi_c)^2\Big\}\Big]
\end{aligned}$$

[2]Similar derivation in Ref.[59, 115] has a problematic point: $\exp(iqx)$ is handled as not a distribution but an ordinary function.

[3]Hereafter, we also use notations like $\overline{V}' = V(\bar{\phi})$ as values of functions at constant configuration, $\phi_c(x) = \bar{\phi} = const.$

$$+\cdots+(\textit{terms which vanish at } \phi_c(x)=\bar{\phi} \textit{ like } \widetilde{V}\times(\textit{something})),$$

where $\nu=\overline{K}_0 p_0^2+\overline{K}_s\mathbf{p}^2+\overline{V}''$, $\nu'=\overline{K}_0' p_0^2+\overline{K}_s'\mathbf{p}^2+\overline{V}'''$ (with $p_0=2\pi nT(n=0,\pm1,\cdots)$ and $\mathbf{p}^2\equiv\sum_{i=1}^3 p_i^2$) and "$\int_{px}$" is an abbreviation of "$T\sum_{n=-\infty}^{\infty}\int d^3p/(2\pi)^3\int d^4x$".

We match the both side of Eq.(6.1) using Eq.(6.3) and Eq.(6.7) and equate the coefficient function of $(\partial\phi_c)$ respectively. After the matching, we put $\phi_c(x)=\bar{\phi}$ and get the following simultaneous partial differential equation,

$$\frac{\partial\overline{V}}{\partial m^2} = \frac{1}{2}\bar{\phi}^2+\frac{1}{2}\int_p\frac{1}{\nu} \tag{6.8}$$

$$\begin{aligned}\frac{\partial\overline{K}_0}{\partial m^2} &= -\frac{1}{2}\overline{K}_0''\int_p\frac{1}{\nu^2}\\ &\quad +\overline{K}_0^2\int_p\frac{p_0^2}{\nu^3}+2\overline{K}_0'\int_p\frac{\nu'}{\nu^3}\\ &\quad -2\overline{K}_0'\overline{K}_0\int_p p_0^2\frac{\nu'}{\nu^4}-\frac{1}{2}\overline{K}_0\int_p\frac{\{\nu'\}^2}{\nu^4}\end{aligned} \tag{6.9}$$

$$\begin{aligned}\frac{\partial\overline{K}_s}{\partial m^2} &= -\frac{1}{2}\overline{K}_s''\int_p\frac{1}{\nu^2}\\ &\quad +\frac{\overline{K}_s^2}{3}\int_p\frac{\mathbf{p}^2}{\nu^3}+2\overline{K}_s'\int_p\frac{\nu'}{\nu^3}\\ &\quad -\frac{2}{3}\overline{K}_s'\overline{K}_s\int_p\mathbf{p}^2\frac{\nu'}{\nu^4}-\frac{1}{2}\overline{K}_s\int_p\frac{\{\nu'\}^2}{\nu^4},\end{aligned} \tag{6.10}$$

where, "$\int_p$" is an abbreviation of "$T\sum_{n=-\infty}^{\infty}\int d^3p/(2\pi)^3$". Since we put $\phi_c(x)=\bar{\phi}$ finally, we do not have contribution from the terms in Eq.(6.7) which vanish at $\phi_c(x)=\bar{\phi}$. This is the evolution equation of the next-to-leading approximation of the derivative expansion.

If we set $\overline{K}_S=\overline{K}_0=1$, we have only the first equation, which corresponds to the local potential approximation. In this respect, the local potential approximation is the leading approximation in the derivative expansion of the effective action.

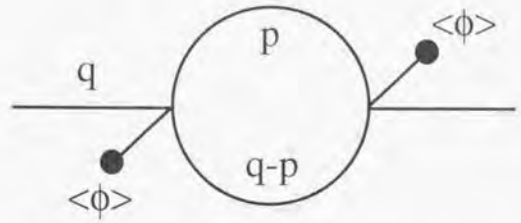

Figure 6.1: Diagram of the external-momentum dependent self-energy at one-loop.

6.2 Initial condition beyond the local potential approximation

We can calculate the initial condition $\Gamma[\bar{\phi};M^2)$ using the perturbation theory within one-loop level reliably thanks to the large auxiliary mass, $M\sim T$. The effective potential, $V(\bar{\phi};M^2)$, is calculated within the one-loop approximation as follows,

$$V(\bar{\phi};M^2)=\frac{1}{2}M^2\bar{\phi}+\frac{\lambda}{24}\bar{\phi}^4+\frac{1}{2}\int_p\log(p_0^2+\mathbf{p}^2+M^2+\frac{\lambda}{2}\bar{\phi}^2). \tag{6.11}$$

The loop correction to $K_0(\bar{\phi};M^2)$ and $K_s(\bar{\phi};M^2)$ comes from the self-energy graph in Fig.6.1 at one-loop level, which depends on external momentum,

$$\Pi(q_0^2,\mathbf{q}^2)=\frac{\lambda^2\bar{\phi}^2}{2}\int_p\frac{1}{p_0^2+\mathbf{p}^2+M^2+\frac{\lambda\bar{\phi}^2}{2}}\frac{1}{(q_0-p_0)^2+(\mathbf{q}-\mathbf{p})^2+M^2+\frac{\lambda\bar{\phi}^2}{2}}. \tag{6.12}$$

The initial conditions of $K_0(\bar{\phi};M^2)$ and $K_s(\bar{\phi};M^2)$ are given by the coefficients of $-q_0^2$ and $-\mathbf{q}^2$ respectively. We, therefore, get[4]

$$K_0(\bar{\phi};M^2) = 1-\left.\frac{d\Pi(q_0^2,\mathbf{q}^2)}{dq_0^2}\right|_{q_i=0,q_0=0} \tag{6.13}$$

[4]Strictly speaking, we first put $q_i=0$ then put $q_0=0$ in taking the limit $q_i=0$ and $q_0=0$. For the function K_0 to be defined this order is essential, while for K_s the order of taking the limit gives no difference. See ref. [1].

$$= 1 - \frac{\lambda^2\bar{\phi}^2}{2}\int_p \left[\frac{1}{(p_0^2+\mathbf{p}^2+M^2+\frac{\lambda\bar{\phi}^2}{2})^3} - \frac{M^2+\frac{\lambda\bar{\phi}^2}{2}}{(p_0^2+\mathbf{p}^2+M^2+\frac{\lambda\bar{\phi}^2}{2})^4}\right],$$

$$K_s(\bar{\phi}; M^2) = 1 - \left.\frac{d\Pi(q_0^2, \mathbf{q}^2)}{d\mathbf{q}^2}\right|_{q_0=0,q_i=0} \tag{6.14}$$

$$= 1 + \frac{\lambda\bar{\phi}^2}{6}\int_p \frac{1}{(p_0^2+\mathbf{p}^2+M^2+\frac{\lambda^2\bar{\phi}^2}{2})^3}.$$

We have calculated the evolution equation in Sec.6.1 and the initial condition in this section. Since some of them, e.g. the one-loop effective potential, has an ultraviolet divergence, we have to renormalize it by the counter terms. Instead of considering this contribution, we simply assume that the renormalization effect is small and discard it. The contribution is, actually, small comparing with the finite temperature contribution around a critical temperature in most cases because of long correlation length. We thus need to deal with only the temperature dependent pieces in the integrals of $\frac{\partial\Gamma}{\partial m^2}$ and the initial condition. To do so, we only perform the following replacement in Eq.(6.8),(6.9),(6.10),(6.11),(6.13) , and (6.14),

$$\int_p \quad \text{with} \quad 2\int \frac{d^4p}{(2\pi)^4 i}\frac{1}{\exp(p_0/T)-1}.$$

6.3 Numerical results

We solved the simultaneous evolution equation Eq.(6.8), Eq.(6.9) and Eq.(6.10) with the initial condition Eq.(6.11), Eq.(6.13) and Eq.(6.14) numerically. We used an extended Crank-Nicholson method, which is explained in the appendix C, to solve the partial differential equation. We can solve the equation at most temperatures above the critical one. Unfortunately, we can not, however, solve the equation at temperatures very close to the critical one due to numerical problems. We tried several improvements of the numerical method but failed. We, therefore, show only the obtained results in the present paper. This equation may be solved at arbitrary temperature if excellent numerical methods to solve a partial differential equation are invented. Or ability of computers progresses highly so that we can calculate with much higher precision. We use a mass unit, $\mu = 1$

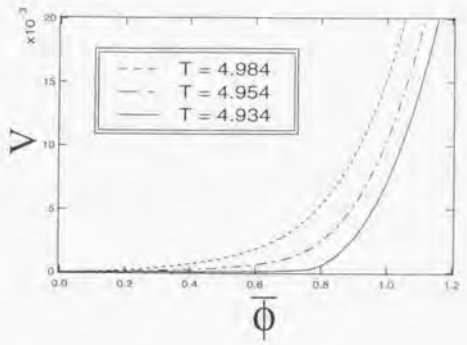

Figure 6.2: Effective potential around the critical temperature ($\lambda = 1$).

We show the effective potential above the critical temperature in Fig.6.2 for $\lambda = 1$. We observe behavior of a second order phase transition up to this temperature. This effective potential seems to be cone-shaped. The critical temperature is estimated to be lower than that of the local potential approximation by 2%.

We show K_0 and K_s in Fig.6.3 for $\lambda = 1$. They are very similar in spite of the violation of the Lorentz invariance in this case while the initial condition is quite different.

In summary, we derived an evolution equation of the effective action with respect to the mass squared in the Z_2-invariant scalar theory. We then approximated the effective action by the derivative expansion. We showed that the previous evolution equation of the effective potential can be derived as the leading approximation, the local potential approximation. We next derived the evolution equation of the next-to-leading approximation which is the simultaneous partial differential equation. We finally solved the equation numerically. Though we could solve it at most temperatures above the critical one, we could not do it under a certain temperature very close to the critical one unfortunately. However, this equation may be solved at arbitrary temperatures if excellent numerical methods to solve a partial differential equation are invented or ability of computers progresses highly. Anyway, we constructed a systematic method to improve the auxiliary mass method in principle.

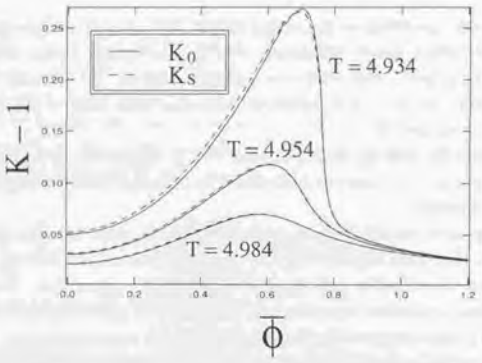

Figure 6.3: The coefficient functions of the second derivative terms in the effective action, K_0 and K_s ($\lambda = 1$).

Chapter 7

Summary

In the first half of the present paper, Ch.1 and Ch.2, we introduced the finite temperature field theory and its breakdown around the critical temperature. We also introduced some known approaches to overcome the problem. The ring resummation method is the most popular one and is explained in some details.

We proposed the auxiliary mass method in Ch.3 to overcome this problem. We applied this method to the Z_2-invariant scalar model in Sec.4.1.2 to examine how well the method works. This model is adequate for the examination since its phase transition can not be investigated well by the perturbation theory; though the phase transition of the model is known to be of second order, the ring resumed perturbation indicates it to be of first order. We, however, needed to approximate somehow to make the auxiliary method to be of solvable form. We tried two approximation: the "super daisy approximation" and the "local potential approximation". We numerically calculated the effective potential of the theory using the both methods. We found that the super daisy approximation is not adequate to investigate the phase transition since it indicates the first order phase transition for this model. On the other hand, we found that the local potential approximation works well both qualitatively and quantitatively.

In Sec.4.2, we applied the method to the O(N)-invariant scalar model, of which phase transition is also investigated well by other approaches. We found that the local potential approximation also works well here.

In Sec.5.1, we applied the method to the Abelian Higgs model. The phase transition of this model is interesting since it describes some physical

systems: for example, superconductors and liquid crystals. The properties of the model, however, have not been understood well, yet. The analysis of the auxiliary mass method with the local potential approximation indicates that there is an end-point, where the phase transition crosses over from the second order phase transition to the first order phase transition. This qualitative result is similar to that obtained by the lattice Monte Carlo simulations. We further investigated the boundary of the phase diagram in detail.

In Sec.5.2, we applied the method to the electroweak phase transition. This phase transition are very important since it may account for the baryon number of the present universe. The properties of the model also have not yet been understood well. The analysis of the auxiliary mass method with the local potential approximation indicates that there is an end-point, where the first order phase transition vanishes. We investigated the phase diagram in Higgs mass-top quark mass plane. We concluded from this phase diagram that we need some extension of the standard model in order to obtain the sufficient baryon number by the electroweak baryogenesis.

In Ch.6, we tried to improve the local potential approximation. We found that the local potential approximation is a leading approximation of the derivative expansion of the effective action in the evolution equation. We derived the evolution equation of the next to leading approximation, which becomes a simultaneous partial differential equation. In this way, we can improve the approximation in principle though we have not yet done it due to numerical difficulties.

We, however, should improve the method in some other aspects. First, we neglected the effects of the ultraviolet renormalization. It is better to deal with the effects more carefully though we expect that the long range effects dominate physics around the critical temperature and the ultraviolet renormalization effect would be small. Second, we had better improve the convergence of the loop of the non-abelian gauge fields.

The most attractive point of this method is the fact that it is based only on the statistical mechanics and is free from the infrared bad behaviour of the loop expansion. We can, therefore, investigate both of a first order phase transition and a second order phase transition. Besides, we can investigate the boundary of them as we have actually done in the present paper. In this respect, this method will have broad applications. We would like to apply it to other interesting phase transitions(e.g. supersymmtric extension of the electro weak phase transition) in future work.

Acknowledgment

I thank my parents for their overall support. I thank Professor J.Arafune for his instructions and encouragements. I thank Dr.T.Inagaki and Dr.J.Sato for their fruitful collaborations. I thank my colleagues for their supplying me with a good environment for research. I thank JSPS for their financial support.

Appendix A

High temperature expansion of one loop integrals

We show the high temperature expansion of one loop diagram with zero external momentum in the present appendix: for Bose field,

$$J_0(m) \equiv \frac{1}{2}\mu^{2\epsilon}T\sum_{n=-\infty}^{n=\infty}\int\frac{d^3\mathbf{k}}{(2\pi)^3}\log\{(2\pi nT)^2+\mathbf{k^2}+m^2\} \quad (A.1)$$

$$J_n(m) \equiv \frac{1}{2}\mu^{2\epsilon}T\sum_{n=-\infty}^{n=\infty}\int\frac{d^3\mathbf{k}}{(2\pi)^3}\frac{1}{\{(2\pi nT)^2+\mathbf{k^2}+m^2\}^n},$$

and for Fermi field,

$$I_0(m) \equiv -2\mu^{2\epsilon}T\sum_{n=-\infty}^{n=\infty}\int\frac{d^3\mathbf{k}}{(2\pi)^3}\log\left[\{(2n+1)\pi T\}^2+\mathbf{k^2}+m^2\right] \quad (A.2)$$

$$I_n(m) \equiv -2\mu^{2\epsilon}T\sum_{n=-\infty}^{n=\infty}\int\frac{d^3\mathbf{k}}{(2\pi)^3}\frac{1}{\left[\{(2n+1)\pi T\}^2+\mathbf{k^2}+m^2\right]^n}.$$

We use the dimensional regularisation with renormalization scale, μ to avoid the ultraviolet divergence for $n \leq 2$. We show only the high temperature expansion of J_0 and I_0 since we can get the others easily using the identities, $J_n(m) = (-1)^{n-1}\frac{1}{(n-1)!}(\frac{\partial}{\partial m^2})^n J_0(m)$ and $I_n(m) = (-1)^{n-1}\frac{1}{(n-1)!}(\frac{\partial}{\partial m^2})^n I_0(m)$. We first calculate the high temperature expansion of J_0.

We can rewrite J_0 as follows,

$$J_0(m) = \frac{1}{2}\mu^{2\epsilon}T\sum_{n=-\infty}^{n=\infty}\int\frac{d^3\mathbf{k}}{(2\pi)^3}\frac{\partial}{\partial\alpha}\{(2\pi nT)^2+\mathbf{k^2}+m^2\}^{\alpha}\Big|_{\alpha=0}. \quad (A.3)$$

Defining $M^2 \equiv m^2+(2\pi nT)^2$, we can perform the three dimensional integral as the ordinary quantum field theory,

$$\begin{aligned} J_0(m) &= \frac{\mu^{2\epsilon}T}{2^{4-2\epsilon}\sqrt{\pi}^{3-2\epsilon}}\frac{\partial}{\partial\alpha}\frac{\Gamma(\epsilon-\alpha-\frac{3}{2})}{\Gamma(-\alpha)}\sum_{n=-\infty}^{\infty}M^{3-2\epsilon+2\alpha}\Big|_{\alpha=0} \\ &= \frac{\mu^{2\epsilon}T}{2^{4-2\epsilon}\sqrt{\pi}^{3-2\epsilon}}\frac{\partial}{\partial\alpha}\{\Gamma(\epsilon-\frac{3}{2})(-\alpha)\sum_{n=-\infty}^{\infty}M^{3-2\epsilon}+\mathcal{O}(\alpha^2)\}\Big|_{\alpha=0} \\ &= -\frac{\mu^{2\epsilon}T}{2^{4-2\epsilon}\sqrt{\pi}^{3-2\epsilon}}\Gamma(\epsilon-\frac{3}{2})\sum_{n=-\infty}^{\infty}M^{3-2\epsilon}. \end{aligned} \quad (A.4)$$

We then expand $J_0(m)$ with respect to $\frac{m}{T}$,

$$\begin{aligned} J_0(m) &= -\frac{\mu^{2\epsilon}T}{2^{4-2\epsilon}\sqrt{\pi}^{3-2\epsilon}}\Gamma(\epsilon-\frac{3}{2})(2\sum_{n=1}^{\infty}M^{3-2\epsilon}+m^{3-2\epsilon}) \\ &= -\frac{\mu^{2\epsilon}T}{2^{4-2\epsilon}\sqrt{\pi}^{3-2\epsilon}}\Gamma(\epsilon-\frac{3}{2})(2\sum_{n=1}^{\infty}(2\pi nT)^{3-2\epsilon}\{1+(\frac{m}{2\pi nT})^2\}^{\frac{3-2\epsilon}{2}}+m^{3-2\epsilon}) \\ &= -\frac{\mu^{2\epsilon}T}{2^{4-2\epsilon}\sqrt{\pi}^{3-2\epsilon}}\Gamma(\epsilon-\frac{3}{2})\{2\sum_{n=1}^{\infty}(2\pi nT)^{3-2\epsilon}\sum_{l=1}^{\infty}\frac{\prod_{i=1}^{l}(\frac{3-2\epsilon}{2}-i+1)}{l!}(\frac{m}{2\pi nT})^{2l} \\ &\qquad +m^{3-2\epsilon}\}. \end{aligned} \quad (A.5)$$

Interchanging the summations, we get,

$$\begin{aligned} J_0(m) &= -\frac{\mu^{2\epsilon}T}{2^{4-2\epsilon}\sqrt{\pi}^{3-2\epsilon}}\Gamma(\epsilon-\frac{3}{2})\{2\sum_{l=1}^{\infty}(2\pi nT)^{3-2\epsilon-2l}m^{2l}\frac{\prod_{i=1}^{l}(\frac{3-2\epsilon}{2}-i+1)}{l!}\sum_{n=1}^{\infty}n^{3-2\epsilon-2l} \\ &\qquad +m^{3-2\epsilon}\}. \\ &= -\frac{\mu^{2\epsilon}T}{2^{4-2\epsilon}\sqrt{\pi}^{3-2\epsilon}}\Gamma(\epsilon-\frac{3}{2})\{2\sum_{l=1}^{\infty}(2\pi nT)^{3-2\epsilon-2l}m^{2l}\frac{\prod_{i=1}^{l}(\frac{3-2\epsilon}{2}-i+1)}{l!}\zeta(2\epsilon+2l-3) \\ &\qquad +m^{3-2\epsilon}\}. \end{aligned} \quad (A.6)$$

We calculate a few first terms explicitly from this,

$$J_0(m) = -\frac{\pi^2T^4}{90}+\frac{m^2T^2}{24}-\frac{m^3T}{12\pi}-\frac{m^4}{64\pi^2}(\frac{1}{\epsilon}+\log\frac{\mu^2}{4\pi T^2}+\epsilon\gamma_E).$$

Here, we used properties and values of the ζ-function, the γ-function, and the poli-γ-function $\psi(z)$,

$$\zeta(1-z) = 2^{1-z}\pi^{-z}\zeta(z)\Gamma(z)\cos(\frac{\pi z}{2}),\ \zeta(0)=-\frac{1}{2},\ \zeta(2)=\frac{\pi^2}{6},\ \zeta(0)=\frac{\pi^4}{90},$$

$$\Gamma(z+1) = z\Gamma(z),\ \Gamma(1)=1,\ \Gamma(\frac{1}{2})=\sqrt{\pi},$$
$$\psi(z) \equiv \frac{\Gamma'(z)}{\Gamma(z)},\ \psi(\frac{1}{2}) = -\log 4 - \gamma_E. \tag{A.7}$$

The high temperature expansion of the other J_n can be calculated by derivating Eq.(A.6).

We can get the high temperature expansion of the Fermionic integrals $I_n(m)$ from $J_n(m)$ using a trick,

$$\begin{aligned} I_0(m) &= -2\mu^{2\epsilon}T\sum_{n=-\infty}^{n=\infty}\int\frac{d^3\mathbf{k}}{(2\pi)^3}\log\left[\{(2n+1)\pi T\}^2+\mathbf{k^2}+m^2\right] \\ &= -2\mu^{2\epsilon}T\sum_{n=-\infty}^{n=\infty}\int\frac{d^3\mathbf{k}}{(2\pi)^3}[\log\{(n\pi T)^2+\mathbf{k^2}+m^2\} \\ &\qquad -\log\{(2n\pi T)^2+\mathbf{k^2}+m^2\}] \\ &= -2\mu^{2\epsilon}2\frac{T}{2}\sum_{n=-\infty}^{n=\infty}\int\frac{d^3\mathbf{k}}{(2\pi)^3}\log\{(2n\pi\frac{T}{2})^2+\mathbf{k^2}+m^2\} \\ &\quad +2\mu^{2\epsilon}T\sum_{n=-\infty}^{n=\infty}\int\frac{d^3\mathbf{k}}{(2\pi)^3}\log\{(2n\pi T)^2+\mathbf{k^2}+m^2\} \\ &= -8J_0(m;\frac{T}{2})+4J_0(m;T). \end{aligned} \tag{A.8}$$

We write down a few first term explicitly,

$$I_0(m) = -\frac{7\pi^2T^4}{180}+\frac{m^2T^2}{12}+\frac{m^4}{16\pi^2}(\frac{1}{\epsilon}+\log\frac{4\mu^2}{\pi T^2}+\epsilon\gamma_E). \tag{A.9}$$

The high temperature expansion of the other I_n can be calculated by derivating this. We notice that this does not have the third term with respect to m due to the absence of the zero mode.

Appendix B

Conversion of the summation form to the integration form

In the present appendix, we convert the summation of a loop at finite temperature to the integration. While we take an example,

$$V^{(1)} = \frac{T}{2}\sum_{n=-\infty}^{\infty}\int\frac{d^3k}{(2\pi)^3}\log\{(2\pi nT)^2+\mathbf{k}^2+m^2\}, \tag{B.1}$$

we can apply to the other summation straitforwardly.

We first consider sum of a general function $f(i\omega_n)$,

$$I = T\sum_{n=-\infty}^{\infty}f(i\omega_n) \qquad (\omega_n = 2\pi nT). \tag{B.2}$$

Using the residue theorem, we can convert this summation to the integral,

$$I = \sum_{c_i}\frac{T}{2\pi i}\oint_{c_i}dp_0 f(p_0)\frac{1}{2T}\coth\frac{p_0}{2T} \tag{B.3}$$

Here, the integration path is taken as Fig.B.1(a). If we assume regularity of $f(p_0)$ around the imaginary axis like Eq.(B.1), it can be converted further,

$$\begin{aligned} I = &\frac{1}{2\pi i}\int_{i\infty-\epsilon}^{-i\infty-\epsilon}dp_0 f(p_0)\{-\frac{1}{2}-\frac{1}{\exp(-\beta p_0)-1}\} \\ &+\frac{1}{2\pi i}\int_{-i\infty+\epsilon}^{i\infty+\epsilon}dp_0 f(p_0)\{\frac{1}{2}+\frac{1}{\exp(\beta p_0)-1}\}. \end{aligned} \tag{B.4}$$

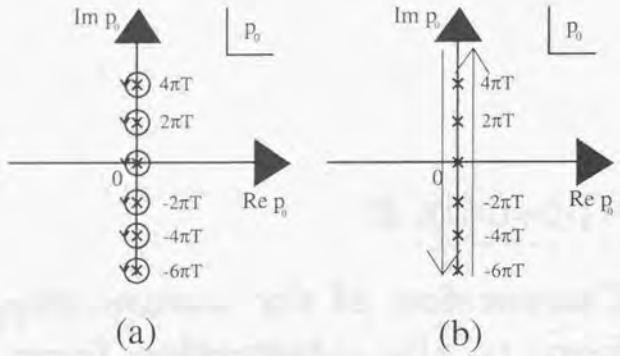

Figure B.1: (a)Integration path in Eq.(B.3) (b)The integration path is changed from (a) to the simpler one by the Causy's theorem.

Here, we take the path as Fig.B.1(b). Changing the integration variable as $p_0^{'} = -p_0$, we have,

$$I = T\sum_{n=-\infty}^{\infty} f(i\omega_n) = \frac{1}{2\pi i}\int_{-i\infty}^{i\infty} dp_0 \frac{1}{2}\{f(p_0)+f(-p_0)\} + \frac{1}{2\pi i}\int_{-i\infty+\epsilon}^{i\infty+\epsilon} dp_0\{f(p_0)+f(-p_0)\}\frac{1}{\exp(\beta p_0)-1}. \quad \text{(B.5)}$$

Applying this identity to Eq.(B.1), we have,

$$\begin{aligned} V^{(1)} &= V_0^{(1)} + V_T^{(1)} \\ V_0^{(1)} &= -\frac{i}{2}\int_{-i\infty}^{i\infty}\frac{dp_0}{2\pi}\int\frac{d^3\mathbf{p}}{(2\pi)^3}\log(-p^2+m^2) \quad \text{(B.6)} \\ V_T^{(1)} &= -i\int_{-i\infty+\epsilon}^{i\infty+\epsilon}\frac{dp_0}{2\pi}\int\frac{d^3\mathbf{p}}{(2\pi)^3}\frac{1}{\exp(\beta p_0)-1}\log(-p^2+m^2). \end{aligned}$$

We next convert the integral, $V_0^{(1)}$ to a simpler form. We rewrite $V_0^{(1)}$ as follows,

$$V_T^{(1)} = -i\int_{-i\infty+\epsilon}^{i\infty+\epsilon}\frac{dp_0}{2\pi}\int\frac{d^3\mathbf{p}}{(2\pi)^3}\frac{1}{\exp(\beta p_0)-1}\{\log(-p_o+\sqrt{\omega_{\mathbf{p}}^2})+\log(p_o+\sqrt{\omega_{\mathbf{p}}^2})\} \quad (\omega_{\mathbf{p}}^2 \equiv \mathbf{p}^2+m^2). \quad \text{(B.7)}$$

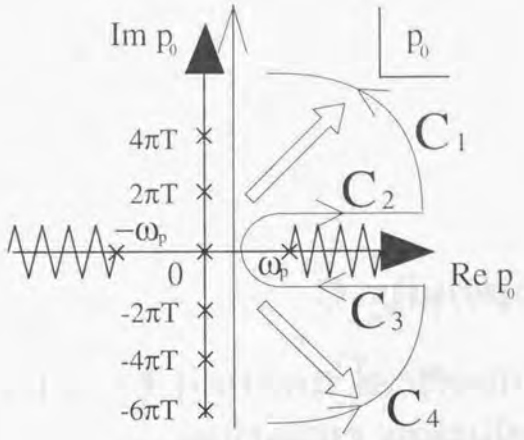

Figure B.2: The integration path is changed by the Causy's theorem.

Defining that the branch cut of $\log x$ locates along the negative real axis, we can change the integration path as Fig.B.2. We have contribution only from the difference C_2 and C_3 and obtain,

$$\begin{aligned} V_T^{(1)} &= -i\int\frac{d^3\mathbf{p}}{(2\pi)^3}(-2\pi i)\int_{\sqrt{\omega_{\mathbf{p}}^2}}^{\infty}\frac{dp_0}{2\pi}\frac{\exp(-\beta p_0)}{1-\exp(-\beta p_0)} \\ &= T\int\frac{d^3\mathbf{p}}{(2\pi)^3}\log\{1-\exp(-\frac{1}{T}\sqrt{\mathbf{p}^2+m^2})\} \\ &= \frac{T}{2\pi^2}\int_0^{\infty} dr\ r^2\ \log\{1-\exp(-\frac{1}{T}\sqrt{r^2+m^2})\} \quad \text{(B.8)} \end{aligned}$$

Appendix C

Numerical method to solve the evolution equation

The numerical method, which we use to solve the partial differential equations in the present paper like Eq.(4.20), is explained in this appendix. Such partial differential equations can be written as follows,

$$\frac{\partial V}{\partial m^2} = \frac{1}{2}\vec{\phi}^2 + f(\frac{\partial^2 V}{\partial \phi^2}). \tag{C.1}$$

Here, $f(x)$ is some function like the integral in Eq.(4.20). First, we make a lattice shown in Fig.C.1. The partial differential equations are, then, differenced as follows [116],

$$\begin{aligned}\frac{V_{i,j+1} - Vi,j}{\Delta m^2} &= \frac{1}{2}\phi_i^2 + f\left(\alpha(\frac{V_{i+1,j+1} - 2V_{i,j+1} + V_{i-1,j+1}}{(\Delta\phi)^2}\right. \\ &\left. +(1-\alpha)(\frac{V_{i+1,j} - 2V_{i,j} + V_{i-1,j}}{(\Delta\phi)^2})\right). \end{aligned}\tag{C.2}$$

The parameter α decides where the Laplacian $\frac{\partial^2 V}{\partial \phi^2}$ is evaluated. If $\alpha = 0$ is chosen, the Laplacian is evaluated at (a) in Fig.C.1. The method with this choice is called the explicit method. This method is simple, because $V_{x,j+1}$ is determined only by substituting $V_{x,j}$ into the right hand side. It, however, suffers from the numerical instability, when smaller mesh size$\Delta\phi$ is chosen [116]. If $\alpha = 1$ is chosen, the Laplacian is evaluated at (b) in Fig.C.1. The method with this choice is called the implicit method, which does not suffer

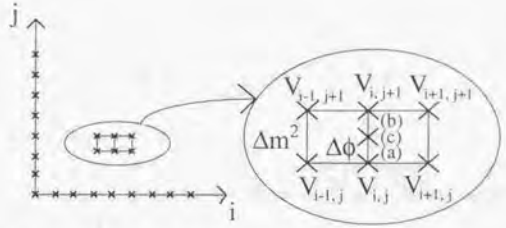

Figure C.1: Lattice used to difference the partial differential equations.

from the numerical instability at least if f(x) is a linear function [116] — as far as we know, when $f(x)$ is not linear function like our case, not many things are known— . If $\alpha = 1/2$ is chosen, the Laplacian is evaluated at (c) in Fig.C.1. The method with this choice is called the Crank-Nicholson method, which also does not suffer from the numerical instability at least if f(x) is a linear function. What is more, the result converges rapidly with decreasing Δm^2 using this method [116]. Both the implicit and the Crank-Nicholson method, however, requires us to solve coupled non-linear equation (C.2); this prevents us from using established method in the case $f(x) = x$.

We developed two methods in order to overcome this difficulty. First method is based on the Taylor expansion of $f(x)$. The equation (C.2) is rewritten as follows,

$$\begin{aligned}\frac{V_{i,j+1} - V_{i,j}}{\Delta m^2} &= \frac{1}{2}\phi_i^2 + f\left(\frac{V_{i+1,j} - 2V_{i,j} + V_{i-1,j}}{(\Delta\phi)^2}\right. \\ &\left. +\alpha(\frac{V_{i+1,j+1} - 2V_{i,j+1} + V_{i-1,j+1}}{(\Delta\phi)^2} - \frac{V_{i+1,j} - 2V_{i,j} + V_{i-1,j}}{(\Delta\phi)^2})\right)\end{aligned}\tag{C.3}$$

Since the quantity in the bracket behind α is the variation of the Laplacian per one step, it is small if Δm^2 is sufficiently small. We, then, expand $f(x)$

around $\frac{V_{i+1,j}-2V_{i,j}+V_{i-1,j}}{(\Delta\phi)^2}$.

$$\begin{aligned}\frac{V_{i,j+1}-V_{i,j}}{\Delta m^2} &= \frac{1}{2}\phi_i^2 + f\left(\frac{V_{i+1,j}-2V_{i,j}+V_{i-1,j}}{(\Delta\phi)^2}\right) \\ &+\alpha\left(\frac{V_{i+1,j+1}-2V_{i,j+1}+V_{i-1,j+1}}{(\Delta\phi)^2} - \frac{V_{i+1,j}-2V_{i,j}+V_{i-1,j}}{(\Delta\phi)^2}\right) \\ &\times f'\left(\frac{V_{i+1,j}-2V_{i,j}+V_{i-1,j}}{(\Delta\phi)^2}\right) + \textit{higher order terms} \quad \text{(C.4)}\end{aligned}$$

This coupled equation is linear with respect to $V_{x,j+1}$ and can be solved easily [116].

The second method is based on an iteration. In order to solve equation (C.2), we iterate as follows until a solution is found,

$$\begin{aligned}\frac{V_{i,j+1}^{n+1}-V_{i,j}}{\Delta m^2} &= \frac{1}{2}\phi_i^2 + f\left(\alpha\left(\frac{V_{i+1,j+1}^{n+1}-2V_{i,j+1}^{n}+V_{i-1,j+1}^{n}}{(\Delta\phi)^2}\right.\right. \\ &\left.\left.+(1-\alpha)\left(\frac{V_{i+1,j}-2V_{i,j}+V_{i-1,j}}{(\Delta\phi)^2}\right)\right)\right. \quad \text{(C.5)}\end{aligned}$$

Here, n is the number of the iteration. Note that we can not replace $V_{i,j+1}^{n}$ with $V_{i,j+1}^{n+1}$ unlike the Gauss-Seidel method, which is a powerful method if $f(x)$ is a linear function [116]. Next, relaxation method is used in order to improve the convergence [116]. Since this procedure is identical with the linear case, we only write down the iteration equation without an explanation.

$$\begin{aligned}\frac{V_{i,j+1}^{n+1}-V_{i,j}}{\Delta m^2} &= \omega\left(\frac{1}{2}\phi_i^2 + f\left(\alpha\left(\frac{V_{i+1,j+1}^{n+1}-2V_{i,j+1}^{n}+V_{i-1,j+1}^{n}}{(\Delta\phi)^2}\right.\right.\right. \\ &\left.\left.\left.+(1-\alpha)\left(\frac{V_{i+1,j}-2V_{i,j}+V_{i-1,j}}{(\Delta\phi)^2}\right)\right)\right)\right. \\ &+(1-\omega)V_{i,j}^{n}. \quad \text{(C.6)}\end{aligned}$$

Here, the relaxation parameter ω is determined only by experience. The results by the two methods agree greatly.

Appendix D

Details of the derivative expansion

In this appendix, we show the derivation of $\partial\Gamma/\partial m^2$ in detail. Some notations are given in the Ch.6. The effective action, $\Gamma[\phi_c]$ for the Lagrangian Eq.(4.30) is defined as usual,

$$\begin{aligned}Z[J_m] &\equiv \int \mathcal{D}[\phi]\exp\left(\int d^4x\mathcal{L}_E\right), \\ W[J_m] &\equiv \log(Z[J_m]), \\ \Gamma[\phi_c] &\equiv W[J_m] - \int d^4x J_m(x)\phi_c(x). \quad \text{(D.1)}\end{aligned}$$

The equation(6.1) is, then, derived as follows,

$$\begin{aligned}\frac{\partial\Gamma[\phi_c]}{\partial m^2} &= \frac{1}{Z[J_m]}\int\mathcal{D}[\phi]\left[\int\left\{d^4x\frac{1}{2}(-\phi(x)^2)+\frac{\partial J_m(x)}{\partial m^2}\phi(x)\right\}\exp\left\{\int d^4x\mathcal{L}_E\right\}\right] \\ &\quad -\int d^4x\frac{\partial J_m(x)}{\partial m^2}\phi_c(x) \\ &= -\frac{1}{2}\int d^4x <\phi(x)^2> \\ &= -\frac{1}{2}\int d^4x\ \phi_c(x)^2 - \frac{1}{2}\int d^4x(M)^{-1}_{xx}. \quad \text{(D.2)}\end{aligned}$$

This equation can not be solved exactly. We, therefore, limit the functional space and expand $\Gamma[\phi_c]$ in powers of derivatives [59, 115], (see Eq.(6.2))

$$\Gamma[\phi_c] = \int d^4x\left[-V(\phi_c^2) - \frac{1}{2}K_0(\phi_c^2)(\partial_0\phi_c)^2 - \frac{1}{2}K_s(\phi_c^2)(\nabla\phi_c)^2 + \cdots\right],$$

where "$\cdots$" denotes terms with higher derivative which are omitted here and equating the coefficient functionals of $(\partial\phi_c)$ in the both side of Eq.(6.1).

The left hand side of Eq.(D.2) is calculated to be Eq.(6.3) by simply differentiating Γ with respect to m^2,

$$-\frac{\partial\Gamma}{\partial m^2} = \int d^4x \left[\frac{\partial V}{\partial m^2} + \frac{1}{2}\frac{\partial K_0}{\partial m^2}(\partial_0\phi_c)^2 + \frac{1}{2}\frac{\partial K_s}{\partial m^2}(\nabla\phi_c)^2\right].$$

It is very complicated to calculate r.h.s. of Eq.(D.2). First, we calculate M_{yx}. The derivative of the effective action, $\Gamma[\phi_c]$ with respect to, $\phi_c(x)$ is,

$$\begin{aligned}\frac{\delta\Gamma[\phi_c]}{\delta\phi_c(x)} = & - V'(\phi_c(x)) \\ & + \frac{1}{2}K_0'(\phi_c(x))(\partial_0\phi_c(x))^2 + K_0(\phi_c(x))(\partial_0^2\phi_c(x)) \\ & + \{K_0 \leftrightarrow K_s, \partial_0 \leftrightarrow \nabla\}.\end{aligned} \tag{D.3}$$

Here, we assume that we can make a partial integral freely without a surface term.

We define the operator, M_{xy} as the following. An operator O_{xy} defined through functional derivative with respect to $\phi(x)$, say $\delta F(\phi(y))/\delta\phi(x)$, acts on any appropriate test function, say $T(y)$,

$$OT(x) \equiv \int d^4y \left\{\frac{\delta}{\delta\phi(x)}F(\phi(y))\right\}T(y).$$

In particular, if $F(\phi(y))$ contains the derivative of $\phi(y)$, say $F(\phi(y)) = G(\phi(y))\partial\phi(y)$,

$$\begin{aligned}OT(x) &\equiv \int d^4y \left\{\frac{\delta}{\delta\phi(x)}G(\phi(y))\partial\phi(y)\right\}T(y). \\ &\equiv \int d^4y\delta(y-x)\left[G'(\phi(y))\partial\phi(y)T(y) - \partial\left\{G(\phi(y))T(y)\right\}\right]\end{aligned} \tag{D.4}$$

In order to obtain Eq.(6.4) and to determine the inverse of M_{yx} around $\bar{\phi}$, we divide the Eq.(6.4) into two pieces (Eq.(6.6)),

$$\begin{aligned}M_{yx} &= A_{yx} - B_{yx}, \\ A_{yx} &= \delta(y-x)(-\overline{K}_0\partial_0^2 - \overline{K}_s\nabla^2 + \overline{V}''),\end{aligned}$$

$$\begin{aligned}B_{yx} = & -\delta(y-x)\left[\widetilde{V}''(\phi_c(y))\right. \\ & - \left\{\frac{1}{2}K_0''(\phi_c(y))(\partial_0\phi_c(y))^2 + K_0'(\phi_c(y))\partial_0\phi_c(y)\partial_{y_0}\right. \\ & + \left.\left. K_0'(\phi_c(y))\partial_0^2\phi_c(y) + \widetilde{K}_0(\phi_c(y))\partial_{y_0}^2\right\}\right. \\ & \left. - \{K_0 \leftrightarrow K_s, \partial_{y_0} \leftrightarrow \nabla_y\}\right].\end{aligned}$$

The inverse of M_{yx} is, then, expanded as,

$$(M^{-1})_{xy} = \{(A^{-1})(\sum_{n=0}^{n=\infty}(BA^{-1})^n)\}_{xy}. \tag{D.5}$$

Here, the multiplication of the "matrix" A and B is taken as the following,

$$(AB)_{xy} = \int d^4z A_{xz}B_{zy}.$$

The inverse of A_{xy} is calculated easily,

$$(A^{-1})_{xy} = \int_p \frac{1}{\nu_p}\exp\{ip(x-y)\}, \tag{D.6}$$

where $\nu_p = \overline{K}_0p_0^2 + \overline{K}_s\mathbf{p}^2 + \overline{V}''$.

We need terms with $(\partial\phi_c)^n$ for n=0,2 to evaluate r.h.s of Eq.(D.2). Such terms are contained only in the first three terms in Eq.(D.5),

$$\begin{aligned}(M^{-1})_{xy} = & (A^{-1})_{xy} \\ & + (A^{-1}BA^{-1})_{xy} \\ & + (A^{-1}BA^{-1}BA^{-1})_{xy}.\end{aligned} \tag{D.7}$$

The relevant terms in Eq.(D.2) are, therefore, the following,

$$\int d^4x(M^{-1})_{xx} = \int d^4x(A^{-1})_{xx} \tag{D.8}$$

$$+ \int d^4x(A^{-1}BA^{-1})_{xx} \tag{D.9}$$

$$+ \int d^4x(A^{-1}BA^{-1}BA^{-1})_{xx}. \tag{D.10}$$

We next calculate Eq.(D.8)-(D.10) up to terms with the second derivative of $\phi_c(x)$. From Eq.(D.6) the first term (D.8) is easy to calculate,

$$\int d^4x(A^{-1})_{xx} = \int d^4x \int_p \frac{1}{\nu_p}. \tag{D.11}$$

The second term in Eq.(D.9) is

$$
\begin{aligned}
& \int d^4x (A^{-1}BA^{-1})_{xx} \\
= & \int d^4x \int d^4y \int d^4z \int_p \frac{1}{\nu_p} \exp\{ip(x-y)\} \\
& \delta(y-z)\Big[-\tilde{V}''(\phi_c(y)) + \Big\{\frac{1}{2}K_0''(\phi_c(y))(\partial_0\phi_c(y))^2 + K_0'(\phi_c(y))\partial_0\phi_c(y)\partial_{y_0} \\
& + K_0'(\phi_c(y))\partial_0^2\phi_c(y) + \tilde{K}_0(\phi_c(y))\partial_{y_0}^2\Big\} + \{K_0 \leftrightarrow K_s, \partial_{y_0} \leftrightarrow \nabla_y\}\Big] \\
& \int_q \frac{1}{\nu_q} \exp\{iq(z-x)\} \\
& \text{(integrating over } z.) \\
= & \int d^4x \int d^4y \int_p \int_q \frac{1}{\nu_p}\frac{1}{\nu_q} \exp\{ip(x-y)\} \exp\{iq(y-x)\} \\
& \Big[-\tilde{V}''(\phi_c(y)) + \Big\{\frac{1}{2}K_0''(\phi_c(y))(\partial_0\phi_c(y))^2 + K_0'(\phi_c(y))\partial_0\phi_c(y) iq_0 \\
& + K_0'(\phi_c(y))\partial_0^2\phi_c(y) - \tilde{K}_0(\phi_c(y))q_0^2\Big\} + \{K_0 \leftrightarrow K_s, \partial_0 \leftrightarrow \nabla, q_0 \leftrightarrow \mathbf{q}\}\Big] \\
& \text{(integrating over } x \text{ and } q \text{ then replacing } y \text{ by } x.) \\
= & \int d^4x \int_p \frac{1}{\nu_p^2} \\
& \Big[-\tilde{V}''(\phi_c(x)) + \Big\{\frac{1}{2}K_0''(\phi_c(x))(\partial_0\phi(x))^2 + K_0'(\phi_c(x))\partial_0\phi(x) ip_0 \\
& + K_0'(\phi_c(x))\partial_0^2\phi(x) - \tilde{K}_0(\phi_c(x))p_0^2\Big\} + \{K_0 \leftrightarrow K_s, \partial_0 \leftrightarrow \nabla, p_0 \leftrightarrow \mathbf{p}\}\Big] \\
& \text{(partially integrating the fourth term.)} \\
= & \int d^4x \int_p \frac{1}{\nu_p^2}\Big[-\tilde{V}''(\phi_c(x)) - \Big\{\frac{1}{2}K_0''(\phi_c(x))(\partial_0\phi_c(x))^2 + \tilde{K}_0(\phi_c(x))p_0^2\Big\} \\
& - \{K_0 \leftrightarrow K_s, \partial_0 \leftrightarrow \nabla, p_0 \leftrightarrow \mathbf{p}\}\Big]. \\
= & \int d^4x \int_p \frac{1}{\nu_p^2}\Big[-\Big\{\frac{1}{2}\overline{K}_0''(\partial_0\phi_c)^2 + \frac{1}{2}\overline{K}_s''(\nabla\phi_c)^2\Big\}\Big] \\
& + (\textit{terms which vanish at } \phi_c(x) = \bar{\phi} \textit{ like } \tilde{V}'' \times (\textit{something})). \qquad \text{(D.12)}
\end{aligned}
$$

Since we set $\phi_c(x) = \bar{\phi}$ after the matching of Eq.(6.1), we have no contribution to the evolution equation from the terms which vanish at $\phi_c(x) = \bar{\phi}$. We thus

leave only terms which remain finite at $\phi_c(x) = \bar{\phi}$ from now on. The third term (D.10) is very complicated to evaluate,

$$
\begin{aligned}
& \int d^4x (A^{-1}BA^{-1}BA^{-1})_{xx} \\
= & \int d^4x \int d^4y \int d^4z \int d^4u \int d^4v \int_p \frac{1}{\nu_p} \exp\{ip(x-y)\} \\
& \delta(y-z)\Big[-\tilde{V}''(\phi_c(y)) + \Big\{\frac{1}{2}K_0''(\phi_c(y))(\partial_0\phi_c(y))^2 + K_0'(\phi_c(y))\partial_0\phi_c(y)\partial_{y_0} \\
& + K_0'(\phi_c(y))\partial_0^2\phi_c(y) + \tilde{K}_0(\phi_c(y))\partial_{y_0}^2\Big\} + \{K_0 \leftrightarrow K_s, \partial_{y_0} \leftrightarrow \nabla_y\}\Big] \\
& \int_q \frac{1}{\nu_q} \exp\{iq(z-u)\} \\
& \delta(u-v)\Big[-\tilde{V}''(\phi_c(u)) + \Big\{\frac{1}{2}K_0''(\phi_c(u))(\partial_0\phi_c(u))^2 + K_0'(\phi_c(u))\partial_0\phi_c(u)\partial_{u_0} \\
& + K_0'(\phi_c(u))\partial_0^2\phi_c(u) + \tilde{K}_0(\phi_c(u))\partial_{u_0}^2\Big\} + \{K_0 \leftrightarrow K_s, \partial_{u_0} \leftrightarrow \nabla_u\}\Big] \\
& \int_r \frac{1}{\nu_r} \exp\{ir(v-x)\} \\
& \text{(integrating over } x, z, v, r \text{ and replacing } u \text{ with } x) \\
= & \int d^4x \int d^4y \int_p \int_q \frac{1}{\nu_p^2}\frac{1}{\nu_q} \exp\{i(p-q)(x-y)\} \\
& \Big[-\tilde{V}''(\phi_c(x)) + \Big\{\frac{1}{2}K_0''(\phi_c(x))(\partial_0\phi_c(x))^2 + K_0'(\phi_c(x))\partial_0\phi_c(x) ip_0 \\
& + K_0'(\phi_c(x))\partial_0^2\phi_c(x) - \tilde{K}_0(\phi_c(x))p_0^2\Big\} + \{K_0 \leftrightarrow K_s, \partial_0 \leftrightarrow \nabla, p_0 \leftrightarrow \mathbf{p}\}\Big] \\
\times & \Big[-\tilde{V}''(\phi_c(y)) + \Big\{\frac{1}{2}K_0''(\phi_c(y))(\partial_0\phi_c(y))^2 + K_0'(\phi_c(y))\partial_0\phi_c(y) iq_0 \\
& + K_0'(\phi_c(y))\partial_0^2\phi_c(y) - \tilde{K}_0(\phi_c(y))q_0^2\Big\} + \{K_0 \leftrightarrow K_s, \partial_0 \leftrightarrow \nabla, q_0 \leftrightarrow \mathbf{q}\}\Big]. \\
& \text{(partially integrating the term with } \partial_0^2\phi.) \\
= & \int d^4x \int d^4y \int_p \int_q \frac{1}{\nu_p^2}\frac{1}{\nu_q} \exp\{i(p-q)(x-y)\} \\
& \Big[-\tilde{V}''(\phi_c(x)) + \Big\{-\frac{1}{2}K_0''(\phi_c(x))(\partial_0\phi_c(x))^2 + K_0'(\phi_c(x))\partial_0\phi_c(x) iq_0 \\
& - \tilde{K}_0(\phi_c(x))p_0^2\Big\} + \{K_0 \leftrightarrow K_s, \partial_0 \leftrightarrow \nabla, p_0 \leftrightarrow \mathbf{p}, q_0 \leftrightarrow \mathbf{q}\}\Big] \\
\times & \Big[-\tilde{V}''(\phi_c(y)) + \Big\{-\frac{1}{2}K_0''(\phi_c(y))(\partial_0\phi_c(y))^2 + K_0'(\phi_c(y))\partial_0\phi_c(y) ip_0
\end{aligned}
$$

$$- \tilde{K}_0(\phi_c(y))q_0^2\Big\} + \{K_0 \leftrightarrow K_s, \partial_0 \leftrightarrow \nabla, p_0 \leftrightarrow \mathbf{p}, q_0 \leftrightarrow \mathbf{q}\}\Big] .$$

By the following variable exchange,

$$\begin{cases} p & \longrightarrow & p+q \\ q & \longrightarrow & p \end{cases} ,$$

we obtain,

$$\begin{aligned}
&= \int d^4x \int d^4y \int_p \int_q \frac{1}{\nu_{p+q}^2} \frac{1}{\nu_p} \exp\{iq(x-y)\} \\
&\Big[-\tilde{V}''(\phi_c(x)) + \Big\{-\frac{1}{2}K_0'''(\phi_c(x))(\partial_0\phi_c(x))^2 + K_0''(\phi_c(x))\partial_0\phi_c(x)ip_0 \\
&- \tilde{K}_0(\phi_c(x))(p+q)_0^2\Big\} + \{K_0 \leftrightarrow K_s, \partial_0 \leftrightarrow \nabla, p_0 \leftrightarrow \mathbf{p}, q_0 \leftrightarrow \mathbf{q}\}\Big] \\
\times &\Big[-\tilde{V}''(\phi_c(y)) + \Big\{-\frac{1}{2}K_0'''(\phi_c(y))(\partial_0\phi_c(y))^2 + K_0''(\phi_c(y))\partial_0\phi_c(y)i(p+q)_0 \\
&- \tilde{K}_0(\phi_c(y))p_0^2\Big\} + \{K_0 \leftrightarrow K_s, \partial_0 \leftrightarrow \nabla, p_0 \leftrightarrow \mathbf{p}, q_0 \leftrightarrow \mathbf{q}\}\Big] . \\
&= \int d^4x \int d^4y \int_p \int_q \frac{\exp\{iq(x-y)\}}{\nu_p^3} \qquad \text{(D.13)} \\
&\left\{1 - \frac{\left\{\overline{K}_0(4p_0q_0 + 2q_0^2) + \overline{K}_s(4\mathbf{pq} + 2\mathbf{q}^2)\right\}}{\nu_p} + \frac{12\left\{\overline{K}_0p_0q_0 + \overline{K}_s\mathbf{pq}\right\}^2}{\nu_p^2} + \cdots\right\} \\
&\Big[-\tilde{V}''(\phi_c(x)) + \Big\{-\frac{1}{2}K_0'''(\phi_c(x))(\partial_0\phi_c(x))^2 + K_0''(\phi_c(x))\partial_0\phi_c(x)ip_0 \\
&- \tilde{K}_0(\phi_c(x))(p+q)_0^2\Big\} + \{K_0 \leftrightarrow K_s, \partial_0 \leftrightarrow \nabla, p_0 \leftrightarrow \mathbf{p}, q_0 \leftrightarrow \mathbf{q}\}\Big] \\
\times &\Big[-\tilde{V}''(\phi_c(y)) + \Big\{-\frac{1}{2}K_0'''(\phi_c(y))(\partial_0\phi_c(y))^2 + K_0''(\phi_c(y))\partial_0\phi_c(y)i(p+q)_0 \\
&- \tilde{K}_0(\phi_c(y))p_0^2\Big\} + \{K_0 \leftrightarrow K_s, \partial_0 \leftrightarrow \nabla, p_0 \leftrightarrow \mathbf{p}, q_0 \leftrightarrow \mathbf{q}\}\Big] ,
\end{aligned}$$

where we take the terms up to q^2 since we will replace q to the derivative and need terms with second derivatives. Similarly, by the following exchange of the variables,

$$\begin{cases} p & \longrightarrow & p \\ q & \longrightarrow & p+q \end{cases} ,$$

we have,

$$\begin{aligned}
&= \int d^4x \int d^4y \int_p \int_q \frac{1}{\nu_{p+q}} \frac{1}{\nu_p^2} \exp\{iq(x-y)\} \\
&\Big[-\tilde{V}''(\phi_c(x)) + \Big\{-\frac{1}{2}K_0'''(\phi_c(x))(\partial_0\phi_c(x))^2 + K_0''(\phi_c(x))\partial_0\phi_c(x)ip_0 \\
&- \tilde{K}_0(\phi_c(x))(p+q)_0^2\Big\} + \{K_0 \leftrightarrow K_s, \partial_0 \leftrightarrow \nabla, p_0 \leftrightarrow \mathbf{p}, q_0 \leftrightarrow \mathbf{q}\}\Big] \\
\times &\Big[-\tilde{V}''(\phi_c(y)) + \Big\{-\frac{1}{2}K_0'''(\phi_c(y))(\partial_0\phi_c(y))^2 + K_0''(\phi_c(y))\partial_0\phi_c(y)i(p+q)_0 \\
&- \tilde{K}_0(\phi_c(y))p_0^2\Big\} + \{K_0 \leftrightarrow K_s, \partial_0 \leftrightarrow \nabla, p_0 \leftrightarrow \mathbf{p}, q_0 \leftrightarrow \mathbf{q}\}\Big] . \\
&= \int d^4x \int d^4y \int_p \int_q \frac{\exp\{iq(x-y)\}}{\nu_p^3} \qquad \text{(D.14)} \\
&\left\{1 - \frac{\left\{\overline{K}_0(2p_0q_0 + q_0^2) + \overline{K}_s(2\mathbf{pq} + \mathbf{q}^2)\right\}}{\nu_p} + \frac{4\left\{\overline{K}_0p_0q_0 + \overline{K}_s\mathbf{pq}\right\}^2}{\nu_p^2} + \cdots\right\} \\
&\Big[-\tilde{V}''(\phi_c(x)) + \Big\{-\frac{1}{2}K_0'''(\phi_c(x))(\partial_0\phi_c(x))^2 + K_0''(\phi_c(x))\partial_0\phi_c(x)ip_0 \\
&- \tilde{K}_0(\phi_c(x))(p+q)_0^2\Big\} + \{K_0 \leftrightarrow K_s, \partial_0 \leftrightarrow \nabla, p_0 \leftrightarrow \mathbf{p}, q_0 \leftrightarrow \mathbf{q}\}\Big] \\
\times &\Big[-\tilde{V}''(\phi_c(y)) + \Big\{-\frac{1}{2}K_0'''(\phi_c(y))(\partial_0\phi_c(y))^2 + K_0''(\phi_c(y))\partial_0\phi_c(y)i(p+q)_0 \\
&- \tilde{K}_0(\phi_c(y))p_0^2\Big\} + \{K_0 \leftrightarrow K_s, \partial_0 \leftrightarrow \nabla, p_0 \leftrightarrow \mathbf{p}, q_0 \leftrightarrow \mathbf{q}\}\Big] .
\end{aligned}$$

By comparing Eq.(D.13) with Eq.(D.14), we have the following "identity",

$$\begin{aligned}
0 &= \int d^4x \int d^4y \int_p \int_q \frac{\exp\{iq(x-y)\}}{\nu_p^3} \qquad \text{(D.15)} \\
&\left\{-\frac{\left\{\overline{K}_0(2p_0q_0 + q_0^2) + \overline{K}_s(2\mathbf{pq} + \mathbf{q}^2)\right\}}{\nu_p} + \frac{8\left\{\overline{K}_0p_0q_0 + \overline{K}_s\mathbf{pq}\right\}^2}{\nu_p^2} + \cdots\right\} \\
&\Big[-\tilde{V}''(\phi_c(x)) + \Big\{-\frac{1}{2}K_0'''(\phi_c(x))(\partial_0\phi_c(x))^2 + K_0''(\phi_c(x))\partial_0\phi_c(x)ip_0 \\
&- \tilde{K}_0(\phi_c(x))(p+q)_0^2\Big\} + \{K_0 \leftrightarrow K_s, \partial_0 \leftrightarrow \nabla, p_0 \leftrightarrow \mathbf{p}, q_0 \leftrightarrow \mathbf{q}\}\Big] \\
\times &\Big[-\tilde{V}''(\phi_c(y)) + \Big\{-\frac{1}{2}K_0'''(\phi_c(y))(\partial_0\phi_c(y))^2 + K_0''(\phi_c(y))\partial_0\phi_c(y)i(p+q)_0 \\
&- \tilde{K}_0(\phi_c(y))p_0^2\Big\} + \{K_0 \leftrightarrow K_s, \partial_0 \leftrightarrow \nabla, p_0 \leftrightarrow \mathbf{p}, q_0 \leftrightarrow \mathbf{q}\}\Big] .
\end{aligned}$$

Indeed, this identity holds exactly for the coefficient functions of $(\nabla\phi_c)^2$, though it is not the case for that of $(\partial_0\phi_c)^2$. Anyway, we use this identity and rewrite (or define) the third term (D.10) in the following,

$$
\begin{aligned}
&\int d^4x (A^{-1}BA^{-1}BA^{-1})_{xx} \\
&= \int d^4x \int d^4y \int_p \int_q \frac{\exp\{iq(x-y)\}}{\nu_p^3} \\
&\quad \left\{1 - \frac{1}{2}\frac{\left\{\overline{K}_0(2p_0q_0+q_0^2)+\overline{K}_s(2\mathbf{pq}+\mathbf{q}^2)\right\}}{\nu_p} + \cdots\right\} \\
&\quad \left[-\tilde{V}''(\phi_c(x)) + \left\{-\frac{1}{2}K_0''(\phi_c(x))(\partial_0\phi_c(x))^2 + K_0'(\phi_c(x))\partial_0\phi_c(x)ip_0\right.\right. \\
&\quad \left.\left. - \tilde{K}_0(\phi_c(x))(p+q)_0^2\right\} + \{K_0 \leftrightarrow K_s, \partial_0 \leftrightarrow \nabla, p_0 \leftrightarrow \mathbf{p}, q_0 \leftrightarrow \mathbf{q}\}\right] \\
&\times \left[-\tilde{V}''(\phi_c(y)) + \left\{-\frac{1}{2}K_0''(\phi_c(y))(\partial_0\phi_c(y))^2 + K_0'(\phi_c(y))\partial_0\phi_c(y)i(p+q)_0\right.\right. \\
&\quad \left.\left. - \tilde{K}_0(\phi_c(y))p_0^2\right\} + \{K_0 \leftrightarrow K_s, \partial_0 \leftrightarrow \nabla, p_0 \leftrightarrow \mathbf{p}, q_0 \leftrightarrow \mathbf{q}\}\right].
\end{aligned}
\tag{D.16}
$$

Note that there is no contribution from Eq.(D.16) to the evolution equation for the effective potential, V since the constant terms always include $\tilde{K}$ and $\tilde{V}''$ which are zero at $\phi_c(x) = \bar{\phi}$ by the definition.

From now on, we evaluate the coefficient functions of $(\partial\phi_c(x))^2$. First we calculate the first term of Eq.(D.16). There are three contributions from this term,

$$
\begin{aligned}
&\int d^4x \int d^4y \int_p \int_q \frac{\exp\{iq(x-y)\}}{\nu_p^3} \\
&\left\{K_0'(\phi_c(x))\partial_0\phi_c(x)ip_0 + K_s'(\phi_c(x))\nabla\phi_c(x)i\mathbf{p}\right\} \\
&\times \left\{K_0'(\phi_c(y))\partial_0\phi_c(y)ip_0 + K_s'(\phi_c(y))\nabla\phi_c(y)i\mathbf{p}\right\} \\
&\text{(integrating over } q \text{ and } y.) \\
&= \int d^4x \int_p \frac{-1}{\nu_p^3}\left\{\overline{K}_0'(\partial_0\phi_c)p_0 + \overline{K}_s'(\nabla\phi_c)\mathbf{p}\right\}^2,
\end{aligned}
\tag{D.17}
$$

$$
\int d^4x \int d^4y \int_p \int_q \frac{\exp\{iq(x-y)\}}{\nu_p^3}
$$

$$
\begin{aligned}
&\left[\left\{K_0'(\phi_c(x))\partial_0\phi_c(x)iq_0 + K_s'(\phi_c(x))\nabla\phi_c(x)i\mathbf{q}\right\} \times \right. \\
&\qquad \left.\left\{-\tilde{K}_0(\phi_c(y))p_0^2 - \tilde{K}_s(\phi_c(y))\mathbf{p}^2 - V''(\phi_c(y))\right\}\right. \\
&+ 2\left\{K_0'(\phi_c(x))\partial_0\phi_c(x)ip_0 + K_s'(\phi_c(x))\nabla\phi_c(x)i\mathbf{p}\right\} \times \\
&\qquad \left.\left\{-\tilde{K}_0(\phi_c(y))p_0q_0 - \tilde{K}_s(\phi_c(y))\mathbf{pq}\right\}\right] \\
&= \int d^4x \int d^4y \int_p \int_q \frac{1}{\nu_p^3} \\
&\left[\left\{K_0'(\phi_c(x))\partial_0\phi_c(x)\partial_{x_0} + K_s'(\phi_c(x))\nabla\phi_c(x)\nabla_x\right\} \times \right. \\
&\qquad \left.\left\{-\tilde{K}_0(\phi_c(y))p_0^2 - \tilde{K}_s(\phi_c(y))\mathbf{p}^2 - V''(\phi_c(y)\right\}\right. \\
&+ 2\left\{K_0'(\phi_c(x))\partial_0\phi_c(x)ip_0 + K_s'(\phi_c(x))\nabla\phi_c(x)i\mathbf{p}\right\} \times \\
&\qquad \left.\left\{\tilde{K}_0(\phi_c(y))ip_0\partial_{x_0} + \tilde{K}_s(\phi_c(y))i\mathbf{p}\nabla_x\right\}\right] \\
&\times \exp\{iq(x-y)\} \\
&\text{(partially integrating over x and then integrating over } q \text{ and } y.) \\
&= \int d^4x \int_p \frac{1}{\nu_p^3}\left[\left\{\overline{K}_0'(\partial_0\phi_c)^2 + \overline{K}_s'(\nabla\phi_c)^2\right\}\left\{\overline{K}_0'p_0^2 + \overline{K}_s'\mathbf{p}^2 + \overline{V}''\right\}\right. \\
&\left. +2\left\{\overline{K}_0'(\partial_0\phi_c)p_0 + \overline{K}_s'(\nabla\phi_c)\mathbf{p}\right\}^2\right],
\end{aligned}
\tag{D.18}
$$

and

$$
\begin{aligned}
&\int d^4x \int d^4y \int_p \int_q \frac{\exp\{iq(x-y)\}}{\nu_p^3} \\
&\left[\left\{-\tilde{K}_0(\phi_c(x))q_0^2 - \tilde{K}_s(\phi_c(x))\mathbf{q}^2\right\} \times \right. \\
&\qquad \left.\left\{-\tilde{K}_0(\phi_c(y))p_0^2 - \tilde{K}_s(\phi_c(y))\mathbf{p}^2 - V''(\phi_c(y))\right\}\right] \\
&= \int d^4x \int_p \frac{1}{\nu_p^3}\left\{\overline{K}_0'(\partial_0\phi_c)^2 + \overline{K}_s'(\nabla\phi_c)^2\right\}\left\{\overline{K}_0'p_0^2 + \overline{K}_s'\mathbf{p}^2 + \overline{V}''\right\}
\end{aligned}
\tag{D.19}
$$

As a whole, we have the following contribution from the first term of Eq.(D.16),

$$
\begin{aligned}
&\int d^4x \int_p \frac{1}{\nu_p^3}\left[2\left\{\overline{K}_0'(\partial_0\phi_c)^2 + \overline{K}_s'(\nabla\phi_c)^2\right\}\nu_p'\right. \\
&\left. + \left\{\overline{K}_0'\partial_0\phi_c p_0 + \overline{K}_s'\nabla\phi_c\mathbf{p}\right\}^2\right].
\end{aligned}
\tag{D.20}
$$

Similarly, we have the following contribution from the second term of Eq.(D.16),

$$\int d^4x \int_p \frac{1}{\nu_p^4} \left[-\frac{1}{2} \left\{ \overline{K}_0' p_0^2 + \overline{K}_s' \mathbf{p}^2 + \overline{V}''' \right\}^2 + \left\{ \overline{K}_0 (\partial_0 \phi_c)^2 + \overline{K}_s (\nabla \phi_c)^2 \right\} \right.$$
$$\left. -2 \left\{ \overline{K}_0' (\partial_0 \phi_c) p_0 + \overline{K}_s' (\nabla \phi_c) \mathbf{p} \right\} \left\{ \overline{K}_0 (\partial_0 \phi_c) p_0 + \overline{K}_s (\nabla \phi_c) \mathbf{p} \right\} \nu_p' \right]. \quad \text{(D.21)}$$

Combining Eq.(D.11), Eq.(D.12), Eq.(D.20) and Eq.(D.21), we obtain the evolution equation, Eq.(6.7).

Bibliography

[1] M.Le Bellac "Thermal Field Theory"(1996)Cambridge.

[2] T. Banks and A. Zaks, Nucl. Phys. **B196** (1982) 189.

[3] T. Appelquist, J. Terning and L. C. R. Wijewardhana, Phys. Rev. Lett. **77** (1996) 1214.

[4] R. Oehme and W. Zimmermann, Phys. Rev. **D21** (1980) 474, 1661.

[5] Y. Iwasaki, K. Kanaya, S. Kaya, S. Sakai, and T. Yoshie Nucl.Phys.Proc.Suppl.**53** (1997) 449.

[6] M. Tachibana Phys.Rev. **D58** (1998) 045015.

[7] G. 'tHooft Nucl. Phys. **B190** (1981) 455.

[8] V.Kuzmin ,V.Rubakov and M.E.Shaposhnikov Phys.Lett.**B155** (1985) 36.

[9] A.G.Cohen ,D.B.Kaplan and A.E.Nelson Nucl.Phys.**B349** (1991) 727.

[10] V. A. Rubakov and M. E. Shaposhnikov, Usp.Fiz.Nauk **166** (1996) 493; Phys.Usp. **39** (1996) 461; hep-ph/9603208.

[11] V.L.Ginzberg and L.D.Landau Zh.Eksp.Teor.Fiz.**20** (1950) 1064.

[12] P.G.de.Gennes, Solid State Commun. **10** (1972) 753.

[13] J. Zinn-Justin, Quantum Field Theory and Critical Phenomena, (Oxford Univ. Press, 1996).

[14] K.Higashijima. Prog.Theor.Phys.Suppl. **104** (1991) 1.

[15] V.A.Miransky, "Dynamical Symmetry Beaking in Quantum Field Theory" (World Scientific, 1993) 1.

[16] M. E. Shaposhnikov, hep-ph/9610247.

[17] P. Arnold, *Proceedings of Quarks '94* (1994) 71 (hep-ph/9410294).

[18] T.Mastsubara Prog.Theor.Phys.**14**(1955)351.

[19] N.P.Landsman and Ch.G.van Wheet Phys.Rep.**145**(1987) 141.

[20] H.Umezawa, " Advanced Field Theory" (1993)AIP.

[21] P.Fendley Phys.Lett.**B196**(1987)175.

[22] J.I.Kapusta "Finite Temperature Field Theory"(1989) Cambridge.

[23] J.Dolan and R.Jackiw Phys.Rev.**D9**(1974)3320.

[24] P.Ginsparg Nucl.Phys.B170(1980)388

[25] T.Appelquist and R.Pisrski Phys.Rev.D23(1981)2305

[26] S.Nadkarni Phys.Rev.D27(1983)917

[27] N.P.Landsman Nucl.Phys.B322(1989)498

[28] K. Rummukainen, M. Tsypin, K. Kajantie, M. Laine and M. E. Shaposhnikov Nucl.Phys. **B532** (1998) 283 (references therein)

[29] T. Appelquist and J.Carazzone Phys.Rev.**D11**(1974)2856.

[30] K. Symmanzik Comm.Math.Phys.**34** (1973) 7.

[31] F. Csikor and Z. Fodor Phys.Lett. **B380**(1996)113.

[32] F. Karsch Nucl.Phys.**B205**(1982)285.

[33] F. Karsch and I. O. Stamatescu Phys.Lett.**B227**(1989)153.

[34] S. Chiku and T. Hatsuda Phys. Rev. **D58**(1998)076001.

[35] H- S Roh and T. Matsui Eur.Phys.J. **A1**(1998)205.

[36] J. Cornwall, R. Jackiw, and E. Tomboulis, Phys. Rev. **D10** (1974) 2428.

[37] G. Amelino-Camelia and S. Y. Pi, Phys. Rev. **D47** (1993), 2356.

[38] A. Camelia, Phys.Rev. **D49** (1994) 2740.

[39] P. Arnold and L. G. Yaffe, Phys. Rev. **D49** (1994) 3003.

[40] W. Buchmuller and O. Philipsen, Nucl. Phys. **B443** (1995) 47.

[41] W. Buchmuller and O. Philipsen, Phys. Lett. **B354** (1995) 403.

[42] I. T. Drummond, R. R. Horgan, P. V. Landshoff and A. Rebhan, Phys. Lett.**B398** (1997) 326.

[43] T. Inagaki, K. Ogure and J. Sato, Prog.Theor.Phys. **99** (1998) 1069.

[44] J.Arafune, K.Ogure and J.Sato, Prog.Theor.Phys. **99** (1998) 119.

[45] K. Ogure and J. Sato, Phys.Rev. **D57** (1998) 7460.

[46] K. Ogure and J. Sato, Phys.Rev. **D58** (1998) 085010.

[47] K. Ogure and J. Sato, Prog.Teor.Phys.**102** (1999).

[48] K. Ogure and J. Sato, hep-ph/9905482.

[49] K. Ogure and J. Sato, hep-ph/9909306.

[50] K.Takahashi Z.Phys.**C26** (1985) 601.

[51] P. Arnold and O. Espinosa, Phys. Rev. **D47** (1993) 3546.

[52] Itzykson and Drouffe "Statistical Field Theory"(1989)Cambridge.

[53] G.Parisi "Statistical Field Theory"(1988)Addison Wesley.

[54] M.Le Bellac "Quantum and Statistical Field Theory"(1988)Oxford.

[55] N.Goldenfeld "Lecture On Phase Transition And the Renormalization Group"(1992) Addison Wesley.

[56] P. D. Morley and M. B. Kislinger, Phys. Rep. **51** (1979), 63.

[57] E. Weinberg and A. Wu , Phys. Rev. **D36** (1987), 2474.

[58] K. Aoki, K. Morikawa, W. Souma, J. Sumi and H. Terao, Prog. Theor. Phys. **95** (1996) 409.

[59] T. R. Morris and M.D. Turner, Nucl. Phys. **B509** (1998) 637.

[60] H.W.J.Blöte, A.Compagner, J.H.Croockewit, Y.T.J.C.Fonk, J.R.Heringa, A.Hoogland, T.S.Smit and A.L.van Villingen, Physica **A161** (1989) 1.

[61] R. Guida, J. Z. Justin em Nucl.Phys. **B489** (1997) 626.

[62] R.B.Griffiths, J. chem. Phys. **43** (1965) 1958.

[63] R.Pisarski and F.Wilczek, Phys.Rev. **D29** (1984) 338.

[64] S.A.Antonenko and A.I.Sokolov Phys.Rev.**E51** (1995)1984

[65] M. E. Carrington, Phys. Rev. **D45** (1992) 2933.

[66] F. Csikor, Z. Fodor and J. Heitger, Phys.Rev.Lett. **82** (1999) 21-24 (references therein)

[67] E.- M. Ilgenfritz, A. Schiller and C. Strecha, Eur.Phys.J. **C8** (1999) 135-150 (references therein)

[68] F. Karch, T. Neuhaus, A. Patós and J. Rank, Nucl.Phys.**474** (1996) 217

[69] Y. Aoki, F. Csikor, Z. Fodor, and A. Ukawa, hep-lat/9901021

[70] N. Tetradis, Phys.Lett. **B409** (1997) 355

[71] S. J. Huber, A. Laser, M. Reuter and M. G. Schmidt, Nucl.Phys. **B539** (1999) 477

[72] B. I. Halperin, T. C. Lubensky and S. K. Ma, Phys.Rev.Lett. **32** (1974) 292.

[73] C. Dasgupta and B. I. Halperin, Phys. Rev. Lett.**47** (1981) 1556.

[74] J. Bartholomew, Phys. Rev.**B28** (1983) 5378.

[75] Y. Munehisa, Phys. Lett.**B155** (1985) 159.

[76] K. Farakos, G. Koutsoumbas and S. Sarantakos, Z.Phys.**C40** (1988) 465.

[77] K. Kajantie, M. Karjalainen, M. Laine and J. Peisa, Phys.Rev. **B57** (1998) 3011.

[78] K. Kajantie, M. Karjalainen, M. Laine and J. Peisa, Nucl.Phys. **B520** (1998) 345.

[79] J. H. Chen and T. C. Lubensky and D. R. Nelson, Phys.Rev.**B17** (1978) 4274.

[80] S. Hikami, Prog.Theor.Phys.**62** (1979) 226.

[81] I. D. Lawrie, Nucl.Phys. **B200** (1982) 1.

[82] H. Kleinert, Phys.Lett. **A93** (1982) 86.

[83] J. M. Russell, Phys.Lett. **B296** (1992) 364.

[84] M. Kiometzis, H. Kleinert and A. M. J. Schakel, Phys.Rev.Lett. **73** (1994) 1975.

[85] L. Radzihovsky, Europhys.Lett. **29** (1995) 227.

[86] I. F. Herbut, and Z. Tešanović Phys.Rev.Lett. **76** (1996) 4588, Phys.Rev.Lett. **78** (1997) 981. I. D. Lawrie, Phys.Rev.Lett. **78** (1997) 978.

[87] R. Fork and Y. Holovatch, J.Phys.A: Math. Gen. **29** (1996) 3409.

[88] B. Bergerhoff, F. Freire, D. F. Litim, S. Lola and C. Wetterich, Phys.Rev. **B53** (1996) 5735.

[89] I. F. Herbut, J.Phys.A **30** (1997) 423, cond-mat/9702167. H. Kleinert and A. M. J. Schakel cond-mat/9702159.

[90] C. J. lobb, Phys.Rev. **B36** (1987) 3930.

[91] M. B. Salamon, W. Lee, K. Ghiron, N. Overend and M. A. Howson , Physica **A200** (1993) 365.

[92] Z.- H. Lin, G. C. Spalding, A. M. Goldman, B. F. Bayman and O. T. Valls , Euro.Phys.Lett. **32** (1995) 573.

[93] W. L. Mcmillan, Phys.Rev. **A7** (1973) 1419.

[94] J. A. Nielsen, R. J. Birgeneau, M. Kaplan, J. D. Lister and C. R. Safinya , Phys.Rev.Lett. **39** (1977) 352.

[95] D. L. Johnson, C. F. Hayes, R. J.deHoff and C. A. Schantz, Phys.Rev.**B18** (1978) 4902.

[96] C. W. Garland, G. B. Kasting and K. J. Lushington, Phys.Rev.Lett. **39** (1979) 1420.

[97] D. Brisbin, R. DeHoff, T. E. Lockert and D. L. Johnson, Phys.Rev.Lett. **43** (1979) 1171.

[98] J. M. Viner and C. C. Huang, Sol.State.Com. **39** (1981) 789.

[99] R. J. Birgeneau, C. W. Garland, G. B. Kasting and B. M. Ocko, Phys.Rev.**A24** (1981) 2624.

[100] C. W. Garland, M. Meichle, B. M. Ocko, A. R. Kortan, C. R. Safinya, L. J. Yu, J. D. Lister and R. J. Birgeneau, Phys.Rev.**A27** (1983) 3235.

[101] J. Thoen, H. Marynissen and W. V. Dael, Phys.Rev.Lett. **52** (1984) 204.

[102] B. M. Ocko, R. J. Birgeneau, J. D. Litster and M. E. Neubert , Phys.Rev.Lett. **52** (1984) 208.

[103] K. K. Chan, P. S. Pershan and L. B. Sorensen, Phys.Rev.Lett. **54** (1985) 1694.

[104] K. K. Chan, P. S. Pershan, L. B. Sorensen and F. Hardouin, Phys.Rev. **A34** (1986) 1420.

[105] M. A. Anisimov, P. E. Cladis, E. E. Gorodetskii, D. A. Huse, V. E. Podnecks, V. G. Taratuta, W. Saarloos and V. P. Voronov , Phys.Rev. **A41** (1990) 6749.

[106] L. Chen, J. D. Brock, J. Huang and S. Kumar, Phys.Rev.Lett. **67** (1991) 2037.

[107] G. Nounesis, K. I. Blum, M. J. Young, C. W. Garland and R. J. Birgeneau , Phys.Rev. **E47** (1993) 1910.

[108] L. Wu, M. J. Young, Y. Shao, C. W. Garland, R. J. Birgeneau and G. Heppke, Phys.Rev.Lett. **72** (1994) 376.

[109] C. W. Garland and G. Nounesis, Phys.Rev. **E49** (1994) 2964.

[110] P. Arnold, Phys. Rev. **D46** (1992) 2628.

[111] A. Jakovác and A. Patkós, Z. Phys. **C60** (1993) 361.

[112] A. Hebecker, Z. Phys. **C60** (1993) 271.

[113] M. S. Manton, Phys.Rev. **D28** (1983) 2019.

[114] F. R.Kllinkhamer and M. S. Manton, Phys.Rev. **D30** (1984) 2212.

[115] T. R. Morris, Phys. Lett. B329 (1994) 241.

[116] W. H. Press, B. P. Flannery, S. A. Teukolsky and W. T. Vetterling, " Numerical Recipes in C" (Cambridge Univ. Press, 1988).